DISSERTATION

Titel der Dissertation

Structural features of TNF-α lectin-like domain derived peptides for activation of amiloride-sensitive sodium current

angestrebter akademischer Grad

Doktorin der Naturwissenschaften (Dr. rer.nat.)

Verfasserin / Verfasser:	Parastoo Hazemi
Dissertationsgebiet (lt. Studienblatt):	Pharmazie A449
Betreuerin / Betreuer:	a.o.Univ.-Prof. Mag. Dr. Rosa Lemmens-Gruber

Wien, im Jänner 2011

Contents

Acknowledgements

Once one starts a doctoral thesis you'll find out that indeed you're going on a quest. And as for any other adventure, you need a lot of friends and meet a lot of people who help you master the quest successfully and safely.

After working for a long time on a project like the here presented doctoral thesis, the time has come for me to bring my thanks to the companions of my personal voyage.

First of all I want to thank my teacher a.o. Univ.Prof. Mag. Dr. Rosa Lemmens-Gruber for all the support she gave me since the very beginning of my thesis. You helped me in the best tradition of the German word "Doktorvater", being for me like a mother, a counsellor, a critic, a teacher, all in one person. And even if I try, my words are not enough to express my gratitude for your patience and the most comprehensive support in the last years.

Furthermore, let me thank Apeptico Forschung und Entwicklung GmbH, Austria. By funding it, Apeptico made this research project possible at all, mentioning before all, Univ.-Doz. Dr. Bernhard Fischer and Dr. Susan Tzotzos from Apeptico who supported me by their invaluable advice in the different stages of the project.

My thanks go to Dr. Majid Reza Kamyar who got me started in the project, sharing with me his knowledge about the methods in electrophysiology and how to setup a research project. As on many quests one needs a person who tells you to continue from time to time even when times get rough.

In my daily work in the laboratory, my good ghost Pakiza Rawnduzi helped me wherever she could, not only limited to purely professional knowledge. Thank you a lot for all that! Also my sincere gratitude to my PhD student colleagues Gowri Shankar B.A. and Waheed Shabbir for their valuable support, whenever help was required.

Last but not least I owe so much thanks to my family: my grandmother who made it possible to study abroad without obligations at home, my parents who made me curious for knowledge and always supported my educational career in any ways, my sister Sara, my aunt Shaharzad, my uncle Kaivan and my aunt Azita. Without your help I never would have started nor finished this ouevre.

Thank you all!

1. INTRODUCTION

Fluid balance in the healthy adult mammalian lung depends on the regulation of re-absorption of fluid and solutes by the alveolar and distal epithelia on the one hand and passive secretion of fluid, driven by hydrostatic pressure, from the vascular space into the alveolar lumen, on the other (Matthay et al. 2002, Eaton et al. 2009). Excessive accumulation of fluid in the alveolar spaces can be accompanied by reduction of alveolar liquid clearance (ALC) capacity, an epithelial and endothelial hyper-permeability, or a disruption of the epithelial and endothelial barriers caused by increased apoptosis or necrosis (Lucas et al. 2009). Pulmonary oedema is a major complication of acute lung injury (ALI), severe pneumonia, and acute respiratory distress syndrome (ARDS), where failure of lungs to rapidly clear oedema fluid is associated with higher morbidity and mortality (Verghese et al. 1999, Ware and Matthay 2001). Resolution of alveolar oedema depends on the active removal of salt and water from the distal air spaces of the lung across the distal lung epithelial barrier (Matthay et al. 2002, Sartori and Matthay 2002). Evidence from clinical studies shows that increased ALC leads to better clinical outcome in cases of pulmonary oedema and ALI/ARDS (Sartori and Matthay 2002). Apart from ventilation strategies, no specific treatment exists for pulmonary oedema and novel therapies need to be developed to improve clinical outcome (Johnson and Matthay 2010).

The involvement of Na^+ transporters in alveolar fluid clearance in the mammalian lung has been well established in recent years (Berthiaume et al. 2002, Berthiaume and Matthay 2007, Eaton et al. 2009, Hummler and Planès 2010). Transport via the amiloride-sensitive epithelial sodium channel (ENaC) in particular is one of the major pathways for Na^+ entry across alveolar and distal epithelial cells (Folkesson and Matthay 2006). Although the primary site of oedema fluid clearance appears to be in the alveolar epithelium, distal airway epithelial cells can also absorb Na^+ (Berthiaume et al. 2002). The current understanding of alveolar fluid clearance is that Na^+ ions passively enter alveolar epithelial cells through the apically located ENaC and are extruded into the interstitium by basally located Na^+/K^+-ATPase accompanied by transport of water in the same direction, following the osmotic gradient generated (Guidot et al. 2006, Berthiaume and Matthay 2007). The large variety of metabolites and intricate signaling pathways involved in regulation of ENaC activity in lung epithelia illustrates the central role of regulation of lung Na^+ absorption and ENaC activity in lung fluid balance and

function (Eaton et al. 2009, Lucas et al. 2009). For this reason, enhancement of ENaC activity in pathological conditions such as ALI and ARDS has been the focus of intense research.

Tumor necrosis factor α (TNF-α) has been shown to produce an amiloride-sensitive increase in ALC in *Pseudomonas aeruginosa* induced pneumonia in rats and to stimulate amiloride-sensitive Na^+ uptake by type II pneumocytes (Rezaiguia et al. 1997, Fukuda et al. 2001). Furthermore, TNF-α has been shown to stimulate ALC during intestinal ischemia-reperfusion and during bronchial asthma in rats (Borjesson et al. 2000, Tillie-Leblond et al. 2002). The activating effect of TNF-α on ALC is mediated by its lectin-like domain (Lucas et al. 1994, Ridge et al. 1997, Hribar et al. 1999, Tillie-Leblond et al. 2002, Lucas et al. 2009, Hamacher et al. 2010).

AP301 was designed over 15 years ago with the aim of mimicking the loop containing the lectin-like domain of TNF-α (TIP), corresponding to residues C101-E116 of wild type human TNF-α (Lucas et al. 1994). The cyclic TIP peptide AP301 contains an artificial disulphide bridge, which effectively restrains the sequence of amino acid residues representing the lectin-like domain into a cyclic structure. However, from a pharmacological standpoint, the peptide AP301 has limitations for therapeutic use as the disulphide bridge is easily reduced and is therefore unstable. For medicinal use, a molecule with improved stability and increased activity is desirable. For this reason, the new TIP peptides described in this thesis were designed containing different, more stable chemical structures across the bridging part of the molecule.

The cyclic peptide AP301 has been granted orphan drug status both in Europe for treatment of ALI and ARDS and in the USA for prevention of ischemia reperfusion injury in the lung during transplantation.

1.1 Alveolar liquid clearance and ion channels

The lungs of mammals are covered with epithelium and have a larger surface area in total than the outer surface area of the lung itself. The fetal lung converts from fluid secretion to fluid re-absorption only shortly before birth. After birth, the regulation of the amount of fluid in the thin (average 0.2 μm) liquid layer, lining the alveolar epithelium, affects the efficient gas exchange (Johnson et al. 2006). In the normal lung, fluid first moves from the blood circulation through the capillary endothelium into the lung interstitium. Afterwards, it is cleared by the lymphatics on a continuous basis. This mechanism secures the dryness of the

alveolar surface in order to allow gas exchange withous a fluid barrier (Zemans et al. 2004). But in cardiogenic pulmonary oedema or ALI, alveolar fluid transport impairs from alveolar to interstitial spaces. As a result the fluid is more than normal and the exchange of CO_2/O_2 will be disordered. It is proved that ALC is achieved by active ion transport in the lung epithelial cells.

1.1.1. Different types of lung cells and their functions

The alveolar epithelium covers >99% of the large internal surface area of the lung. It is composed of two cell types, alveolar type I (TI) and type II (TII) cells (Figure 1).
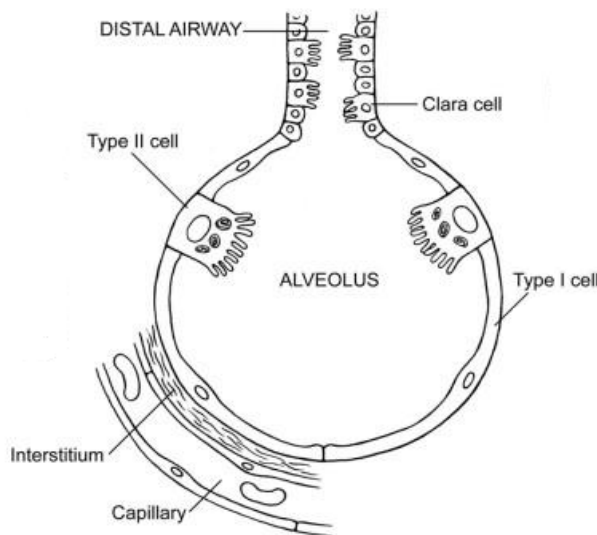
Figure 1: The distal airway epithelium contains alveolar type I and type II cells and Clara cells, which possess various pumps and channels that achieve clearance of oedema fluid (Zemans et al.2004).

TII cells are cuboidal cells that synthesize and secrete pulmonary surfactant. These cells cover 2–5% of the internal surface area of the lung (Johnson et al. 2006). TI cells, however, cover >95% of the surface area of the lung. TI cells express aquaporin 5, which is a water channel. They have the highest known osmotic water permeability of any mammalian cell type (Johnson et al. 2006).

1.1.2. Different types of ion channels in isolated type I and type II lung cells

Freshly isolated type I cells of adult Sprague-Dawley rat lungs contain (Figure 2):
  ➢ Amiloride-sensitive epithelial sodium channels (ENaC, HSC)
  ➢ pimozide-sensitive cyclic nucleotide-gated cation channels (CNG channels)
  ➢ voltage-gated potassium (K^+) channels and
  ➢ the cystic fibrosis transmembrane regulator (CFTR Cl⁻ channels)

Freshly isolated type II cells contain:

➢ ENaC and

➢ cystic fibrosis transmembrane regulator
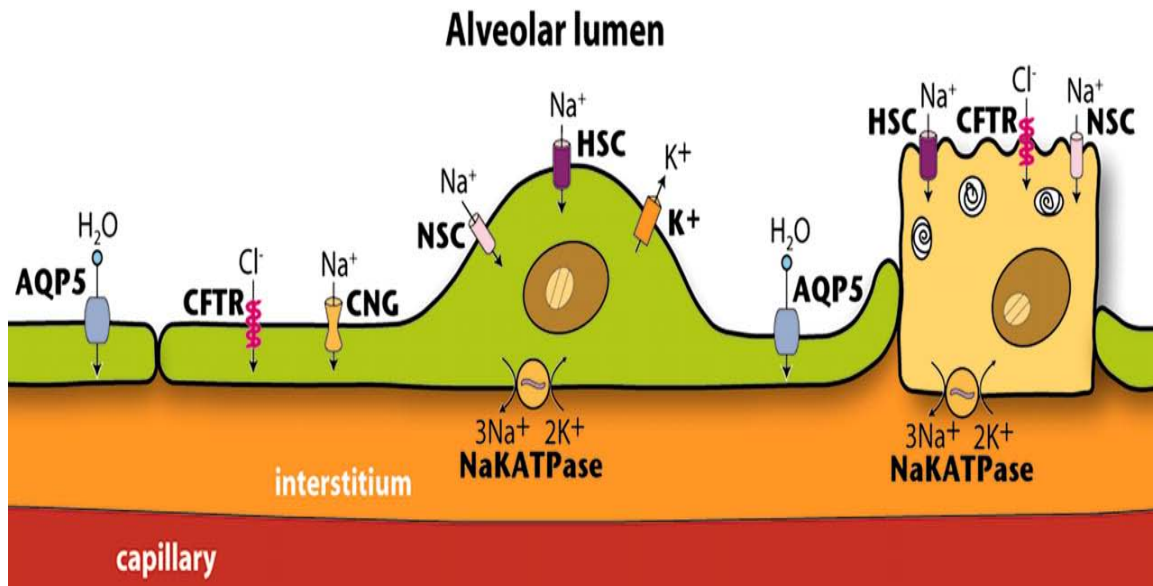
Figure 2: Sodium is transported through channels on the apical membrane and extruded from the cell by the Na^+/K^+-ATPase located on the basolateral membrane. This transport generates a sodium gradient that drives the transport of water, which is accomplished in part through water channels. AQP, aquaporin; CFTR, cystic fibrosis transmembrane conductance regulator; CNG, cyclic nucleotide-gated; ENaC, epithelial Na^+channel, HSC, highly selective channel, NSC, non-selective channel, TI cells (green), TII cells (yellow). From Johnson et al. (2006).

Cultured TII cells have been proposed as a model for TI cells because type I cells are difficult to isolate. Moreover, cultured type II cells express some markers shared by type I cells (Johnson et al. 2006).

Cultured type II cells contain epithelial ENaC, CNG channels, K^+ channels and CFTR Cl^- channels. The expression of CNG and K^+ channels depends on duration of cultivation, though. TII cells contained CNG channels only when cultured for 2 days (Kemp et al. 2001). Studies on TII cells on the other hand give evidence for K^+ channels when cultured for 5–7 days (O'Grady et al. 2003). This clearly demonstrates that culture conditions can alter channel expression.

1.1.3. CNG channels, K$^+$ channels and CFTR Cl$^-$ channels

1.1.3.1. <u>Location and function of CNG channels</u>

The ***cyclic nucleotide-gated ion channel*** is any ion channel that opens in the presence of cyclic nucleotides. As a result, cations flow into the cell and cause depolarization. Cyclic GMP stimulates currents through CNG channels, which are inhibited by pimozide (Kemp et al. 2001).

CNG channels are particularly important in several tissues. Examples would be the retinal photoreceptor cells, and the kidney where they promote Na$^+$ reabsorption. In addition, it was demonstrated that mRNA for primary and secondary subunits of CNG channels, hαCNG1 and hβCNG1, respectively, are expressed in several human airway cell lines. These include normal and cystic fibrosis bronchial airway cells, normal and cystic fibrosis tracheal airway cell lines and nasal polyp tissue from a cystic fibrosis patient. By increasing circulating glucocorticoids or mineralocorticoids, the mRNA of αCNG1 in rat lung and in cultured alveolar airway cells increases. αCNG1 is a functional sodium entry channel in both rat and human airway epithelial cells. This channel could mediate an increase in sodium absorption across lung epithelia in response to circulating hormones, if channel protein is also elevated (Oiu et al. 2000).

1.1.3.2. <u>Location and function of CFTR</u>

The ***cystic fibrosis transmembrane conductance regulator*** is an ABC transporter-class protein and ion channel. The ion channel transports chloride ions across epithelial cell membranes. Whole cell patch-clamp experiments revealed cAMP-stimulated, 5-nitro-2-(3-phenylpropyl-amino)-benzoate-sensitive Cl$^-$ conductance with a linear current-voltage relationship. In cell-attached membrane patches with 100 µM amiloride in the pipette solution, forskolin stimulated channels of approximately 4 pS conductance. It is concluded that functional CFTR Cl$^-$ channels occur in adult alveolar cells and could contribute to alveolar liquid homeostasis (Brochiero et al. 2004).

In epithelial cells of many organs including lung, liver, pancreas, digestive tract, reproductive tract and skin, the CFTR can be traced. Mutations that result in decreased expression or function of the membrane Cl$^-$ channel CFTR, result in a decrease in the volume and hence the depth of liquid on the airway surface, impaired ciliary function, and dehydrated glandular secretions (Nichols et al. 2008).

1.1.3.3. _Location and function of potassium channels_

Voltage-gated potassium channels are transmembrane channels specific for potassium. They are sensitive to voltage changes in the cell's membrane potential and play a central role in mediating hypoxic pulmonary vasoconstriction. During inflammatory lung processes such as pneumonia or ARDS, hypoxic pulmonary vasoconstriction is impaired (Spöhr et al. 2007). In the lung epithelia repair processes, the stimulation of K^+ channels through autocrine activation of epidermal growth factor receptors could play a crucial role (Trinh et al. 2007).

Calcium activated K^+ channels can be divided into different categories such as BK channels, IK channels, and SK channels. The distinction is made based on their conductance (big, intermediate, and small conductance). In epithelia from tissues outside the airway that have similar transport mechanisms to airway cells, large Ca^{2+}-activated potassium channels have been found (Ridge et al.1997). BK channels may play a role in repolarizing cells following depolarization or calcium entry (Morin et al. 2007). Nevertheless, the question of the physiological role of BK channels in primary alveolar epithelial cells remains to be answered. IK channels are prominently expressed in cells of the hematopoietic system. Moreover, they can be found in organs involved in salt and fluid transport, including the colon, lung, and salivary glands.

1.1.4. Epithelial sodium channel (ENaC)

The epithelial sodium channel belongs to a new class of ion channels, which were found at the beginning of the 1990s. It is a member of the ENaC/degenerin family of nonvoltage-gated ion channels (Garty and Palmer 1997, Alvarez de la Rosa et al. 2000, Kellenberger and Schild 2002, Rossier et al. 2002). The ENaC (synonyms: sodium channel non-neuronal 1 (SCNN1) or amiloride sensitive sodium channel (ASSC)) is permeable for Li^+-ions, protons and especially Na^+-ions. It is an active ion-channel, and it belongs to the most selective ion channels. It is proved that ENaC, compared to other channels, which are found in early stage evolution like potassium, chloride and water channels, is expressed just in animal cells with specialized functions. The members of the ENaC/degenerin gene family show a high degree of functional heterogeneity that is unusual among the known gene families of ion channels. Their wide tissue distribution that includes transporting epithelia as well as neuronal excitable tissues best reflects the functional heterogeneity of the ENaC/degenerin family members. Depending on their function in the cell, these channels are either constitutively active like ENaC or activated by mechanical stimuli as postulated for *C. elegans* degenerins, or by

ligands such as peptides or protons in the case of FMRF (Phe-Met-Arg-Phe-NH$_2$)-amide-gated ion channel (FaNaC) and acid-sensing ion channels (ASICs) (Kellenberger and Schild 2002).

1.1.4.1. *Location and function of ENaC in different organs*

ENaC is localized in the apical membranes of sodium-absorbing epithelia like the aldosterone-sensitive distal nephron, respiratory epithelia, distal colon, and sweat and salivary ducts. In these epithelia ENaC is the rate-limiting step for sodium absorption and plays a critical role in the maintenance of body sodium balance. In addition, ENaC expression has been reported in a number of other tissues, including skin, endothelial cells, vascular smooth muscle cells, and neurons where its physiological role remains to be determined (Kellenberger and Schild 2002).

➢ Kidney and urinary bladder

For regulation of fluid balance, epithelial sodium channels are expressed in the distal convoluted tubule, connecting tubule, cortical collecting tubule and outer medullary collecting tubule.

➢ Intestine

The colon is the important and major part of the gastrointestinal tract of ENaC expression.

➢ Sweat and salivary ducts

ENaC is expressed in human sweat and rabbits salivary ducts. The amiloride sensitive channel works in conjunction with the (CFTR) Cl$^-$ channels to reabsorb salt from the sweat.

➢ Salt-taste cells

These kinds of cells are defined by specialized cells on the tongue that has reaction to NaCl. Recently some studies suggested that the channels play a role in taste. Amiloride can attenuate the perception of salty taste.

➢ Lung

The fluid can be reabsorbed and secreted in airway epithelial cells. In comparison to other cells in different organs with this type of Na$^+$ channel, like kidney, colon, and sweat and salivary ducts, the Na$^+$ transport through ENaC is not only involved in electrolyte balance, but also in maintaining a level of hydration of fluid layer that covers the inner surface of the epithelium. In addition, sodium reabsorption by ENaC is also very

important to keep alveoli dry. To absorb the fluid from the airways and alveolar lumen, an active transport of sodium ions by alveolar type II and possibly type I cells is required (Davis et al. 2007).

In humans, the expression of ENaC in the upper airways like nasal epithelium, trachea and bronchi fluid is demonstrated both *in vivo* and *in vitro*.

In adult rats and humans, all three subunits α, β and γ are highly expressed in small and medium-sized airways. In the lung, where type II cells are located, more α- and γ-subunits are expressed. The α-subunit is essential for ENaC function in the lung. This is based on the evidence that the α-subunit by itself forms functional channels in Xenopus oocytes and that inactivation of this subunit in animal models results in early death with flooded lungs (Chu et al. 2008).

The role of amiloride sensitive Na^+ transport at birth time is important to reabsorb the liquid that fills the alveoli and the airways of the fetal lung. mRNAs for all three subunits is detected in the fetal lung, and expression of α and γ subunits increases in the late fetal and early postnatal life. This is the time when the lung's function is changed from secretion to absorption.

1.1.4.2. *Structure of ENaC in different organs*

Recent research demonstrates that the epithelial sodium channel is a heteromeric protein composed of three well characterized homologous subunits, α, β and γ (Figure 3). In human an additional δ-subunit exists, which alters proteolytic channel activation and enhances base-line channel activity (Haerteis et al. 2009). At the sequence level δ-ENaC is more closely related to α-ENaC (37% amino acid identity) and to the ϵ-subunit of *Xenopus laevis* (Babini et al. 2003) than to the β- and γ-subunits of ENaC. Such δβγ-ENaC is found in pancreas, testes and ovaries. The biophysical properties of the δβγ-hENaC channel are different from those of the αβγ-channel (Waldmann et al. 1995). The δβγ-ENaC is more than an order of magnitude less sensitive to amiloride than αβγ-ENaC (Waldmann et al. 1995, Ji et al. 2004, Ji et al. 2006, Lu et al. 2008).

Each subunit contains two transmembrane domains (M1 and M2), a large extracellular loop, and short intracellular NH_2- and COO^-- termini. With their M2 domains all subunits are thought to contribute to the channel pore (Garty and Palmer 1997, Kellenberger and Schild 2002). In the absence of a crystal structure for ENaC, its subunit stoichiometry remains a matter of debate. Nevertheless, the recently published crystal structure of the related acid-sensing ion channel ASIC1 suggests that ENaC is probably a heterotrimer.
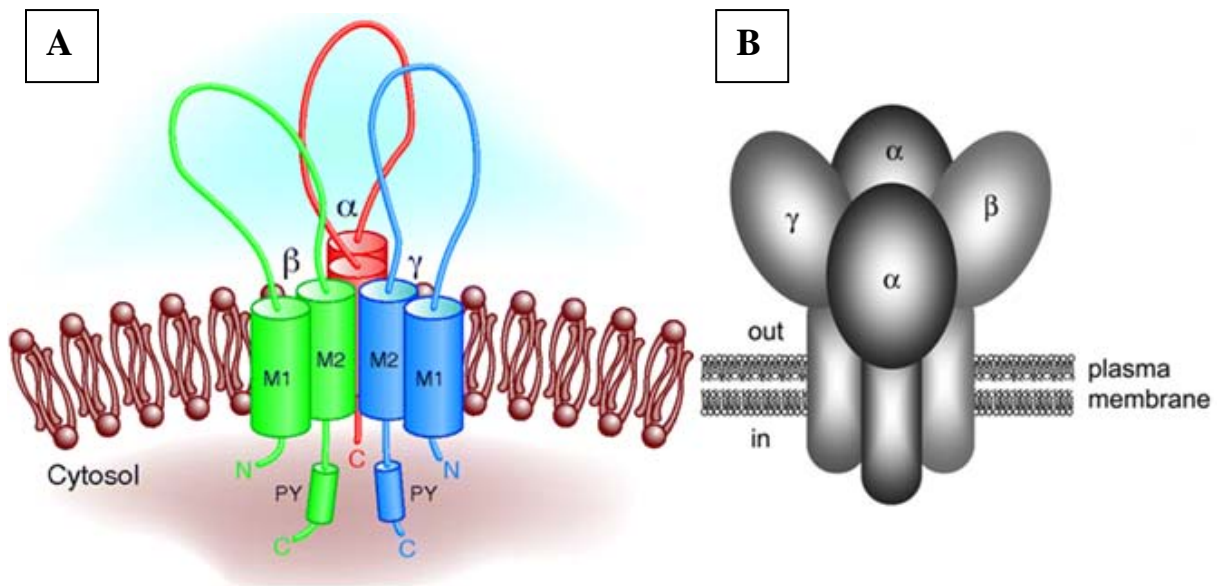
Figure 3: Structure of ENaC

A: ENaC may exist as a heterotrimer composed of an α-, β-, and γ-subunit. Each subunit has two membrane-spanning domains (M1 and M2) with intracellular N- and C-termini (Bhalla et al. 2008.*)*

B: The model shows the tetrameric assembly of ENaC subunits around the central channel pore. The model is based on functional analyses, which showed that all ENaC subunits participate in the formation of the channel pore (Kellenberger and Schild 2002).

The size of the ENaC proteins is from 530 to 740 amino acids. Several studies show that there are different types of epithelial sodium channels, which can conduct sodium and are defined pharmacologically by their sensitivity to potassium sparing diuretic such as amiloride or triamterene. Four Na^+ channel phenotypes have been presented with differing Na^+ selectivities and amiloride sensitivities (Kellenberger and Schild 2002):

Highly selective Na$^+$ channels (HSC):
Selectivity:
HSC is defined by a very high selectivity for Na^+ over K^+ lying between 100:1 and 1000:1. The idea is that the pore of sodium channel selects for Na^+, which is totally dehydrated. This idea can explain why Li^+ and H^+, which are smaller ions than Na^+, can pass the channel, but larger ions like K^+, Rb^+ and Cs^+ cannot.

Single channel currents and conductance:

Single channel current amplitude is between 0.1 and 0.5 pA, depending on membrane voltage and temperature. The single channel conductance is about 4 to 5 pS.

Kinetics of gating:

This kind of channels can have very different kinetics and open probabilities (P_o). It is reported that P_o can range from near zero to close to one. So the channels with high P_o have long open time and short closed time, but in case of low P_o long closed times and short open times. Both open and closed times are between 0.5 to 5 seconds.

Interaction with amiloride:

The interaction with amiloride (Figure 4) depends on the transmembrane voltage, pH of the extracellular solution and the concentration of extracellular Na^+. The concentration of amiloride that can block ENaC is in the range of 0.1 to 1 µM, and it is suggested to apply amiloride to the extracellular surface. However, some studies show that high concentrations of amiloride can block ENaC from the intracellular side in some cells such as from proximal tubules.

Other epithelial amiloride sensitive channels:

➤ *ENaC in the proximal tubule*

This group is ranked between highly selective and moderately selective channels, and the selectivity for Na^+ over K^+ is more than 19:1. Conductivity is approximately 12 pS and the channel can be blocked with 10 µM amiloride from the inside of the cells.

➤ *Moderately selective channels*

The conductivity is between 9 and 21 pS, and the P_o for most of the channels is less than 0.1. This kind of channel can be observed in cultured cells. The ion selectivity for Na^+ over K^+ is about 6:1. The open and closed times are shorter than in highly selective channels with approximately 40 to 100 ms, respectively. The channel can be blocked by 100 µM amiloride. This type of channel is expressed in the cells, which grow in plastic flasks, whereas the highly selective type is expressed when the cells are grown on permeable supports.

➤ *Non-selective cation channel (NSC)*

This kind of channel can be blocked by very low concentrations of amiloride and it has no selectivity between Na^+ and K^+. The conductivity with ~28 pS is rather high compared to highly and moderately selective channels. The mean of open and closed times are

comparable with moderately selective channels with ~40 and 50 ms, respectively (Garty and Palmer 1997).
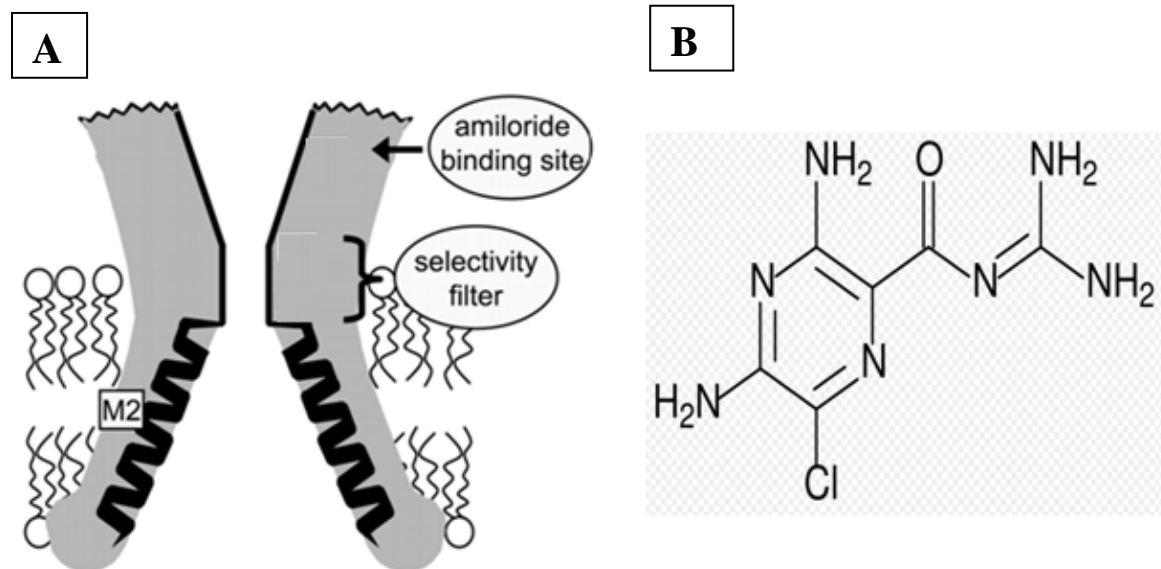
Figure 4.: Block of ENaC by amiloride.

A: Amilorid binds to αS583 and Gly residues in β and γ. The selectivity filter is formed by αG587, βG529, γS541 and the ring of Ser residues (αS589 and homologous residues in β and γ). In this model the M2 domain forms the intracellular part of the pore.

B: Amiloride is a guadinium group containing a pyrazine ring and both are necessary for high affinity binding.

(Kellenberger and Schild 2002)

1.1.4.3. Channelopathies

A number of human diseases that have been linked to malfunction of or mutations in ENaC, including pulmonary oedema, multiple target organ defect pseudohypoaldosteronism type I, Liddle's syndrome and colitis (Staub et al. 2000, Rossier et al. 2002, Bhalla et al. 2008, Chu et al. 2008, Shehata et al. 2009):

Pulmonary oedema:
ALI and ARDS are defined with clinical conditions like respiratory failure and death. One of the important pathologic factors of ALI/ARDS is non-cardiogenic pulmonary oedema.

Pulmonary oedema plays an important role in the recovery phase of ALI/ARDS and is critically dependent on ALC. Unfortunately, a majority of ALI/ARDS patients have less function or expression of ENaC (Chu et al. 2008).
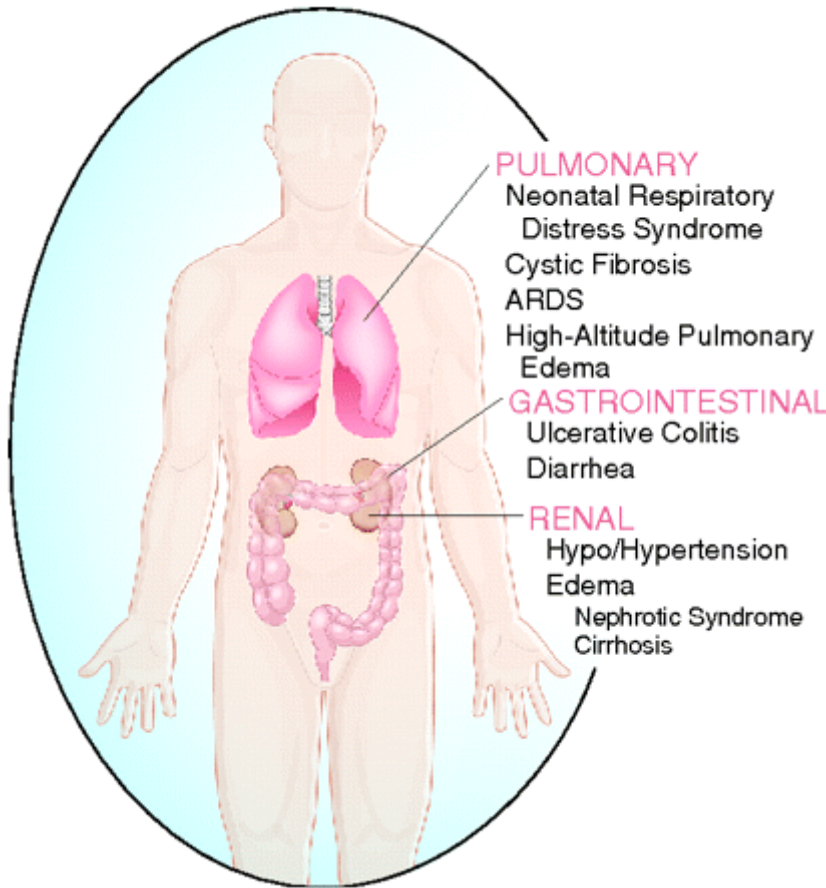
Figure 5: Clinical correlations of ENaC regulation.
ENaC has been well characterized as a regulator of volume status and blood pressure, but more recent studies have demonstrated its role in oedema formation and gastrointestinal and respiratory disorders.
(Bhalla et al. 2008)

Colitis:

Decreased expression of ENaC subunits in human biopsy samples from patients with colitis is demonstrated (Bhalla et al. 2008).

Multiple target organ defect pseudohypoaldosteronism type I (MTODPHA-I), hypotensive syndromes:

Some patients with the autosomal recessive inheritance of this syndrome have been found to carry mutations in one or another of the α, β, or γ subunits. It is a loss-of-function mutation, which results in a defect of sodium transport in many organs such as kidney, lung, colon, sweat and salivary glands. The mutation leads to salt-loss symptoms and is characterized by volume depletion, hypotension, hyperkalemia, and failure to respond to mineralocorticoids.

The importance of ENaC in the absorption of salt and fluid by epithelia has been confirmed by the generation of knockout mice with inactivated subunits of ENaC.

Liddle's syndrome, hypertensive syndromes:

The Liddle's syndrom is an autosomal-dominant form of salt-sensitive hypertension caused by gain-of-function mutations, which leads to constitutively increased channel activity. ENaC is very important for the maintenance of sodium balance, extracellular fluid volume and long term blood pressure control. The syndrome is defined by a severe form of hereditary hypertension, hypokalemia, low aldosterone and plasma renin levels and metabolic alkalosis in human. Studies with patients suffering from Liddle's syndrome demonstrated linkage of hypertension to a segment of chromosome 16, which contains the β- and γ-subunits of the amiloride-sensitive ENaC. Several mutations have been identified in β- and γ-subunits that either deleted most of the carboxy terminus or introduced point mutations in a short carboxy-terminal proline-rich sequence.

1.1.5. Methods to increase the activity of ENaC in lung cells

As described above, ENaC plays a critical role in epithelial cells to absorb Na^+ and also water, and to make the alveoli space dry. Thus, this ion channel is of interest in the treatment of pulmonary oedema. To achieve this goal, an increased activity of ENaC either by stimulation of expression or by stimulation of the ion current is the target.

1.1.5.1 *Stimulation of expression of ENaC*

Most studies are focused on the stimulation of the expression of ENaC. It has been observed that glibenclamide induced the stimulation of the amiloride-sensitive current in oocytes expressing human αβγENaC by 40-50% (Chraibi and Horisberger 1999).

Also in airway and renal epithelia, the glucocorticoid-mediated stimulation of amiloride-sensitive Na^+ transport has been demonstrated, which is caused by the increased expression of the epithelial Na^+ channel α subunit (αENaC) (Sayegh et al. 1999).

Furthermore, some experiments indicate that an increase in channel open probability combined with an increase in channel surface expression are the two mechanisms by which cAMP leads to enhanced ENaC currents (Yang et al. 2006).

1.1.5.2 *Stimulation of epithelial sodium channel by TNF-α*

Recently, several articles confirmed that TNF-α induced up-regulation of alveolar fluid transport in human alveolar epithelial cells. Some of the researches reported that TNF-α creates ion channels in the cells by insertion into the plasma membrane (Baldwin et al. 1995, 1996). On the other hand it has been reported that membrane interaction of TNF-α is not sufficient to trigger an increase in membrane conductance in mammalian cells (Van der Goot et al. 1999), while Fukuda et al. demonstrated in patch clamp studies with human alveolar epithelial cells (A549 cell line) that TNF-α stimulates Na$^+$ influx and that this effect was inhibited by amiloride (Figure 6) (Fukuda et al.2001).
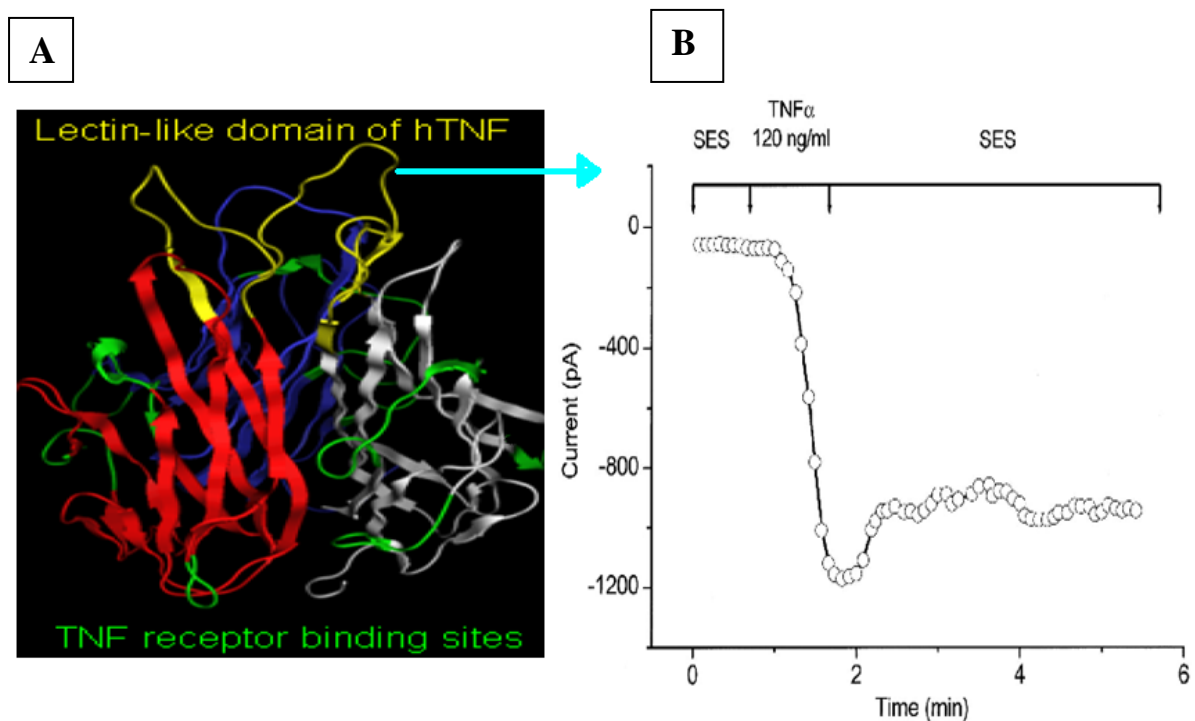
Figure 6: Structure and effect of TNF-α on Na$^+$ current

A: Trimeric molecule of TNF-α and the side of this molecule, which has the ability to actively affect oedema re-absorption (Braun et al. 2005).

B: Effect of TNF-α on Na$^+$ current in A549 cells patched in the whole cell mode (Fukuda et al. 2001). The pipette was filled with standard internal solution. The cell was held at -40 mV, and an inward current was elicited by an application of a -100 mV pulse. The cell was perfused with either standard external solution (SES) or SES containing TNF-α (120 ng/ml) as indicated.

1.2. Structure of lectin-like domain of TNF-α and design of a series of novel peptides

TNF-α is a cytokine that is secreted by macrophages and monocytes. It occurs in many inflammatory diseases, and also as a response to endotoxins from bacteria. This molecule has three chains, which are named A, B and C with 152 residues (Figure 7).
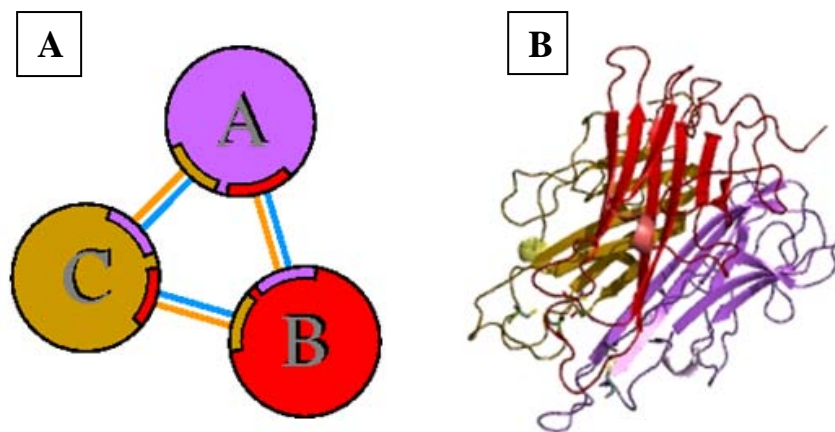
Figure 7: Structure of TNF-α

A: Schematic diagram of interactions between protein chains. The bridges between the chains are mostly hydrogen bonds.

B: Structure of TNF-α at 2.6 Ångstrom resolution.

(From Protein Data Bank)

As described above, it has been demonstrated that TNF-α can stimulate the epithelial sodium channel in the human epithelial cell line A549 (Fukuda et al. 2001). The lectin-like domain (TIP) of the TNF-α molecule is responsible for this effect and presented by C101 to E116 as illustrated in Figure 8.

Native TNF-α is a homotrimer with the lectin-like domain of each subunit (in human TNF-α the sequence of amino acid residues from C101 to E116) located close together at the tip of the structure (Figure 6), whereas the TNF receptor-binding sites are located in the basolateral regions of the molecule. Initially characterized for its trypanolytic effect (Lucas et al. 1994), the lectin-like domain of TNF-α has been shown to activate amiloride-sensitive Na^+ uptake in lung microvascular endothelial cells (Hribar et al. 1999) and in the alveolar epithelial cell line A549 (Fukuda et al. 2001).
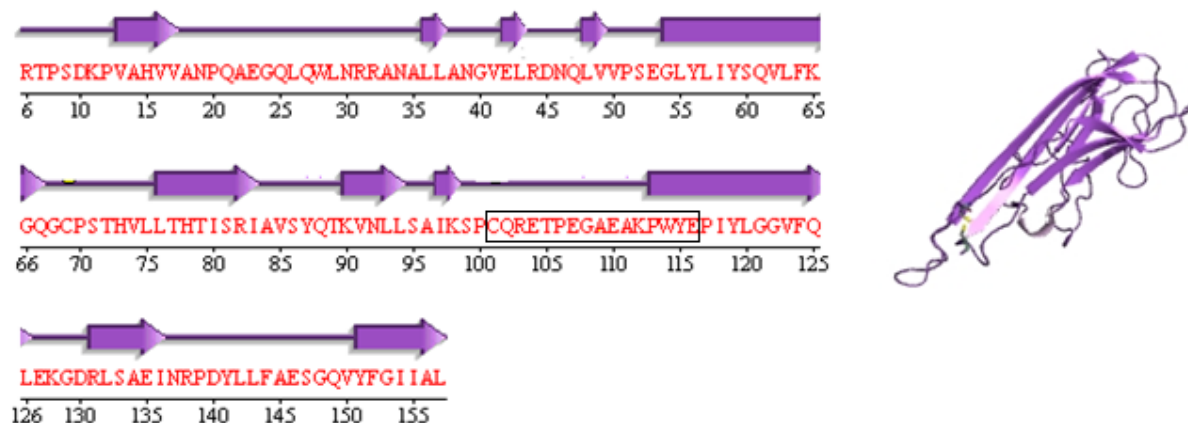
Figure 8: Analysis of sequence's residue in chain A of human TNF-α.
The lectin like domain of TNF-α is highlighted. (From Protein Data Bank)

In the present study, the lectin-like domain of human TNF-α (C101 to E116), previously shown to be implicated in sodium uptake activation in A549 cells (Fukuda et al, 2001), was used as a template for the design of a series of novel peptides, in which cyclisation was achieved, in all cases but one, by amide bond formation between an amino group of an N-terminal lysine or non-protein amino acid and a carboxyl group of a C-terminal α-amino acid residue. The 3D structural model for human TNF-α, PDB ID:1A8M was used as a template to build 3D models of the peptides using molecular graphics software and the models provided estimates of atomic distances in the cyclic molecules (Hazemi et al. 2010).

Cyclic peptides were generally designed such that the distance between the N-terminal and C-terminal α-carbon atoms or atoms in positions equivalent to these, approximated that in AP301 (C1-C17 Cα-Cα distance 7.15Å) or in human TNF -α (P100-E116 Cα-Cα distance 7.23 Å in PDB ID:1A8M A chain) (Figure 9). The 19-residue cysteine-free, cyclic peptide (AP303) comprises the sequence of human TNF-α from K98 to E116, with C101 replaced by glycine and cyclisation achieved by isopeptide bond formation between the ε-amino group of K98 and the γ-carboxyl group of E116 (Figure 9). The cysteine-containing peptide (AP302) has the wild-type sequence of TNF-α from C101 to K112 to which two glycine residues have been added followed by a C-terminal cysteine residue. Disulphide bond formation between the two terminal cysteine residues brings about cyclisation in the 15-peptide AP302. Thus, AP302 lacks P113 and bulky hydrophobic residues W114 and Y115 of TNF-α (P14, W15 and Y16 of AP301), whilst retaining the residues T105, E107 and E110 (T6, E8 and E11 of AP301) (Figure 9), shown to be essential for the ENaC-activating effect of TNF-α and

AP301. A mutant TIP peptide having the same sequence as AP301 with T6, E8 and E11 each replaced by alanine, was included in the study for comparative purposes (Figure 9).
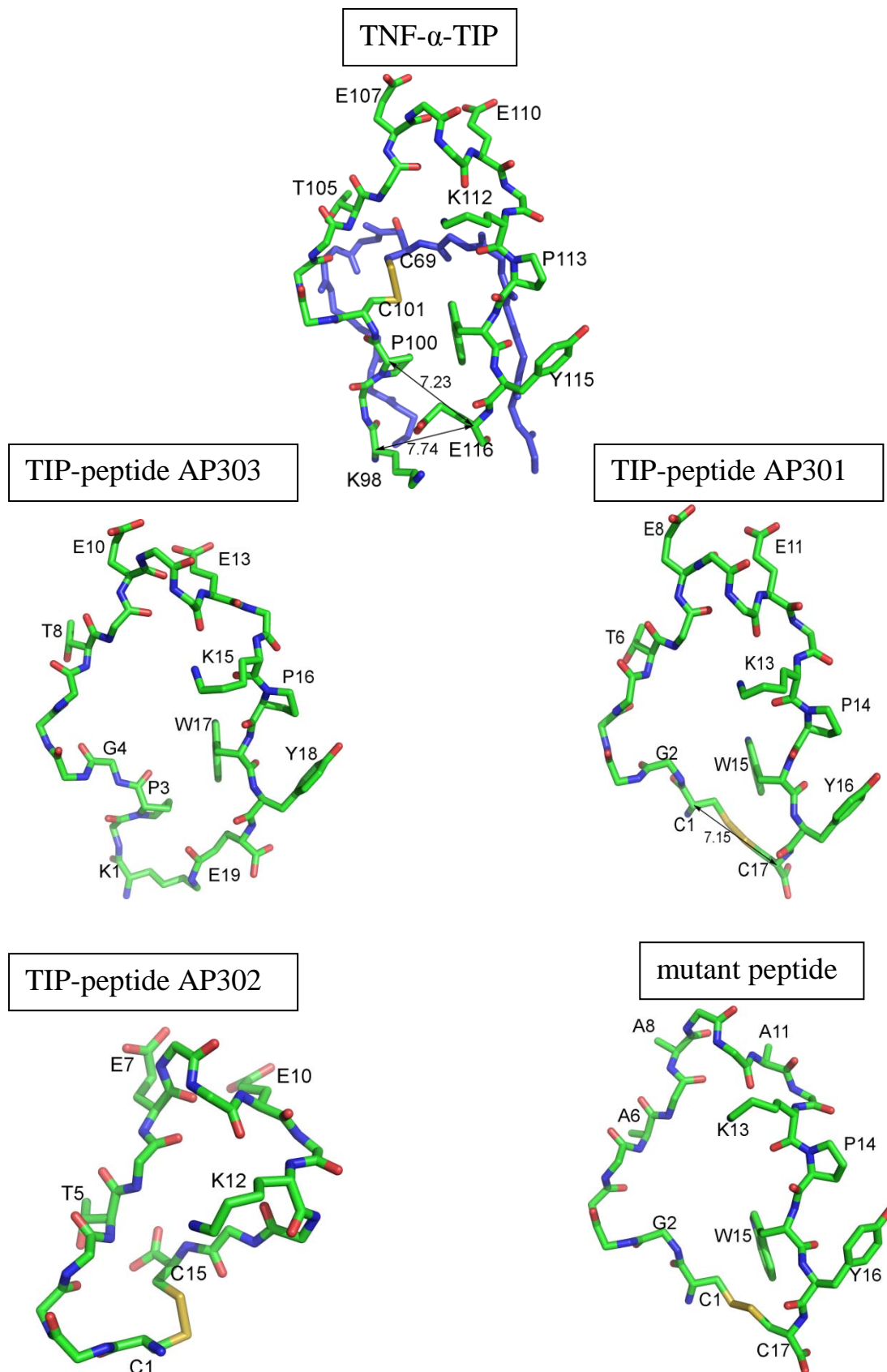
Figure 9: Human TNF-α around TIP or lectin-like domain (C101-E116) according to structure PDB ID:1A8M, and models for the TIP-peptides AP301, AP302, AP303 and mutant peptide based on the 1A8M template.

Side chains are shown only for those residues relevant for structure activity relationship. Numbers adjacent to lines with double arrowheads refer to Cα-Cα distances in Å.

i)   Human TNF-α molecule, A chain, showing parts of polypeptide chain, F64-L76 (blue), K98-E116 (green), disulphide bridge between residues C69 and C101 (yellow) and residues known from previous studies to be essential for trypanolytic and ENaC-activating effects: T105, E107 and E110.

ii) AP303, the TIP-peptide which most resembles wild-type TNF-α, showing isopeptide link between side chains of K1 (K98 in TNF-α) and E19 (E116 in TNF-α) and amino acid change G4 (C101 in TNF-α).

iii) AP301, showing disulphide bond between C1 (P100 in TNF-α) and C17 (E116 in TNF-α) and amino acid change G2 (C101 in TNF-α); residues critical for ENaC-activating activity are T6, E8 and E11.

iv) AP302, showing disulphide bond between C1 (C101 in TNF-α) and C15; sequence C1-K12 is the same as C101-K112 in TNF-α, but residues corresponding to P113, W114 and Y115 are missing.

v)   Mutant peptide, showing disulphide bond between C1 (P100 in TNF-α) and C17 (E116 in TNF-α) and amino acid change G2 (C101 in TNF-α), as well as mutated critical residues A6, A8 and A11 (T105, E107 and E110 in wild-type human TNF-α and T6, E8, E11 in AP301).

(Hazemi et al. 2010)

1.3. Pore-forming bacterial toxins

1.3.1   Panton-Valentine Leukocidin (PVL)

Panton-Valentine Leukocidin (PVL) is a β-barrel pore-forming toxin secreted from *Staphylococcus aureus* (*S. aureus*), a gram positive bacterium. PVL consists of two subunits, LukS-PV and LukF-PV, which in an equimolar ratio, shape the octamer structure (Kaneko et al. 2004, Jayasinghe et al. 2005, Miles et al. 2006, O'Hara et al. 2008) and can form pores on a host cell (Genestier et al. 2005). Bacterial strains carrying the gene for PVL are rare (Genestier et al. 2005) but in last several years due to spread of several methicillin resistant *S. aureus* (MRSA) clones throughout the world, they are becoming more prevalent (Vandenesch et al. 2003). Previous studies show that human and rabbit neutrophils are highly sensitive to pore-forming properties of PVL and thereby undergo cell death rapidly (Colin et al. 1994). Lysing the first cells which come to the site of the infection is a good strategy of bacteria to escape the immune response and this is likely to be a key event of successful MRSA pathogenesis (Genestier et al. 2005).

Within the respiratory tract, alveolar macrophages are considered to be the first lines of defence and express a plethora of pattern recognition receptors**,** including Toll-like receptors (TLR), which recognize pattern associated molecular patterns. Fast and accurate recognition of pattern associated molecular patterns is extremely important in lungs, which are a specialized compartment constantly exposed to air flow and pathogens (Knapp et al. 2006). Toll-like receptor activation results in downstream signaling pathways such as activation of mitogen-activated protein kinases and the transcription factor nuclear factor kappa B (NF-kB). These pathways then modulate inflammatory gene expression, which is crucial to shaping the innate immune response within the lungs.

Previous studies predominantly concentrated on the *in vitro* role of PVL on polymorphonuclear cells (PMNs) and disclosed the toxic properties of PVL (Colin et al. 1994, Genestier et al. 2005). So far data indicate that PVL can induce apoptosis in human PMNs by virtue of its ability to release cytochrome C from mitochondria (Genestier et al. 2005). Also, PVL has been shown to induce granule content release, to interfere with the oxidative burst and to induce IL-8 release (Colin et al. 1994, Colin and Monteil 2003). From other reports that also concentrated on PMNs, it seems that PVL's ability to form pores has to be distinguished from its capacity to open Ca^{2+} channels (Staali et al. 1998, Baba Moussa et al.

1999). A dispute arose over the ability of PVL to directly cause lung inflammation *in vivo*. While one report could demonstrate this effect, the other one found contradictory results and based the pathogenicity of PVL on the concomitant presence of hemolysins (Labandeira-Rey et al. 2007, Bubeck Wardenburg et al. 2007). By using a microarray profiling approach it was shown that PVL induces a highly specific inflammatory transcriptional response in alveolar macrophages. Further biochemical and genetic studies indicated that this response is independent from PVLs pore-forming ability and is mediated via NF-kB, through a TLR2 dependent mechanism (Zivkovic et al., manuscript accepted).
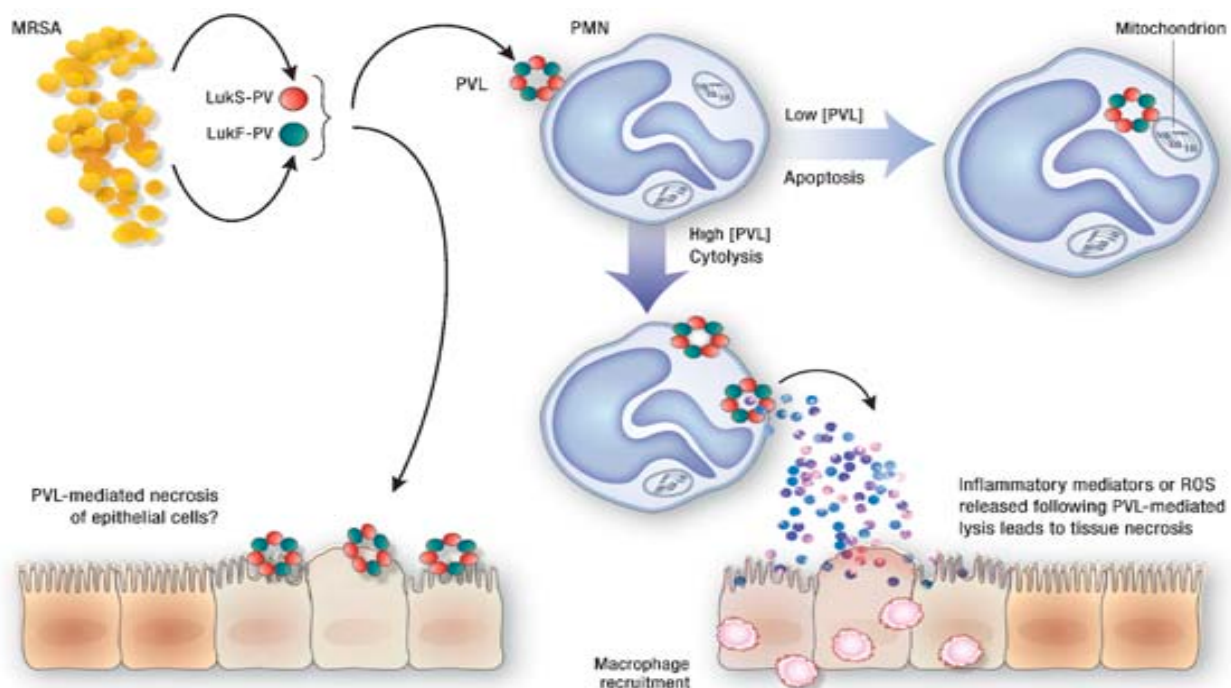
Figure 10: Model for how PVL might mediate tissue necrosis. The two components of PVL, LukS-PV and LukF-PV are secreted from *S. aureus* before they assemble into a pore-forming heptamer on PMN membranes. High PVL concentrations cause PMN lysis whereas low concentrations mediate a novel pathway of PMN apoptosis by directly binding to mitochondrial membranes. Tissue necrosis could result from release of reactive oxygen species (ROS) from lysed PMNs. Alternately, release of granule contents from lysed PMNs could set in motion an inflammatory response, eventually resulting in tissue necrosis. It is unlikely that PVL has a direct necrotic effect on epithelial cells.
(Boyle-Vavra and Daum 2007)

1.3.1.1 *Role of PVL in disease*

Panton-Valentine Leukocidin is a cytotoxin that can destroy white blood cells and cause extensive tissue necrosis and severe infection. The toxin was first described by Panton and Valentine in 1932. Severity of infection ranges from mild skin diseases, such as impetigo and skin abscesses to serious invasive diseases, including sepsis, endocarditis, toxic shock syndrome, and necrotizing pneumonia (Genestier et. al 2005). Presence of PVL-positive MRSA isolates are usually associated with soft tissue (skin and lungs) necrosis and these patients have poor prognosis along with strikingly higher mortality rates (up to 75%) compared to PVL-negative MRSA strains (Gillet et al. 2002).

1.3.1.2 *Pore-forming function of PVL*

As described before, PVL has two components, LukF-PV and LukS-PV. The presence of both components is necessary to form a pore in the cell membrane (Figure 11). Staphylococcal leukocidin (Luk) and α-hemolysin are members of the same family of β-barrel pore-forming toxins. The Luk pore is formed by the co-assembly of four copies each of the two distantly related polypeptides, LukF and LukS, to form an octamer (Miles et al. 2006).
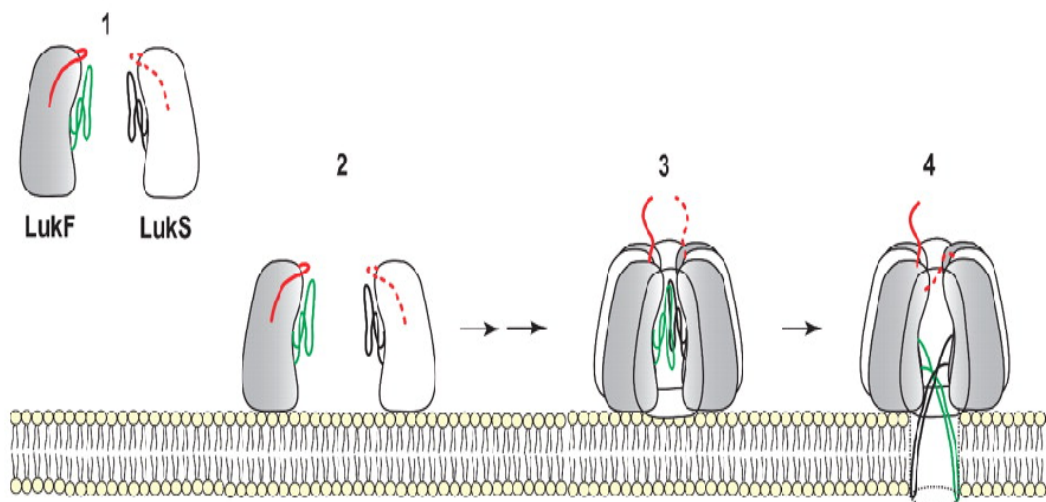
Figure 11: PVL is a β-barrel pore-forming toxin, comprised of two subunits termed LukF-PV and LukS-PV. Both subunits are secreted separately (1) and are thought to oligomerize (2, 3) on the surface of specific cells to assemble the final pore (4).

(Miles et al. 2006)

1.3.2   Listeriolysin O (LLO)

Listeriolysin O (LLO) is a cholesterol-dependent cytolysin, a family of toxins secreted by Gram-positive bacteria (Tweten et al. 2005, Kayal et al. 2006). Structural studies have provided much insight into the molecular mechanism of pore formation by this family. Initially, the secreted monomer binds to cholesterol-containing membranes via the conserved undecapeptide motif in domain 4 (Rossjohn et al. 1997, Ramachandran et al. 2002). Lateral diffusion and oligomerization of the monomers is followed by structural changes in the molecule (Gilbert et al. 1999, Tilley et al. 2005), resulting in pores consisting of 35–50 monomers, with a diameter of 25–35 nm (Gilbert et al. 2005). LLO, together with the other listerial cholesterol-dependent cytolysins (seeligerolysin and ivanolysin), are distinct within the wider family for having an optimum activity at acidic rather than neutral pH (Geoffroy et al. 1987), attributed to a triad of acidic residues unique to this subgroup of toxins (Schuerch et al. 2005). These trigger rapid and irreversible denaturation of the structure at neutral pH at temperatures above 30°C. However, it has been recently shown that binding and permeabilization of cells is possible at neutral pH, provided the cholesterol content of the membrane is sufficiently high (Bavdek et. al 2007).

LLO is critically required during Listeria infection, and Listeria deficient for LLO are avirulent in mouse infection studies (Kathariou et al. 1987). LLO expression allows escape of bacteria from phagosomes into the cytoplasm and secondary cell-to-cell spreading, although in some cell types its loss may be compensated for by bacterial phospholipases (Alberti-Segui et al. 2007). The acidic pH optimum, together with rapid degradation within the cell, restricts its intracellular activity and prevents premature death of the host cell (Schnupf et al. 2006 and Glomski et al. 2002). The action of LLO during infection, however, may not be restricted to the phagosome, given that the toxin will be released from extracellular bacteria and from dead cells. Indeed, lesions in the spleen resulting from extensive lymphocyte death during Listeria infection are shown to be due to extracellular LLO release (Carrero et al. 2004a). These exogenous actions can contribute to the pathogenesis of infection, for example, the apoptotic lymphocyte death previously mentioned is reported to trigger a down-regulation of the inflammatory response, to the detriment of the host (Carrero et al. 2006).

Exogenous LLO, and also other pore-forming toxins, were shown to trigger signaling events in a variety of cell types (Kayal et al. 2006). In some instances, including MAPK activation and calcium signaling, this is attributed to its pore-forming ability at the plasma membrane and also potentially at organelle membranes. It is also suggested that signaling may be

triggered by LLO binding to a cell surface receptor, specifically TLR4 (Repp e. al. 2002, Park et al. 2004, Carrero et al. 2006a, Gekara et. al 2007), although no direct binding was shown. An alternative model for LLO-induced signaling is also proposed, based on the observation that LLO oligomerization induces lipid raft aggregation in the cell membrane (Gekara et al. 2005). Subsequent pore formation is not required for this process, nor for the tyrosine kinase activation, induced presumably through signaling complex congregation in the raft.

Pore-formation and signaling events are linked to cell death induced by LLO and other pore-forming toxins, at concentrations less than those required for instant lysis of nucleated cells (Guzman et a.l 1996). Reports for LLO-induced death include apoptotic death in dendritic cells, and in T lymphocytes (Carrero et al. 2004a), where caspase-dependent and -independent death has been shown. Ion fluxes initiated by pore opening are suggested to be the trigger for death in the case of various other pore-forming toxins, including *Staphylococcus aureus* α-toxin and aerolysin from *Aeromonas hydrophila* (Jonas et al. 1994, Bantel et al. 2001, Nelson et al. 1999).

The case of T lymphocyte death upon LLO treatment is particularly intriguing, as it is shown to be up-regulated upon pretreatment of the lymphocytes with type I interferon (IFN-I) (Carrero et al. 2004b). IFN-I production, induced during early stages of Listeria infection *in vivo*, is detrimental to the innate immune response of the host (Carrero et al. 2004b, O'Connell et al. 2004, Auerbuch et al. 2004). Macrophages are host cells for invading Listeria within the spleen and liver. When activated, they are able to destroy phagocytosed bacteria. However, *in vitro* experiments show that infection of resting macrophages results in a slow, predominantly necrotic death (Barsig et al. 1997), and this death is increased by IFN-β production and signaling triggered by the cytoplasmic invasion of the macrophage (Stockinger et al. 2002). In this case, LLO expression by Listeria is necessary for cytoplasmic invasion and IFN-β production, but the necrotic death is in part attributed to IFN-dependent up-regulation of inducible NO synthase (Zwaferink et al. 2008a). The lytic activity of LLO may both contribute to the death of infected macrophages and affect non-infected cells as in the case of T lymphocytes.

1.3.2.1. *Pore-forming properties of LLO*

Various signalling events and cellular effects, including modulation of gene expression, are triggered by LLO. LLO applied extracellularly at sublytic concentrations causes long-lasting oscillations of the intracellular Ca^{2+} level of human embryonic kidney cells; resulting from a

pulsed influx of extracellular Ca^{2+} through pores that are formed by LLO in the plasma membrane (Figure 12). Calcium influx does not require the activity of endogenous Ca^{2+} channels. LLO-formed pores are transient and oscillate between open and closed states. Pore formation and Ca^{2+} oscillations were also observed after exposure of cells to native *Listeria monocytogenes* (Repp et al. 2002).
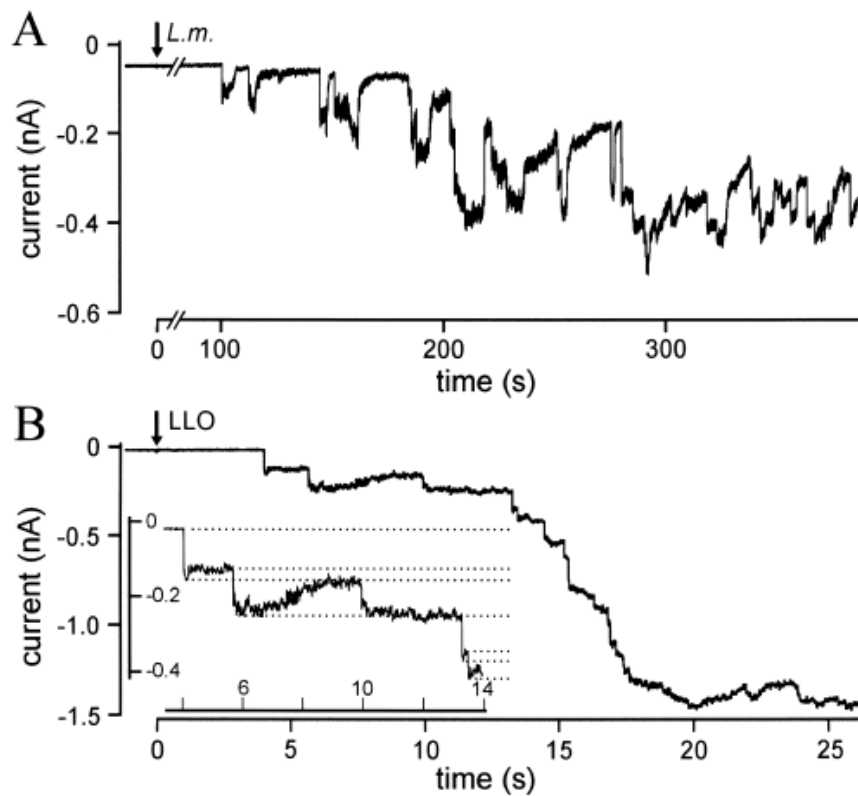
Figure 12: Pore formation after exposure to wild-type *Listeria monocytogenes* and LLO.
A. Section from a 15 min recording. The trace goes downwards after a pore opening and upwards during a pore closing. When the recording was stopped, the membrane current amplitude was ~ −0.6 nA.
B. Pore formation by LLO (100 ng.ml^{-1}). The inset shows the beginning of pore formation on an expanded time and current scale. The dotted lines indicate membrane current levels corresponding to pore openings. The membrane holding potential was −50 mV (Repp et al. 2002).

1.4 Aim of study

The present work investigated the effect of the original TIP peptide AP301, and a series of novel cyclic peptides that also mimic the lectin-like domain of TNF-α, on amiloride-sensitive sodium current in A549 cells. The study was aimed at elucidation of structural features that are important for the ENaC-activating effect in order to achieve an improved TIP peptide for therapeutic use. These novel peptides were compared to the original human TIP analogue, CGQRETPEGAEAKPWYC (AP301), which contains the sequence from P100 to E116 of human TNF-α, but with P100 and E116 replaced by cysteine residues and C101 replaced by glycine, so that cyclisation of the linear sequence was achieved by disulphide bond formation between the two terminal cysteine residues. The disulphide bond in analogue AP301 may be susceptible to reduction and scission leading to complications in medical use. Therefore, the focus of the new peptide design described in the thesis was replacement of the disulphide bridge of the original TIP analogue, AP301, with other molecular arrangements, whilst preserving the sequence of residues T105-E110, shown to be essential for the ENaC-activating effect of TNF-α. The continuous human ATII alveolar cell line A549 was used to test the activity of the peptides by means of the patch clamp technique. Furthermore, the selectivity of the activation effect of Na^+ over K^+ and the effect of deglycosylation of the cell membrane was investigated. Furthermore, the electrophysiological effects of TIP peptides in presence of pore-forming bacterial toxins were studied.

The two studied pore-forming bacterial toxins are produced by MRSA and *Listeria*. MRSA strains can contain genes that encode PVL, which is responsible for many severe clinical symptoms of infection with MRSA. The aim of this study was to determine whether PVL or the two components LukF-PVL and Luks-PVL can induce pores in the cell membrane of macrophages. Besides the pore-forming activity, electrophysiological properties such as ion selectivity and single channel current kinetics had to be characterized. Furthermore, concentration- and potential-dependency as well as site of action were evaluated. As it has been demonstrated that the human TIP-peptide blunts LLO-induced hyperpermeability *in vitro* (Xiong et al. 2010), we aimed to study the effect of TIP-peptides on PVL-induced current. Furthermore, the effect of the bacterial toxin LLO on pore formation was tested after pretreatment of macrophages with IFN-β as it was reported that pore-formation and signaling events are linked to cell death induced by LLO.

2. MATERIAL AND METHODS

2.1. Materials

2.1.1 Cell culture

2.1.1.1 Cells

A549 cells were kindly supplied by W. Berger from the Department of Medicine I, Institute of Cancer Research, Medical University of Vienna, Austria in the 80th passage.

MH-S cells (ATCC) were kindly supplied by S. Knapp from the Center for Molecular Medicine (Ce-M-M) of the Austrian Academy of Sciences, Vienna, in the second passage.

Bone marrow-derived macrophages were obtained by culture of bone marrow from 7- to 11-week-old mice of C57BL/6 genetic background in L cell-derived CSF-1. These cells were kindly supplied by T. Decker from the Department of Microbiology and Immunobiology.

2.1.1.2 Cell culture media

DMEM-F-12 (Dulbecco's modified Eagle's medium/nutrient mixture F12 Ham) was purchased from Sigma-Aldrich GmbH.

RPMI-1640 medium with L-glutamine, without sodium bicarbonat was purchased from Sigma-Aldrich St. Louis USA.

Fetal calf and bovine serum was purchased from Sigma-Aldrich GmbH.

Penicillin-Streptomycin that was added to the media was purchased from Sigma-Aldrich GmbH and stored at -20°C.

PBS without Ca^{2+}/Mg^{2+} 10X: 2.00 g KCl, 2.0 g KH_2PO_4, 80.0 g NaCl, 27.07 g $Na_2PO_4.2H_2O$, 1000 ml distilled H_2O. Mixed to dissolve, this solution was diluted 1:10 with distilled H_2O, sterile filtrated before use and stored at 4 °C.

Trypsin/EDTA 10X: 0.25 g trypsin (1:250), 0.20 g EDTA, 10 ml PBS without Ca^{2+}/Mg^{2+} 1x. Mix to dissolve. This solution was sterile filtrated and stored at –20 °C. Diluted 1:10 with sterile PBS without Ca^{2+}/Mg^{2+} 1X before use.

2.1.2 Solutions for patch clamp experiments

All the solution ingredients were purchased from Sigma-Adrich GmbH, except Amphotericin B, which was from Fluka Biochemika.

2.1.2.1 *Whole cell recording*

Bath solution for experiments with TIP-peptides (in mM):
145 NaCl, 2.7 KCl, 1.8 CaCl$_2$, 2.0 MgCl$_2$, 5.5 glucose, 10 HEPES, pH 7.4 adjusted with NaOH.

Pipette solution for experiments with TIP-peptides (in mM):
135 potassium methylsulfonic acid, 10 KCl, 6 NaCl, 1 Mg$_2$ATP, 2 Na$_3$ATP, 10 HEPES, 0.5 EGTA, pH 7.2 titrated with 1 N KOH.

Bath solution for experiments with bacterial toxins (in mM):
150 NaCl, 5.4 KCl, 1.8 CaCl$_2$, 0.5 MgCl$_2$, 5 glucose, 10 HEPES, pH 7.4 adjusted with NaOH.

Pipette solution for experiments with bacterial toxins (in mM):
140 potassium aspartate, 2 MgCl$_2$, 2 CaCl$_2$, 10 HEPES, pH 7.4 adjusted to KOH.

Amphotericin B from *Streptomyces ssp.* was used in a concentration of 600 µg/ml in the pipette solution when applying the perforated patch clamp configuration in experiments with LLO.

2.1.2.2 *Cell-attached patches*

Bath solution for experiments with TIP-peptides (in mM):
145 potassium methanesulfonate, 5 MgCl$_2$, 40 mannitol, 10 HEPES, 5.5 glucose, pH 7.4.
With this solution the cells were depolarized to 0 mM.

Pipette solution for experiments with TIP-peptides (in mM):
145 sodium methanesulfonate, 5 MgCl$_2$, 40 mannitol, 10 HEPES, 5.5 glucose, pH 7.4.

2.1.2.3   *Inside-out patches*

The pipette and bathing solutions were of the same composition and contained (in mM): 140 potassium aspartate (or NaCl for sodium ions as the charge carrier), 2 $CaCl_2$, 2 $MgCl_2$, 2 Na_2ATP, 10 HEPES, titrated to pH 7.4 with KOH.

or 110 $CaCl_2$, 2 $MgCl_2$ and 10 HEPES (for calcium ions as the charge carrier), titrated at pH 7.4 with $Ca(OH)_2$.

2.1.3. Chemicals

Amiloride hydrochloride hydrate was used at concentrations of 10 to 100 µM in order to block ENaC.

Tetraethylammonium chloride (TEA) was used at a concentration of 10 mM to block the K^+ current.

Both amiloride hydrochloride hydrate and TEA were purchased from Sigma-Aldrich GmbH, Austria.

Peptide-N-glycosidase F cloned from *Flavobacterium meningosepticum* and expressed in E. coli was obtained from Roche Diagnostics GmbH, Germany. Cells were treated with the enzyme in order to study if this has an effect on binding properties of TIP-peptides.

Recombinant murine interferon β (IFN-β, Calbiochem) was used to prove whether IFN-β has an influence on the pore-forming activity of LLO.

2.1.4.   Experimental set-up

The set-up consisted of the microscope (Axiovert 100, Carl Zeiss, Germany), amplifier (Axopatch 200B, Axon Instruments, CA, USA), headstage (CV 203BU Axon Instruments, CA, USA), pipette holder (HL-U, Axon Instruments, Inc., Foster City, Ca, USA), micromanipulator (A WR-60, Narishige Scientific Instrument Lab., Tokyo, Japan), computer, metal cage and vibration isolation table (Newport Coporation, Irvine, CA, USA).

The silver wire was chlorinated every week before using as an electrode.

2.2. Methods

2.2.1   Cell culture

Experiments were carried out on the human epithelial cell line A549 (ATTAC Nr. CCL-185) in passages 80-90. Cells were grown in Dulbecco's modified Eagle's medium/nutrient mixture F12 Ham, supplemented with 10% fetal bovine serum and containing 1% penicillin-streptomycin. The cells were maintained at 37 °C in a humidified atmosphere of 5 % CO_2 in air. The cells were refreshed every 2 or 3 days with new medium according to the specific requirements.

Cells were grown on tissue culture flasks until it has been 70% full of cells. Confluent cells were washed (with 37 °C warm PBS without Ca^{2+}/Mg^{2+}) and detached from the culture dishes by enzymatic digestion using 37°C warm 1X trypsin/EDTA. Following enzymatic digestion, cells were collected in centrifuge tubes and spun down at 1000 rpm for 5 min at 4°C. The pellet was re-suspended in culture medium and the cells seeded and allowed to proliferate onto new culture flasks with splitting rates of 1:4.

Following enzymatic digestion, cells were pelleted and re-suspended in new medium. After addition of 10 µl Tryptan blue to re-suspended cells, viable cells were counted with the cell counter (Hemacytomter; Hausser Scientific, Horsham, PA. USA). The counted cells were pelleted again and re-suspended in a defined volume of freezing medium (50 % heat inactivated FBS, 40 % D-MEM-F-12 and 10 % DMSO). About 4 million cells in 1.5 ml freezing medium were aliquoted in cryogenic vials. The latter were immediately placed in freezing containers (Nalgene, USA) with isopropanol and stored overnight at –80 °C to allow freezing at a constant rate of -1°C/min. These vials were later transferred to liquid nitrogen tanks for long term storage.

After re-suspension of the cells in culture medium, the cells were seeded on coverslips 12 to 24 hours before performing patch clamping experiments. The coverslips were put in small culture plates with 2 ml culture medium and were maintained at 37°C in a humidified atmosphere of 5 % CO_2 in air.

2.2.2   Patch clamp technique

The patch clamp technique is an electrophysiological technique that allows the study of single or multiple ion channels in cells (Hamill et al.1981).

2.2.2.1   *Cell attached patch*

The glass pipette is sealed to the patch of membrane, and the cell remains intact. This allows the recording of currents through single ion channels in that patch of membrane, without disrupting the interior of the cell. Test compounds being studied are included in the pipette solution, where it can contact what had been the external surface of the membrane. While the resulting channel activity can be attributed to the test compounds being used, it is usually not possible to then change the test compounds concentration and it can be a disadvantage. The advantage of this method is the possibility to analyze channel kinetics in more detail like open time and close time of the channel in the patch.
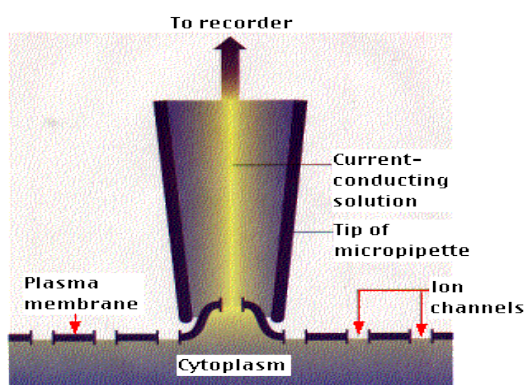
Figure 13: Patch clamp technique in the cell-attached mode.
This mode is used to study single channel kinetics.

2.2.2.2   *Inside-out patch*

After the giga-seal had been made, the pipette is quickly detached from the cell, thus ripping the patch of membrane off the cell, leaving the patch of membrane attached to the tip of the pipette, and exposing the intracellular surface of the membrane to the external solution (bath solution). This mode is useful when the researcher studies the effect of compounds binding from the intracellular side. The concentration of the test substances can easily be changed. This method also allows measuring the current through single ion channels.

2.2.2.3   *Whole cell recording mode*

This method allows to measure whole cell current through entire ion channels on the cell membrane. The pipette is left in place on the cell, but more suction is applied to rupture the membrane patch, thus providing access to the intracellular space of the cell. Alternatively, the pipette can be filled with an amphothericin containing solution, an ionophore which provides perforated patches.

The positive point of whole-cell patch clamp recording compared to sharp microelectrode recording is that the larger opening at the tip of the patch clamp pipette provides lower resistance and thus better electrical access to the inside of the cell. A disadvantage of this technique is that the volume of the electrode is larger than the cell, so the soluble contents of the cell's interior will slowly be replaced by the contents of the electrode.
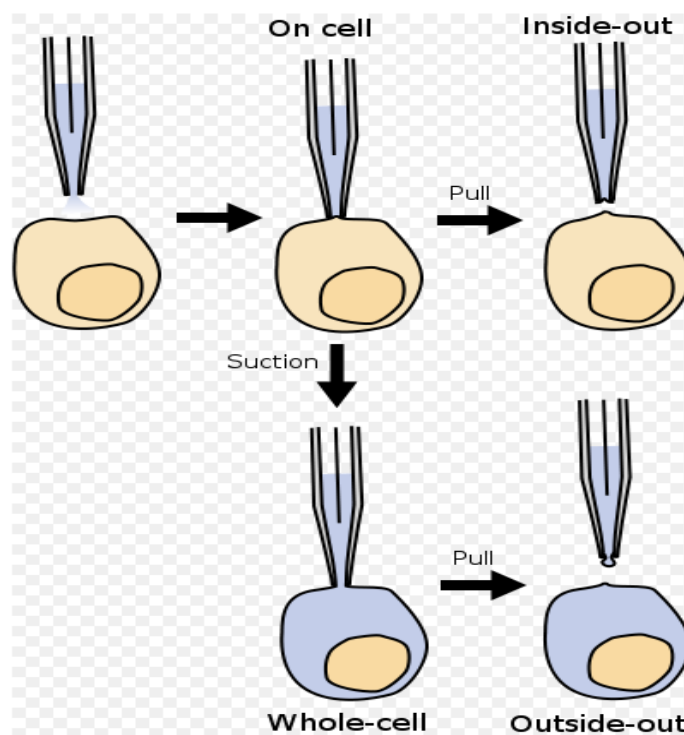
Figure 14: All models of patch clamping.

After putting the pipette on the cell surface, with the first suction, an attached cell patch will be made. After that either, with the second suction, the whole cell patch will be created, or by pulling the pipette an vesicle, and after quickly moving out of the solution, an inside-out patch will be obtained. For an outside-out patch, after formation of the whole cell configuration the pipette must be pulled off the cell.

2.2.2.4 *Pipettes*

Patch pipettes were made in three stages: pipette pulling, heat polishing and filling.

The patch pipettes were pulled from borosilicate glass (WPI, Sarasota, FL, USA) using a programmed Flaming/Brown micropipette puller (P-87, Sutter Instrument Company, CA, USA). The pipette tips were fire-polished on a Micro-Forge model MF-79 (Narishige Scientific Instrument Lab., Tokyo, Japan). The pipette tip polishing was observed at 16 x 35 magnification using a compound microscope with a long distance objective (Leitz Biomed, Wetzlar, Germany). This procedure further reduced the tip opening to a final resistance of 2-10 MΩ.

The tip of the pipettes were dipped into pipette solution for 5 minutes. Then the pipettes were back filled by syringe and needle with pipette solution. The next stage was to drive out the air bubbles by regular strong knocks. The pipette solution must be filtered before using a filter with at a pore size equivalent to 0.2 mm in diameter (Sartorius, Göttingen, Germany).

The pipette resistance was controlled before patch formation. Pipettes with a resistance lower than 1.5 MΩ were rejected and also pipettes with a resistance higher than 10 MΩ. Usually, the pipette resistance between 1.5-3.5 MΩ was used for whole cell patch clamp experiments and 5-10 MΩ for single channel studies.

2.2.3   Experimental procedure

2.2.3.1 *Whole cell recording and cell-attached patches in A549 cells*

Effects on ENaC were studied on A549 cells at room temperature (19-22°C) 24 to 48 h after plating.

Currents were recorded with the patch clamp method in the whole-cell mode and to further evaluate the effects of TIP-peptides on biophysical properties of the epithelial sodium channel, A549 cells were patched in the cell attached mode and single-channel currents were recorded. Glass cover slips with the cultured cells were transferred to a chamber of 1 ml capacity, mounted on the stage of an inverted microscope.

Capacity transients were cancelled, and series resistance was compensated. Whole cell currents were filtered at 5 kHz and sampled at 10 kHz.

Data acquisition and storage were processed directly to a PC equipped with pCLAMP 10.0 software (Axon Instruments, CA, USA).

After GΩ-seal formation, the equilibration period of 5 min was followed by control recordings at at holding potentials (Eh) between –100 and +100 mV in 20 mV increments for 1 min at each Eh.

Then, aliquots of a stock solution, which was prepared with distilled water, were cumulatively added into the bathing solution, resulting in concentrations ranging from 1.75 to 30 nM TNF-α, and from 3.5 to 240 nM TIP peptide, respectively.

The wash-in phase lasted about 1 min. After steady-state had been reached, the same experimental protocol as during control recordings was applied for each concentration of the peptide. Concentration-response curves and EC_{50}-values were fitted and estimated for currents recorded at Eh of –100 mV with SigmaPlot 9.0. Differences in EC_{50} were calculated for statistical significance ($P<0.05$) with the Student's t-test.

For evaluation of ion selectivity, ENaC was blocked by 10 to 100 µM amiloride hydrochloride before the addition of peptide in the whole cell recording mode. Subsequent addition of 10 mM tetraethylammonium chloride (TEA) indicated whether any observed increases in the current were due to potassium current. These experiments were also carried out at Eh = –100 mV.

To study the effect of TNF-α, AP301 and AP318 on ENaC after deglycosilation, N-glycosidase F (PGNase) was applied. Currents were recorded with the patch clamp method in the whole-cell and cell-attached mode. In the whole cell mode the A549 cells were either incubated with 100 units PNGase F for 1 to 5 minutes before doing experiment, and glass cover slips with the cultured cells were rinsed with external solution before transferred to a chamber of 1 ml bath. After control recordings, 30nM TNF-α, 240nM AP301 or AP318 was added. To study more details in single channel kinetics after deglycosilation, the 100 units PNGase F with one of the substance (TNF-α, AP301 or AP318) was added to 1ml pipette solution. TNF-α, AP301 and AP318 were added in concentrations corresponding to their respective EC_{50} values to the pipette solution.

For single channel current measurements 10 mM TEA was added to the pipette solution to block the K^+ channel. It allows us to see the openings of the Na^+ channel without the interference with the K^+ channel, because the amplitude of the K^+ channel is really big in contrast to the Na^+ channel. For control, only TEA was added to the pipette solution, and these controls were recorded at ±60 mV holding potential.

Furthermore, to study the effect of the pore-forming toxin PVL on A549 cells, after control recording of 5 min 200nM PVL was added to the bath solution. After steady-state has been reached, 240 nM AP301 was added to the bath solution.

2.2.3.2 _Whole cell recording and inside-out patches in macrophages_

Currents were recorded with the patch clamp technique in the whole cell and inside out mode. Macrophages of passage 2 to 12 were plated on glass cover slips 12 to 24 h before the experiments were performed.

All measurements were performed at room temperature (19-22°C). Electrodes pulled of borosilicate capillaries had a tip resistance of 3-5 MΩ for whole cell recording and 8-10 MΩ for single channel recording. After patch formation an equilibrium period of 5 min followed, which was succeeded by control recordings at holding potentials ranging from –80 mV to +80 mV with 20 mV increments. During the control period no electrical activity could be observed. Then either of the single components LukF-PV and LukS-PV, or both components together were added to the bathing solution to obtain concentrations of 14 to 280 nM PVL. First channel openings were detected approximately 1 min after addition of the toxin. Then the same experimental protocol was applied as during control recordings.

Electrophysiological measurements were carried out with an Axopatch-1D patch clamp amplifier (Axon Instruments, CA) at a cut-off frequency (-3 dB) of 2 kHz. Currents were filtered at 5 kHz and sampled at 10 kHz. Data acquisition was executed directly to a PC with pCLAMP 6 software (Axon Instruments, CA). Current analysis was performed with ASCD software (G. Droogmans, Leuven, Belgium).

For studies with LLO, macrophages were plated onto glass coverslips and treated with IFN-β (500 U/ml) overnight. Currents were recorded in the perforated patch clamp configuration using amphothericin B (600 µg/ml) in the pipette solution. All measurements were performed at 20–22°C. Electrodes pulled of borosilicate capillaries had a tip resistance of 5–6 MΩ. After patch formation, an equilibrium period of 5 min followed, which was succeeded by a control period of 5 min at a holding potential of –30 mV during which no electrical activity could be observed. Then, LLO was added to the bathing solution at concentrations of 2.5 or 5.0 µg/ml. First channel openings were detected ∼1 min after addition of LLO. Electrophysiological measurements were conducted with an Axopatch-1D patch clamp amplifier (Axon

Instruments) at a cutoff frequency (–3 dB) of 2 kHz. Currents were filtered at 5 kHz and sampled at 10 kHz. Data acquisition was executed directly to a PC with pCLAMP 6 software (Axon Instruments). Current analysis was performed with ASCD software (G. Droogmans, Katholieke Universiteit Leuven, Leuven, Belgium).

2.3 Test substances

2.3.1 TNF-α

TNF-α was purchased from Sigma-Adrich, Saint Louis, USA. Mouse TNF-α, recombinant, expressed in E.coli (T 7539) was used.

To reconstitute the contents of the vial using 0.2 µm filtered, distilled water was used to obtain a concentration of 0.1 mg/ml. For further dilutions, the stock solution with distilled water was prepared and stored in the freezer at -20°C.

The reference compound TNF-α was studied at concentrations ranging from 1.75 to 30 nM.

2.3.2 TIP-peptides

TIP peptides AP301 (cyclic and linear), AP302, AP303, AP309, AP310, AP314, AP317, AP318, AP319, AP321 and AP322 were obtained from Dr. B. Fischer, APEPTICO Forschung und Entwicklung GmbH.

The test compounds were studied at a concentration range of 3.5 to 240 nM.

The stock solutions were prepared with distilled water and stored in the freezer.

The lectin-like domain of human TNF-α (C101 to E116), previously shown to be implicated in sodium uptake activation in A549 cells (Fukuda et al. 2001), was used as a template for the design of a series of novel peptides, in which cyclisation was achieved, in all cases but one, by amide bond formation between an amino group of an N-terminal lysine or non-protein amino acid and a carboxyl group of a C-terminal α-amino acid residue.

The amino acid sequence of the TNF-α lectin like domain is CQRETPEGAEAKPWYE (see Figure 8). The identical sequence of 14 amino acids in lectin-like domain of TNF-α, the lead compound AP301 (CGQRETPEGAEAKPWYC) and other test compounds is highlighted in blue. This amino acid sequence of TNF-α lectin like domain is present in all studied compounds except in AP302 (only 12 identical amino acids, amino acids identical to TNF-α TIP printed in bold letters) and mutant AP301 (amino acids identical to TNF-α TIP printed in bold letters).

Natural and non-protein amino acids and amino carboxylic acids replacing C1 (in red) and C17 (in red) in the molecule of the lead compound AP301 are highlighted in red.

AP301: _Cyclo_(CGQRETPEGAEAKPWYC). Cyclisation was achieved by oxidation of the terminal cysteine residues to form a disulphide bridge. The purity of the peptide was 96.3%. _m/z_ (ESI) 1924.2 (M^++1); theoretical average molecular mass 1923.1.

AP302: _Cyclo_(**CQRETPEGAEAK**GGC). Cyclisation was achieved by oxidation of the terminal cysteine residues to form a disulphide bridge. The purity of the peptide was 97.0%. _m/z_ (MALDI) 1534.8 (M^++1); theoretical average molecular mass 1533.6.

AP303: _Cyclo_(KSPGQRETPEGAEAKPWYE). Cyclisation was achieved by formation of an amide bond between the amino group attached to the ε-carbon of the N-terminal lysine residue and the side chain carboxyl group attached to the γ-carbon of the C-terminal glutamic acid residue. The purity of the peptide was 89%. _m/z_ (MALDI-TOF) 2142.7 (M^++1); theoretical average molecular mass 2142.3.

AP309: _Cyclo_(KGQRETPEGAEAKPWYG). Cyclisation was achieved by creating an amide bond between the amino group attached to the ε-carbon of the side chain of the N-terminal lysine residue and the carboxyl group of the C-terminal glycine residue. The purity of the peptide was 98.8%. _m/z_ (ESI) 1888.2 (M^++1); theoretical average molecular mass 1886.0.

AP310: _Cyclo_(ornithine-GQRETPEGAEAKPWYG). Cyclisation was achieved by creating an amide bond between the amino group attached to the δ-carbon of the side chain of the N-terminal ornithine residue and the carboxyl group of the C-terminal glycine residue. The

purity of the peptide was 97.4%. *m/z* (ESI) 1873.4 (M$^+$+1); theoretical average molecular mass 1872.0.

AP314: *Cyclo*(5-aminopentanoic acid-GQRETPEGAEAKPWYG). Cyclisation was achieved by creating an amide bond between the amino group of N-terminal 5-aminopentanoic acid and the carboxyl group of the C-terminal glycine residue. The purity of the peptide was 100%. *m/z* (MALDI-TOF) 1857.9 (M$^+$+1); theoretical average molecular mass 1857.0.

AP317: *Cyclo*(4-aminobutanoic acid-GQRETPEGAEAKPWYG). Cyclisation was achieved by creating an amide bond between the amino group of the N-terminal 4-aminobutanoic acid and the carboxyl group of the C-terminal glycine residue. The purity of the peptide was 100%. *m/z* (MALDI-TOF) 1843.3 (M$^+$+1); theoretical average molecular mass 1843.0.

AP318: *Cyclo*(4-aminobutanoic acid-GQRETPEGAEAKPWYD). Cyclisation was achieved by creating an amide bond between the amino group of 4-aminobutanoic acid and the side chain carboxyl group attached to the β-carbon of the C-terminal aspartic acid residue. The purity of the peptide was 100%. *m/z* (MALDI-TOF) 1901.6 (M$^+$+1); theoretical average molecular mass 1901.0.

AP319: *Cyclo*(β-alanine-GQRETPEGAEAKPWYE). Cyclisation was achieved by creating an amide bond between the amino group of the N-terminal β-alanine (3-aminopropanoic acid) and the side chain carboxyl group attached to the γ-carbon of the C-terminal glutamic acid residue. The purity of the peptide was 100%. *m/z* (MALDI-TOF) 1902.7 (M$^+$+1); theoretical average molecular mass 1901.0.

AP321: *Cyclo*(7-aminoheptanoic acid-GQRETPEGAEAKPWY). Cyclisation was achieved by creating an amide bond between the amino group of the N-terminal 7-aminoheptanoic acid and the carboxyl group of the C-terminal tyrosine residue. The purity of the peptide was 97.2%. *m/z* (MALDI-TOF) 1828.9 (M$^+$+1); theoretical average molecular mass 1828.0.

AP322: *Cyclo*(6-aminohexanoic acid-GQRETPEGAEAKPWYG). Cyclisation was achieved by creating an amide bond between the amino group of 6-aminohexanoic acid and the carboxyl group of the C-terminal glycine residue. The purity of the peptide was 100%. *m/z* (MALDI-TOF) 1872.6 (M$^+$+1); theoretical average molecular mass 1871.0.

Mutant AP301: *Cyclo*(**CGQRE**A**P**A**GA**A**AKPWYC**). Cyclisation was achieved by oxidation of the terminal cysteine residues to form a disulphide bridge. The purity of the peptide was 98.2%. *m/z* (ESI) 1778.2 (M$^+$+1); theoretical average molecular mass 1777.0.
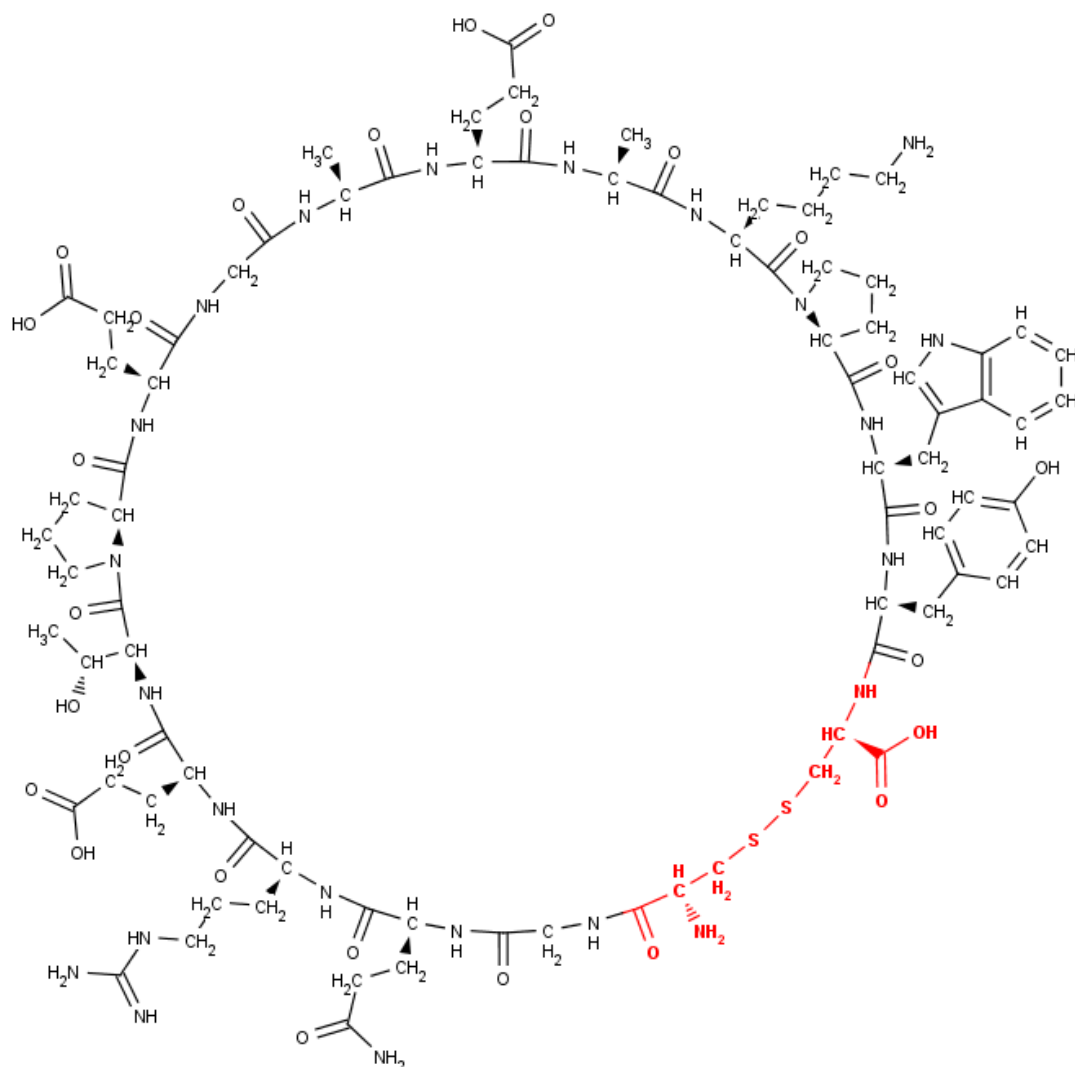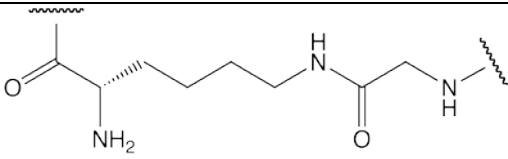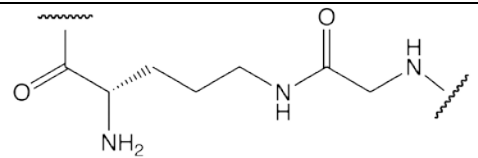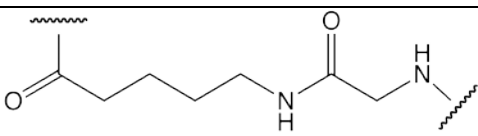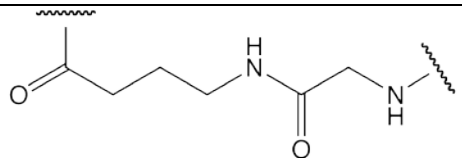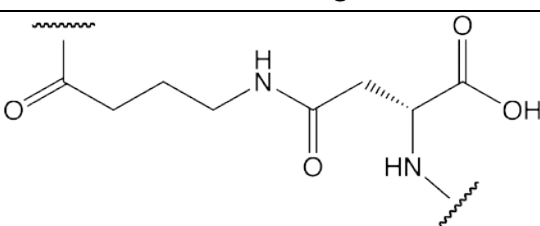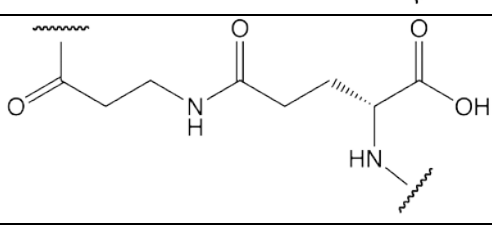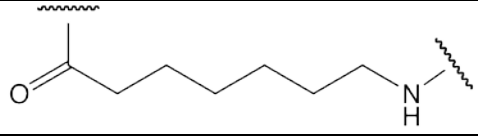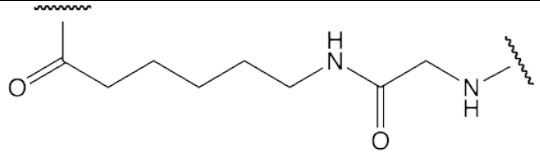
Figure 15: TIP peptide 301, 2D chemical structure.
Atoms replaced in the derived TIP peptides 309, 310, 314, 317, 318, 319, 321 and 322 are shown in bold and coloured red. This part of the molecule refers to the cross linking structures, which are listed in Table 1.

TIP peptides 309, 310, 314, 317, 318, 319, 321 and 322 have the same sequence as AP301 from G2 to Y16, with natural and non-protein amino acids and amino carboxylic acids replacing C1 and C17; AP321 is a 16-peptide in which 7-aminoheptanoic acid replaces C1. In

each peptide the cross-linking structure replaces the atoms shown in bold and red in Figure 15.

Table 1: Cross-linking solutions to replace the disulphide bridge of AP301 in TIP peptide analogues

Peptide	Cross-linking structure (positions 1 and 17)	Characteristics of amide bond in cross-linking structure
AP309		Side chain amino group of lysine (K1) and carboxyl group of glycine (G17)
AP310		Side chain amino group of ornithine and carboxyl group of glycine (G17)
AP314		Amino group of 5-aminopentanoic acid and carboxyl group of glycine (G17)
AP317		Amino group of 4-aminobutanoic acid and carboxyl group of glycine (G17)
AP318		Amino group of 4-aminobutanoic acid and side chain carboxyl group of aspartic acid (D17)
AP319		Amino group of β-alanine (3-aminopropanoic acid) and side chain carboxyl group of glutamic acid (E17)
AP321		Amino group of 7-amino-heptanoic acid and carboxyl group of tyrosine (Y16)
AP322		Amino group of 6-aminohexanoic acid and carboxyl group of glycine (G17)

2.3.3 Panton-Valentine Leukocidin (PVL)

PVL is comprised of two subunits termed LukF-PV and LukS-PV. These components of the PVL toxin were kindly supplied by S. Knapp from the Center for Molecular Medicine (CeMM) of the Austrian Academy of Sciences. The stock solution of each subunit was stored separately in the freezer.

To generate PVL the sequence from *Staphylococcus aureus V8* (ATCC 49775) was amplified as described by Genestier et al. (2005).

2.3.4 Listeriolysin O (LLO)

LLO was kindly supplied by T. Decker from Vienna Biocenter, Department of Microbiology and Immunobiology. Production and purification are described in detail by Zwaferink et al. (2008b). The protein was stored frozen in aliquots at -80°C.

3.   RESULTS

3.1. TIP peptides

3.1.1. Structure-activity relationship

TNF-α has been shown to activate ENaC in alveolar epithelium (Fukuda et al. 2001). Therefore, synthetic peptides that mimic the lectin-like domain of TNF-α (TIP) were synthesised and evaluated for their ability to enhance the amiloride-sensitive sodium current through ENaC in A549 cells. Currents were recorded by means of the patch clamp technique in the whole-cell mode. To prove the specificity of the test compounds on the amiloride-sensitive Na^+ current, firstly, amiloride was added in control experiments to identify the registered current as the amiloride-sensitive Na^+ current. Secondly, after a control period and addition of the tested TIP peptide, amiloride was added after a steady-state effect has been reached in order to prove whether the peptide-induced increase in current is due to the amiloride-sensitive Na^+ current. In this experimental setting it could be shown that, in a similar manner to TNF-α, TIP peptides AP301, AP303, AP309, AP310, AP318 and AP319 induced an amiloride-sensitive sodium ion flux through ENaC at all tested membrane holding potentials ranging from -100 to $+100$ mV (Figure 16 and 17). At a membrane holding potential of $E_h = -100$ mV, a maximal response to TNF-α and each ENaC-activating peptide was reached at a current level of 1073 ± 15 pA, whereas TIP peptides mutant AP301, AP302, AP314, AP317, AP321 and AP322 showed no effect on ENaC at concentrations up to 480 nM.

For comparison of activity, the concentration for half maximal response (EC_{50}) was estimated at $E_h = -100$ mV for TNF-α and all tested TIP peptides. TNF-α as the reference compound increased Na^+ current with an EC_{50} of 8.2 ± 0.1 nM (n=5). The active TIP peptides showed 0.14- (TIP peptide AP303) to 0.43-fold (TIP peptide AP319) the activity of TNF-α. TIP peptide AP303 with an estimated EC_{50} of 56.0 ± 0.8 nM (n=4) increased the Na^+ current to the same extent as compound AP301 (Table 2, Figure 18). All other active TIP peptides, AP309, AP310, AP318 and AP319, were significantly (P<0.05) more effective in increasing the Na^+ current than TIP peptide AP301 (Table 2, Figure 18).
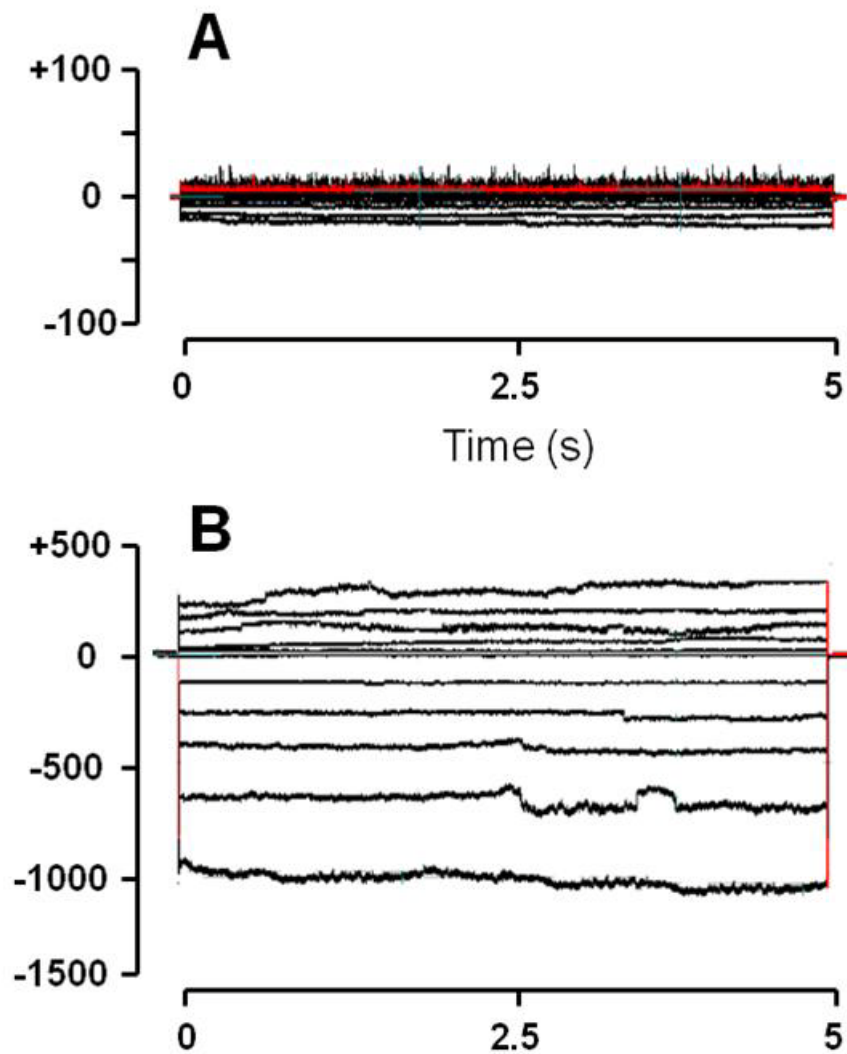
Figure 16: Effect of AP301 on ENaC.

Representative original whole-cell recordings from a cell clamped at holding potentials ranging from –100 to +100 mV (in 20 mV increments) are shown during control (A) and in presence of 120 nM AP301 (B). At this concentration the ENaC-activating effect was maximal.
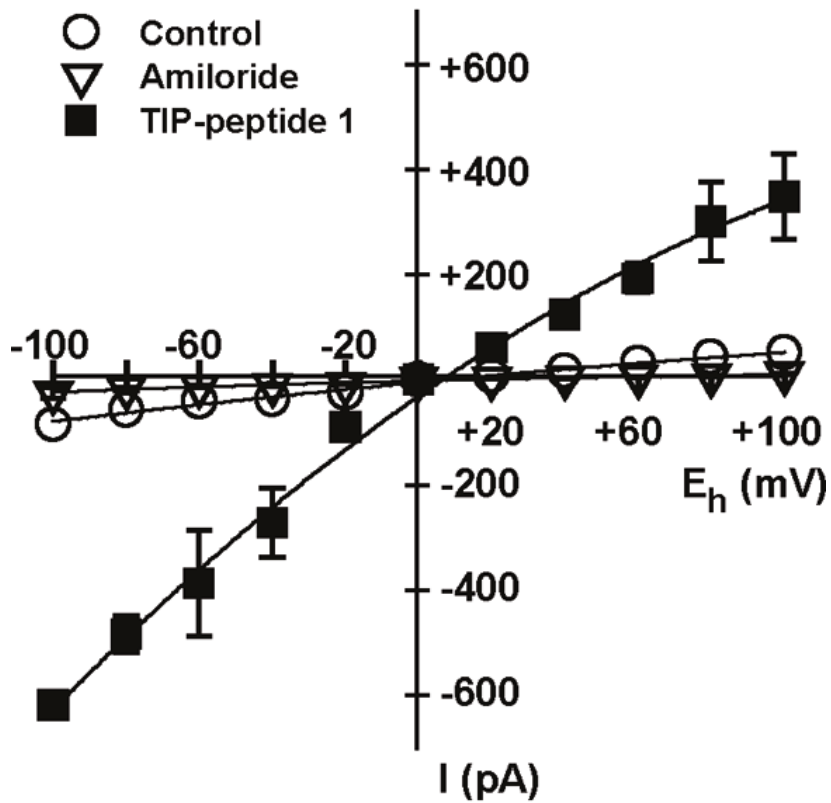
Figure 17: Effect of AP301 on current-voltage (IV) relationship.

IV-curves are illustrated for control (open circles, n=5), in presence of 60 nM AP301 (filled squares, note: concentration of AP301 is 60 nM that is the concentration close to the EC_{50}-value of AP301, n=5). Open triangles represent values obtained after addition of 10 mM amiloride, which blocks the sodium current in control (n=5) as well as in presence of AP301 (n=5). Mean values ± S.E. are given for 5 experiments.

concentration response curves
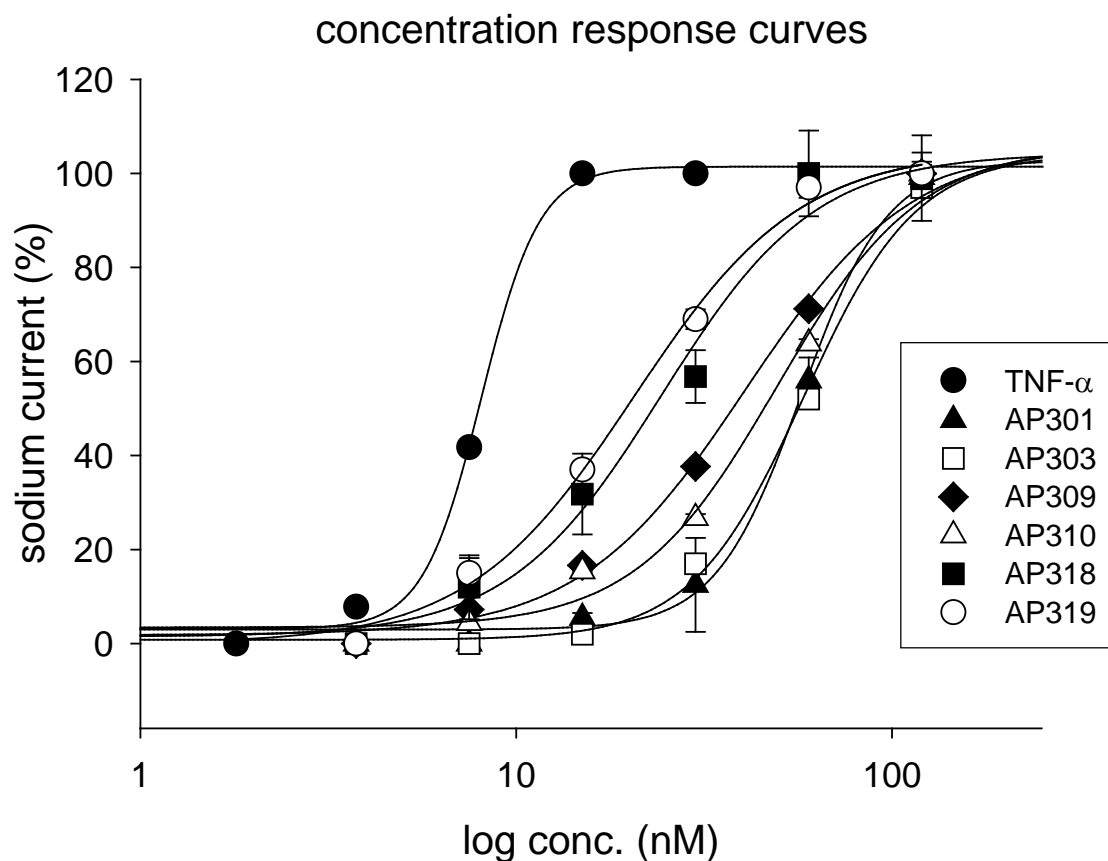
Figure 18: Concentration-response curves.

For all ENaC-activating TIP peptides a maximal effect could be observed at 120 nM. TIP peptides AP309, AP310, AP318 and AP319 were more active than reference compound AP301, but less active than TNF-α, whereas AP303 was as active as AP301. Estimated values for the Hill slope of the concentration-response curves were smaller for TIP peptides than for TNF-α and AP301, indicating attenuated steepness of the curves. Mean values ± S.E. for 3-5 experiments are given.

These data imply that either a free positively-charged N-terminal amino group on residue 1 (AP309 and AP310) or a free negatively-charged carboxyl group on residue 17 (AP318 and AP319) is essential for the ENaC-activating effect. The presence of both types of charged group on the terminal residues, as in compounds AP301 and AP303, results in an ENaC-activating effect, which is less pronounced than when either charged group is present alone.

This structure-activity relationship becomes evident, since the TIP peptides AP314, AP317, AP321 and AP322, which lack a free positively-charged N-terminal amino group on residue 1 as well as a free negatively-charged carboxyl group on residue 17, showed no effect on ENaC at concentrations up to 240 nM. TIP peptides AP302 and mutant AP301 were also ineffective.

Table 2: Potency of ENaC-activating TIP peptides.

Active test compound	EC$_{50}$ (nM)	n
TNF-α	8.2 ± 0.1	5
AP301	54.3 ± 0.8	5
AP303	56.0 ± 0.8	4
AP309	38.3 ± 1.7	3
AP310	45.5 ± 0.6	3
AP318	24.8 ± 0.5	5
AP319	19.9 ± 0.7	4

All studied TIP peptides (AP301, AP302, AP303, AP309, AP310, AP314, AP317, AP318, AP319, AP321, AP322, mutant TIP peptide) have a cyclic structure. In case of AP301, the circular form is intended to restrain the key residues known to be necessary for the ENaC-activating effect: T105, E107 and E110, in the conformation found in native human TNF-α. It is well known that circular peptides are more stable than their linear counterparts. However, cyclization is another additional step in the synthesis of TIP-peptides. Therefore, it was of interest whether the cyclic structure is essential for the ENaC activating effect. When the concentration of the linear peptide AP301 was increased until 600 nM (n=5), no effect on ENaC was observed (Figure 19), whereas subsequent addition of cyclic AP301 increased the sodium current.
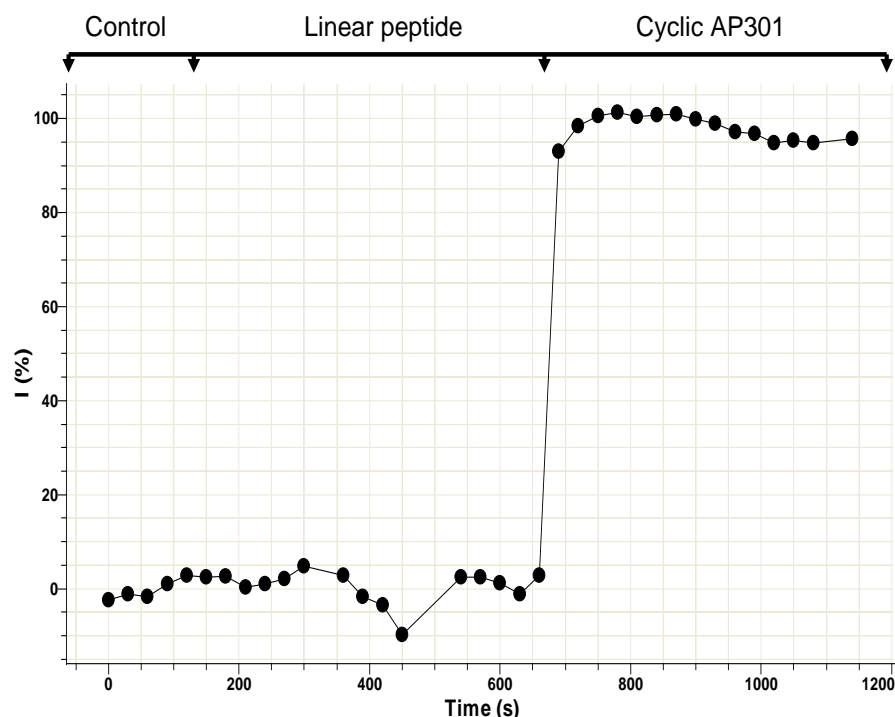
Figure 19: Effect of the linear peptide on ENaC recorded in the whole cell mode. Addition of 600 nM linear peptide did not affect the current whereas the addition of 240 nM cyclic AP301 increased Na^+ current (n=5).

3.1.2. Selectivity of ENaC-activating effect

All TIP peptides showing an activating effect were highly selective for amiloride-sensitive sodium current. The percentage increase in whole-cell current, which could be attributed to ENaC ranged between 89.6% in the case of AP319 and 99.4% for AP301 and AP309. Specifically, TIP peptides AP301, AP309 and AP310 have virtually no effect on potassium channels whereas AP303, AP318 and AP319 do have a slight effect (Table 2, Figure 20). The small current which was induced by these latter peptides, when ENaC was blocked by amiloride, could be reversed by the K^+ channel blocker TEA.

With regard to this point, it is interesting to note that AP309 and AP310 have a free positively-charged, N-terminal amino group on residue 1 and no free negatively-charged

carboxyl group on residue 17, whereas AP318 and AP319 have no free positively-charged amino group, but they do have a free negatively-charged carboxyl group on residue 17. Both AP301 and AP303 have a free amino group on residue 1, but in AP303, residue 1 is equivalent to K98 in native TNF-α, whereas in AP301 residue 1 is equivalent to P100, thus the N-terminal residues in these peptides represent structurally different parts of the native TNF-α molecule.

Table 3: Selectivity of ENaC-activating TIP peptides.

Active test compound	Selectivity		n
	ENaC (%)	Potassium current (%)	
TNF-α	93.4 ± 1.9	6.9 ± 1.8	4
AP301	99.4 ± 0.1	0.6 ± 0.1	3
AP303	93.4 ± 0.6	6.1 ± 0.9	3
AP309	99.4 ± 0.2	0.6 ± 0.1	3
AP310	98.9 ± 0.3	1.1 ± 0.3	3
AP318	91.2 ± 0.2	8.6 ± 0.1	3
AP319	89.6 ± 1.2	10.4 ± 1.1	3
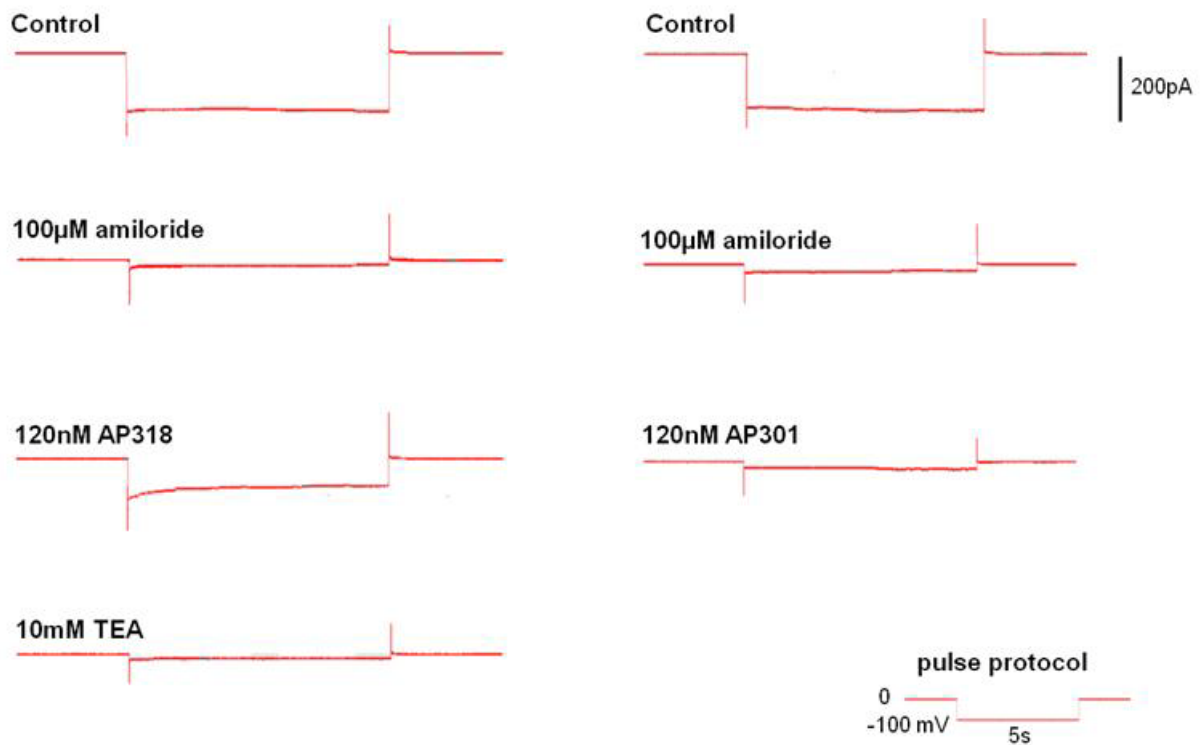
Figure 20: TEA-selective K^+ current

Current traces induced by clamping the cell membrane to a holding potential of –100 mV are presented. The original whole-cell recordings from two cells are illustrated during control, and after addition of 100 µM amiloride, which blocks the amiloride-sensitive Na^+ current through ENaC. Addition of AP301 and AP318 to the bathing solution induced virtually no (AP301, right panel) or only a small (AP318, left panel) current, respectively. This peptide-induced current was completely blocked by TEA indicating that this current is a K^+ current. The pulse protocol and calibration bar is illustrated in the inset.

3.1.3.   Activity of nebulised AP301 solution

The lead compound AP301 is being developed as an aqueous solution, which will be delivered to the patient by inhalation as an aerosol. It is therefore essential to demonstrate that AP301 retains its pharmacological effect after nebulisation. Administration of the lead compound as an aerosol by inhalation is considered the most efficient delivery route, since AP301 exerts its pharmacological effect by activating apically-located ENaC ion channels in alveolar epithelia, resulting in uptake of Na^+ ions from the alveolar fluid and subsequent reabsorption of lung oedema (Lucas et al, 1994; Fukuda et al, 2001; Elia et al, 2003; Braun et al, 2005). The ENaC activation effect of a solution of AP301 which has been introduced into the nebuliser, nebulised and reconstituted by capture ("condensation") of the aerosol particles was tested. It had to be proven that the nebulised AP301 peptide spray generated by the nebuliser retains its activity, because the nebulised form is the finally way to use with patient. The concentrations of nebulised and un-nebulised AP301 were applied in 25, 2.5, 0.5, 0.25, 0.167, 0.125, 0.1 mg/ml.

A solution of AP301 test substance containing 25 mg/ml pure AP301, which had been nebulised using the Aeroneb Solo nebuliser unit (Aerogen Ltd, Ireland) and condensed, showed the same activation effect on ENaC ion channels as the same solution of AP301 which had not been nebulised (Table 4, Figure 21).

Table 4: The data of whole cell patch clamping in A549 cells with nebulised and un-nebulised AP301 in different concentrations.

Concentration (mg/ml)	Un-nebulised AP301 I (pA) at Eh= -100mV	Nebulised AP301 I (pA) at Eh= -100mV
25	1013 ± 35	1085 ± 51
2.50	-	1056 ± 65
0.50	-	1141 ± 30
0.167	1100 ± 40	1041 ± 58
0.125	-	1028 ± 16
0.1 (corresponds to 60 nM)	589 ± 9	586 ± 22
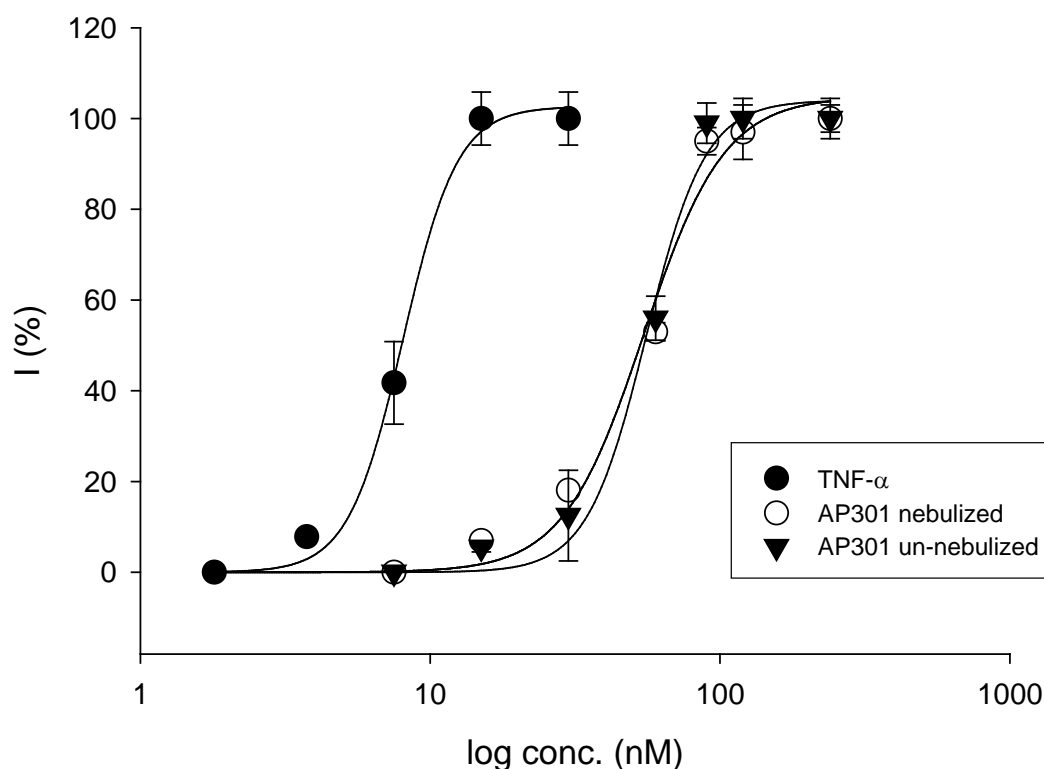
Figure 21: Dose response curves of TNF-α (filled circles), un-nebulized AP301 (filled triangles) and nebulised AP301 (open circles).

3.1.4. Effects on single epithelial sodium channel current in A549 cells

TNF-α and TIP-peptides AP301, AP303, AP309, AP310, AP318 and AP319 induced a marked, concentration-dependent increase of macroscopic Na^+ current. To study the effects on single channel current, TNF-α, AP301 and the most active TIP-peptide, AP318, were examined in the cell-attached mode of the patch clamp technique. Experiments were performed at holding potentials of ±60 mV. For single Na^+ channel measurements, in all experiments 10 mM TEA was added to the pipette solution to block the potassium channel, because otherwise K^+ current with its large amplitude would cover the Na^+ current. TNF-α, AP301 and AP318 were added at respective EC_{50} concentrations to the pipette solution. Na^+ current with a conductivity of 9.4 ± 0.1 pS (n=18) was observed. This parameter was not significantly changed by TNF-α (9.8 ± 0.1 pS, n=10), AP301 (9.7 ± 0.1 pS, n=7) and AP318 (9.6 ± 0.3 pS, n=9). When amiloride (100 µM) was included in the pipette solution, no

channel activity was seen (n=3). The amplitude and open probability (Po) were calculated from all event histograms. In the cell-attached mode, TNF-α, AP301 and AP318 significantly increased Po of single channels without affecting their amplitude (Table 5 and 6, Figure 22 and 23).
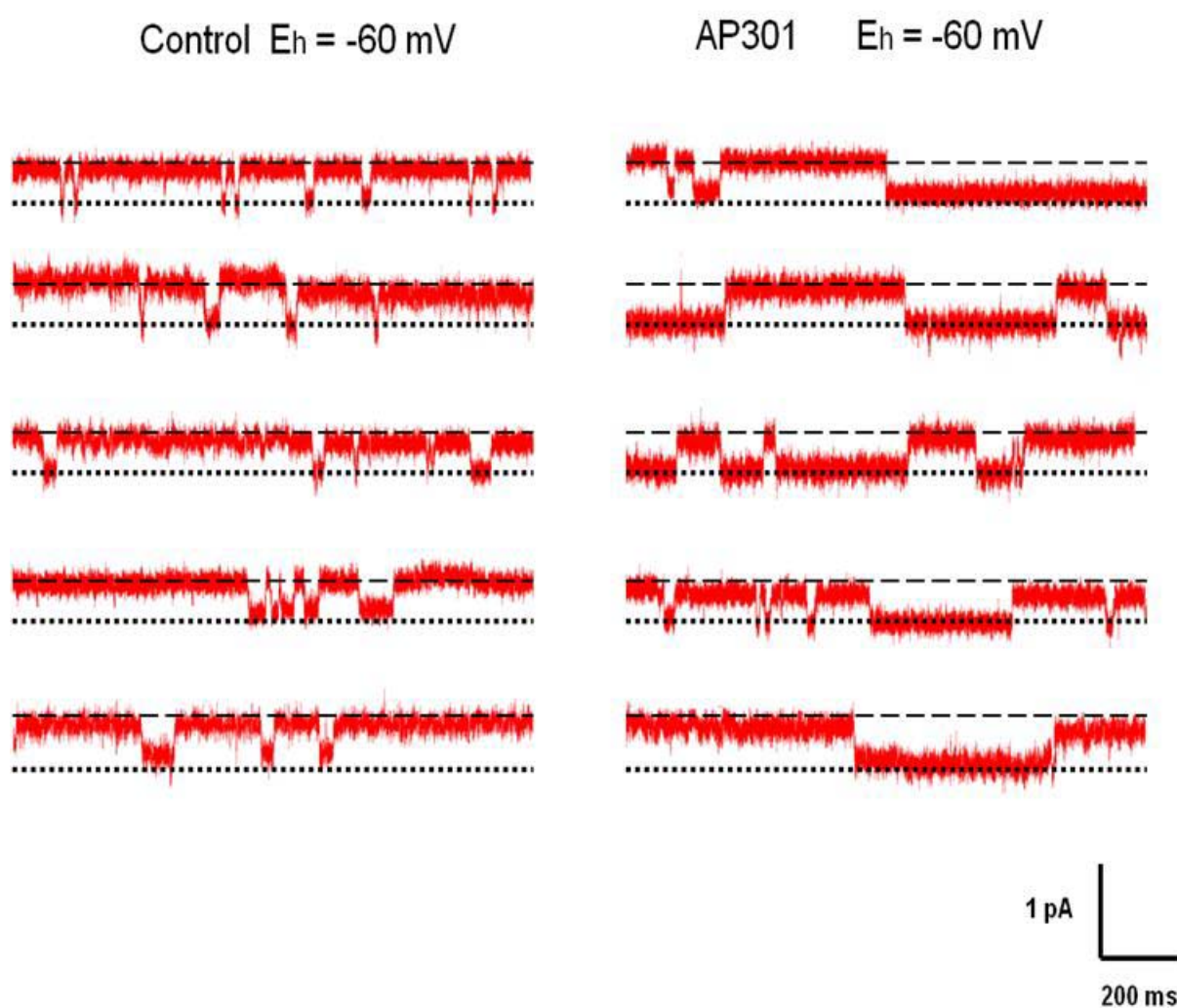
Figure 22: Original recordings from a cell-attached patch at a holding potential of -60 mV during control (left panel) and in presence of AP301 (right panel).

Dashed lines indicate the closed state of the channel, and dotted lines indicate the open state (downward deflections). The recordings clearly indicate the longer duration of single channel openings with AP301.

Table 5: Effect of TNF-α, AP301 and AP318 on single channel kinetics at $E_h = -60$ mV.

	Control	TNF-α	AP301	AP318
P_o	0.37 ± 0.03 n=5	0.77 ± 0.08*** n=4	0.69 ± 0.05*** n=3	0.78 ± 0.05*** n=3
Mean open time (ms)	2.2 ± 0.9 n=5	23.5 ± 4.5*** n=4	24.3 ± 4.8*** n=3	26.5 ± 4.3*** n=4
Number of bursts	993 ± 105 n=5	1274 ± 259* n=4	2365 ± 419*** n=3	1966 ± 402** n=4
Events in burst	7.2 ± 1.7 n=5	46.3 ± 4.3*** n=4	32.3 ± 5.0*** n=3	16.1 ± 4.9** n=4
Duration of burst (ms)	5.7 ± 1.3 n=5	210.6 ± 47.8*** n=4	47.9 ± 1.4*** n=3	42.2 ± 12.5*** n=4
Mean intra-burst interval (ms)	0.29 ± 0.03 n=5	0.60 ± 0.1** n=4	0.63 ± 0.03*** n=3	0.60± 0.12** n=4

* P<0.05, ** P<0.01, *** P<0.001

Table 6: Effect of TNF-α, AP301 and AP318 on single channel kinetics at $E_h = +60$ mV.

	Control	TNF-α	AP301	AP318
P_o	0.09 ± 0.02 n=13	0.49 ± 0.03*** n=6	0.40 ± 0.01*** n=4	0.42 ± 0.03*** n=6
Mean open time	0.9 ± 0.1 n=4	3.4 ± 0.3*** n=6	5.5 ± 1.1*** n=4	4.1 ± 1.2*** n=6
Number of bursts	2300 ± 214 n=4	4179 ± 320*** n=6	5477 ± 517*** n=4	5851 ± 900*** n=6
Events in burst	3.4 ± 1.2 n=4	23.3 ± 5.5*** n=6	6.6 ± 0.6** n=4	8.7 ± 1.3** n=6
Duration of burst (ms)	1.6 ± 0.5 n=4	33.9 ± 12.6*** n=6	7.5 ± 1.7*** n=4	7.5 ± 1.1*** n=6
Mean intra-burst interval (ms)	0.28 ± 0.03 n=4	0.58 ± 0.05*** n=6	0.57 ± 0.01*** n=4	0.48 ± 0.02*** n=6

Figure 23: Original recordings from cell-attached patches at holding potentials of +60 and -60 mV during the respective controls and in presence of the reference peptide TNF-α, and the test peptides AP301 and AP318.

"C" indicates the closed state of the channel, and "O" indicates the open state. The recordings demonstrate the increase in open times caused by TNF-α and the TIP-peptides.

Besides mean open times, also the number of bursts, and the duration of bursts were significantly increased by TNF-α as well as AP301 and AP318 (Table 5 and 6, Figure 24). In Figure 23 typical recordings are shown which demonstrate the increase in burst duration. Accordingly, effects on macroscopic Na^+ current were confirmed by single channel current measurements.
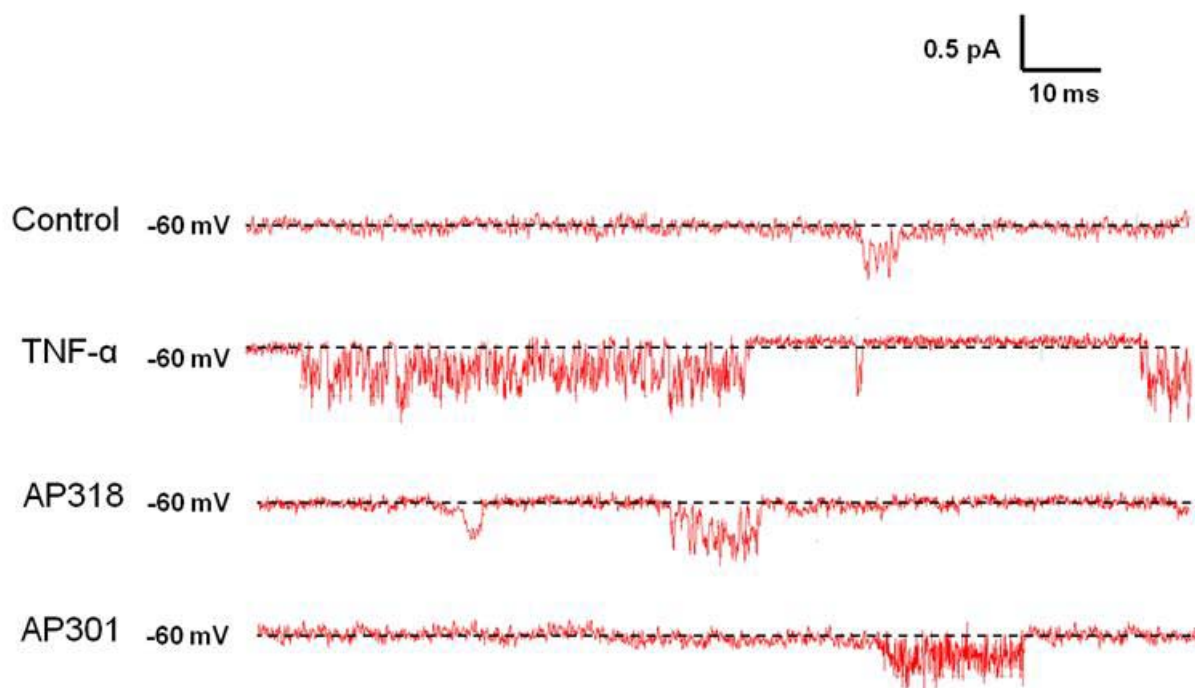
Figure 24: Typical single Na^+ channel current recordings from cell-attached patches of A549 cells demonstrating increased burst duration by AP301 and AP318, and especially TNF-α.

TEA-sensitive K^+ current was measured with a conductivity of 261 ± 20 pS (n=6). This estimated conductance is very close to the value of 242 ± 33 pS reported for the TEA-sensitive Ca^{2+}-activated K^+ channel in A549 cells (Ridge et al. 1997). In Figure 25 typical single channel K^+ currents recorded from cell-attached patches at a holding potential of -60 mV are shown during control and in presence of TNF-α and AP301. In total single channel parameters were not changed significantly by TNF-α and AP301. This confirms the data obtained with whole-cell recordings.
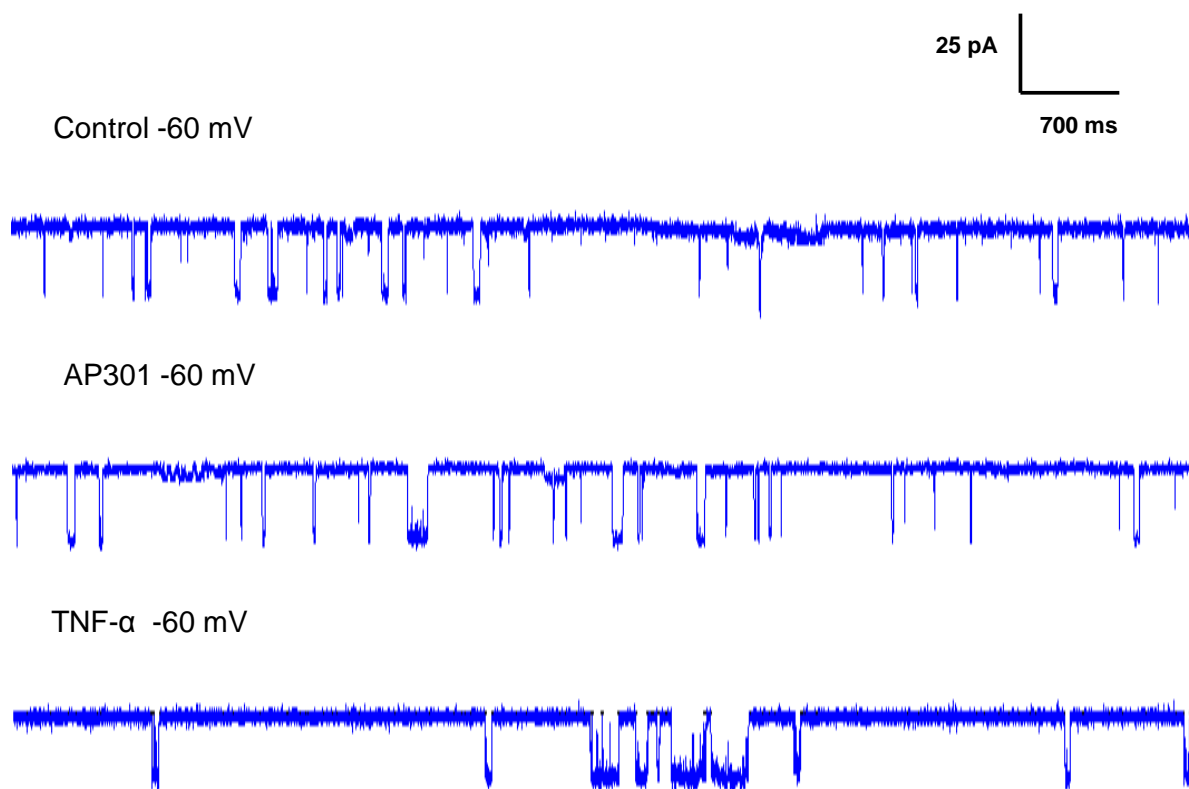
Figure 25: Single channel K$^+$ currents in A549 cells at a holding potential of -60 mV during control and in presence of TNF-α and AP301 are illustrated. Downward deflections indicate single channel openings.

3.1.5. Effect of TNF-α and TIP peptides on ENaC after deglycosylation

A cyclic disulfide heptadecapeptide, TIP17ox, derived from the lectin-like 17-amino acid domain of human TNF-*α* was demonstrated to bind specifically to *N,N*-diacetylchitobiose, a disaccharide present in many glycan structures of glycoproteins. Approximately 30% of the mass of the voltage-dependent sodium channel is carbohydrate, present as glycoconjugate chains, mostly composed of *N*-acetylhexosamines and sialic acid. ESI-FTICR-MS was used as an efficient tool for the direct molecular characterisation of TIP peptide–carbohydrate complexes. The specific binding of the TNF-TIP domain to chitobiose and other carbohydrate

motifs in glycoproteins may explain the high proteolytic stability of these peptides in biological fluids (Marquardt et al. 2007).

To study a theoretical interaction of the TIP-peptides with sugar moieties on the cell membrane, deglycosylation of the A549 cell membrane was performed with PNGase F. Cells were incubated with the enzyme for 1-5 minutes or the enzyme was added to the pipette solution when studying effects on single channel activity. Currents were recorded with the patch clamp method in the whole-cell and cell-attached mode.

Whole cell current was recorded at E_h= -100mV from cells without any pre-treatment during control and in presence of TNF-α, AP301 and AP318 as well as after treatment with PGNase. Test compounds were added at concentrations of 120 and 240 nM to ensure a maximal effect. It could be clearly demonstrated that the ENaC-activating effect of TNF-α and the two studied TIP-peptides got lost when cells were pre-treated with PGNase (Table 7).

Table 7: Effect of deglycosylation on TNF-α-, AP301- and AP318-induced ENaC activation. Whole cell currents were recorded from A549 cells at E_h= -100 mV. The peptide concentrations were 120 and 240 nM.

Test compound	Control	Pre-treatment with PNGase F	untreated cells
TNF-α		24.0 ± 5.9 pA n=3	
AP301	25.4 ± 6.1 pA n= 10	19.6 ± 2.9 pA n=3	1073.3 ± 15.1 pA n= 10
AP318		23.1 ± 5.4 pA n=3	

In single channel studies, this effect of deglycosylation could be verified. In untreated cell membranes P_O was significantly increased by TNF-α and TIP-peptides, whereas after deglycosylation no effect of TIP peptides on P_O could be observed (Table 8). Single channel conductivity was not changed by TIP-peptides, indicating an interference of sugar moieties of the cell membrane with binding of TIP-peptides.

Table 8: Open probability and single channel conductivity (Con.) of ENaC at E_h= -60 mV in untreated and deglycosylated A549 cell membranes.

Test compound	Control		Pre-treatment with PNGase F		untreated cells	
	P_O	$Con.(pS)$	P_O	$Con.(pS)$	P_O	$Con.(pS)$
TNF-α	0.09 ± 0.02 n=18	9.6 ± 0.2 n=18	0.10 ± 0.03 n=4	9.6 ± 0.4 n=10	0.77 ± 0.08 n=4	9.8 ± 0.1 n=10
AP301			0.09 ± 0.02 n=3		0.69 ± 0.05 n=3	9.7 ± 0.1 n=7
AP318			0.10 ± 0.02 n=3		0.78 ± 0.05 n=3	9.6 ± 0.3 n=9

3.2. Pore-forming bacterial toxins

3.2.1. Pore-forming activity of PVL in macrophages

Macrophages were treated with different concentrations of either subunit of rPVL (LukS or LukF) or with an equimolar combination of both subunits. Pore-forming activity was measured with the patch clamp technique in the whole cell recording mode. A concentration-dependent increase of current was observed (Figure 26 and 27).
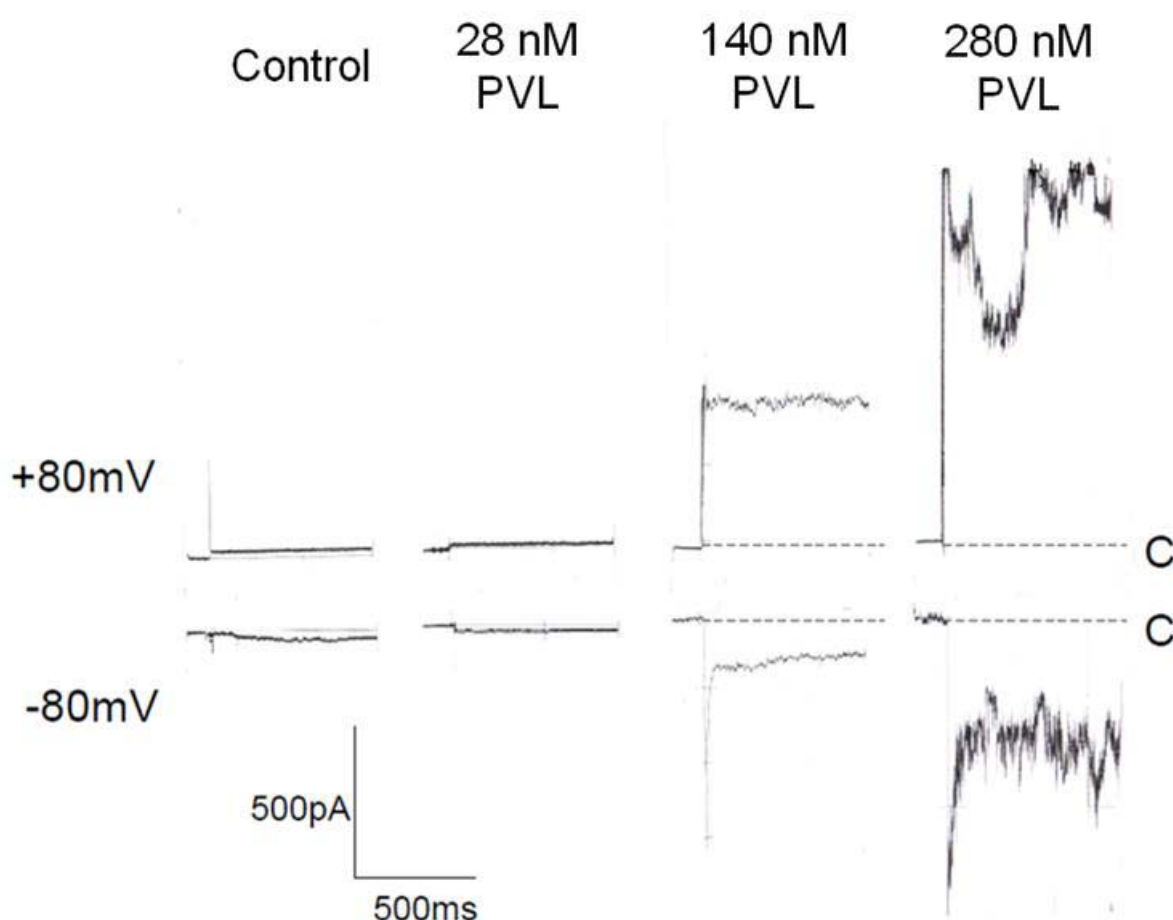
Figure 26: Concentration-dependent effect of PVL.

Original whole-cell recordings are presented at holding potentials of +80 mV (upper row) and –80 mV (lower row). The closed state of the channels is indicated by the dashed lines and is marked with "C". Up- and downward deflections indicate channel openings in the presence of 28, 140 and 280 nM PVL.
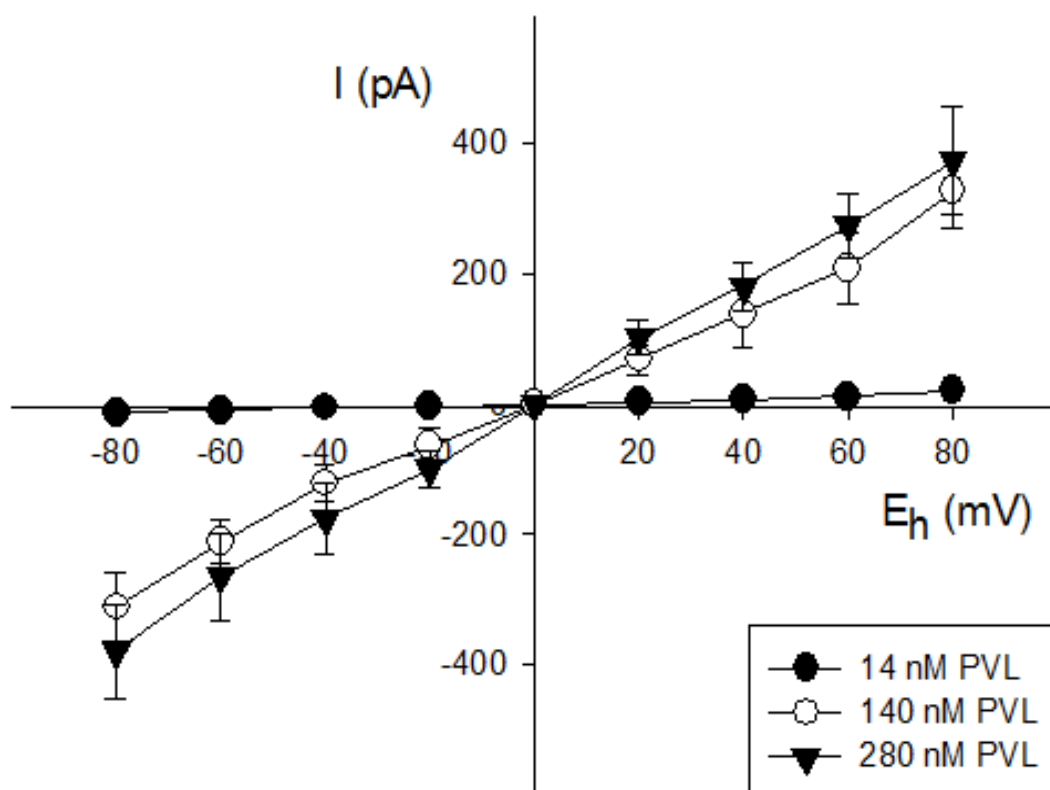
Figure 27: Current-voltage relation of PVL-induced currents at different concentrations and holding potentials ranging from -80 mV to +80 mV.

No pore formation was observed following treatment of macrophages with only one of the subunits of the toxin (Figure 28), but multiple ion channels openings were observed after a 1 min treatment with both subunits at concentrations of 140 (Figure 25 and 26) and 280 nM (Figure 26, 27 and 28). These data are in line with previous observations, showing that both subunits of rPVL in an equimolar ratio are required to create a pore. However, as we found in our studies it has to be mentioned that LukF and LukS only induced pores when administered concomitantly, but not when applied consecutively.
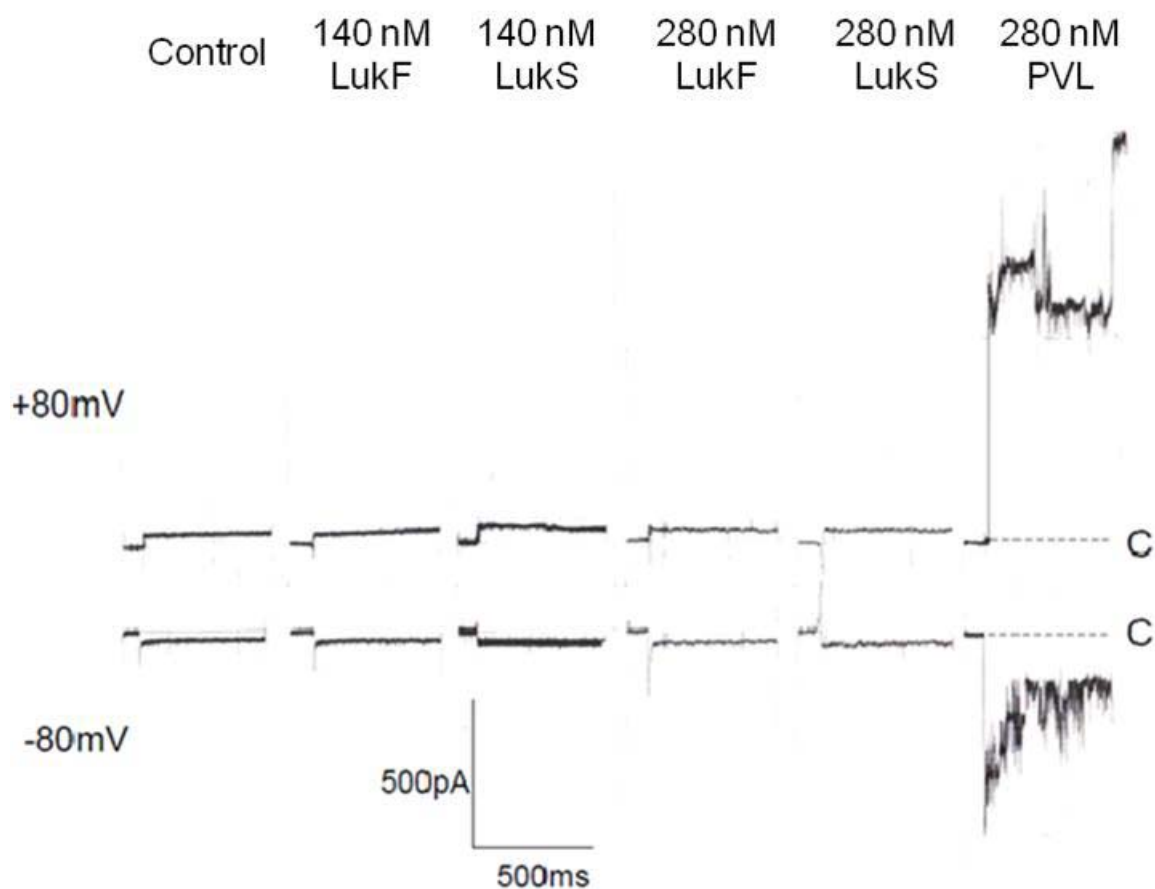
Figure 28: Original whole-cell recordings are presented at holding potentials of +80 mV (upper row) and –80 mV (lower row). The closed state of the channels is indicated by the dashed lines and is marked with "C". Up- and downward deflections indicate channel openings. In the presence of 140 nM LukF, 140 nM LukS, 280 nM LukF and 280 nM LukS no channel openings were observed, while in the presence of both components (140 nM LukF plus 140 nM LukS) multiple channel openings occurred.

Furthermore, in experiments performed in the inside-out configuration of the patch clamp technique, it became obvious that PVL can create pores independent on the site of application, i.e. PVL acts from the extra- as well as from the intracellular side. The PVL-induced pores were not ion selective as they conducted Na^+, K^+ (Figure 29) and Ca^{2+} ions with a single channel conductivity of 207 pS (Na^+), 257 pS (K^+) and 186 pS (Ca^{2+}), respectively.

20 pA

50 ms
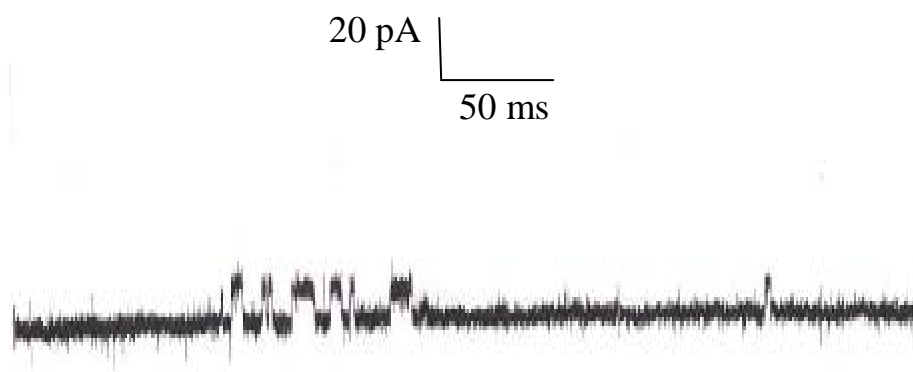
Figure 29: Original recording at a holding potential of +80 mV from an inside-out patch of a macrophage with K^+ as the charge carrier. PVL was applied to the bathing solution at a concentration of 140 PVL. Upward deflections indicate channel openings.

3.2.2. Effect of LLO on membrane permeability of macrophages in presence of IFN-β

Experiments were performed on macrophages with the perforated patch clamp technique in the whole cell configuration. After a control period of 5 min without any electrical activity, LLO was added at concentrations of 2.5 or 5.0 µl/ml to the external solution. About 1 min after addition of the bacterial toxin, single channel currents could be observed. The pore formation progressed rapidly and multiple openings occurred. At least three elementary pore current amplitudes of 16.5 ± 1.5 pA, 32.0 ± 2.0 pA and 64.1 ± 6.2 pA were measured at a holding potential of –30 mV; the latter are multiples of the smallest pore current amplitude. Pore openings were rare and occurred in bursts. At a concentration of 2.5 µ/ml, LLO caused channel openings only of small amplitude (n=3). The current was markedly increased in IFN-β pre-treated macrophages (n=3) (Figure 30). Multiple openings were observed, which never occurred in absence of IFN-β in otherwise same experimental conditions. At 5.0 µl/ml LLO (n=2), obviously more pores were incorporated into the cell membrane as multiple openings were frequently seen, and again membrane current was larger in IFN-β pre-treated cells (n=3). After about 10 min the frequency of pore openings slowly decreased.

control   control

C ━━━━━━━━━━━━━━━━━━━━━━━━━━   ━━━━━━━━━━━━━━━━━━━━━━━━

2.5 µg/ml LLO   5.0 µg/ml LLO

C ━━━━━━━━━━━━━━━━━━━━━━━━━━   ━━━━━━━━━━━━━━━━━━━━━━━━

2.5 µg/ml LLO + IFN-β   5.0 µg/ml LLO + IFN-β

C ━━━━━━━━━━━━━━━━━━━━━━━━━━   ━━━━━━━━━━━━━━━━━━━━━━━━
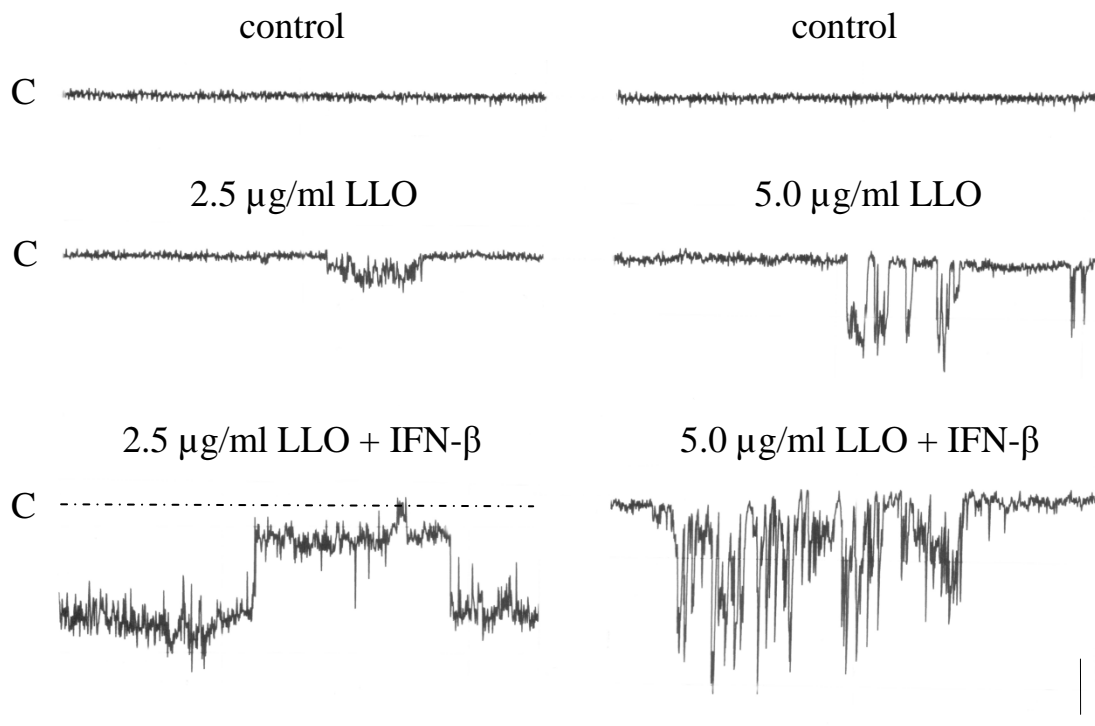
Figure 30: Effect of IFN-β on pore forming activity of LLO.

Original recordings at a holding potential of –30 mV are shown during control (upper traces), in presence of LLO (middle traces) and with LLO in IFN-β pre-treated macrophages (lower traces). Downward deflections represent channel openings, and "C" indicates the closed state of the pore. Single channel and multiple openings are seen in the recording of the IFN-β pre-treated cells. The horizontal and vertical calibration bars indicate 1 s and 25 pA, respectively.

3.3. Electrophysiological effect of AP301 in presence of PVL in A549 cells

Recently it was demonstrated that the human TIP-peptide blunts LLO-induced hyper-permeability *in vitro* (Xiong et al. 2010). Thus, we aimed to study the effect of AP301 on PVL-induced current. As described in the Introduction and in section 3.6., PVL is a β-barrel pore forming toxin. This pore-forming effect was not only observed in macrophages but also in other cells such as the A549 cell line as a model of alveoli type II cells.

280 nM PVL (50 µg/ml LukF-PV plus 50 µg/ml LukS-PV) was added to the standard bath solution. The current was recorded in whole cell patch clamp mode at a holding potential of -100 mV. After addition of 240 nM AP301 the current further increased (Figure 31). These results show that AP301 does not interfere with the current-inducing effect of PVL. It is suggested that signaling pathways might be the targets of TIP-peptides in presence of PVL as previously described for LLO.
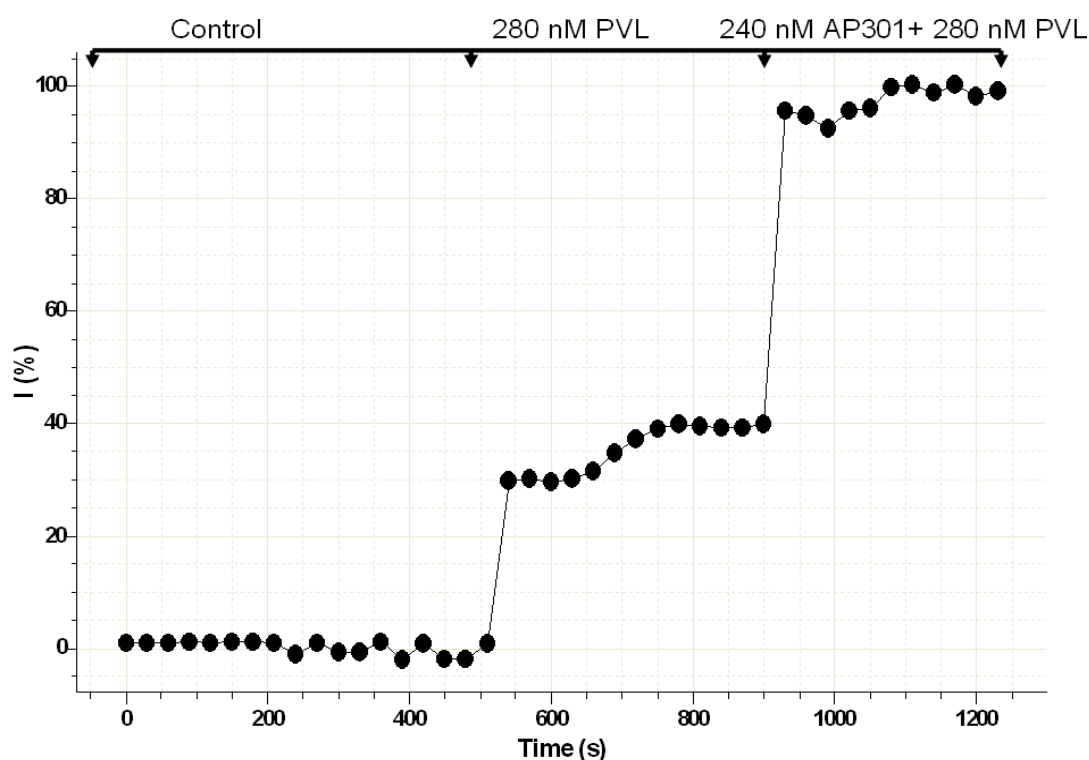
Figure 31: Effect of AP301 on PVL-induced current in A549 cells (n=11).

4. DISCUSSION

Both alveolar type I (ATI) cells (which cover at least 95% of the internal surface area of the lung) and type II (ATII) cells (which cover about 2-5% of the internal surface area of the lung) have several different sodium-permeable channels in their apical membranes that play a role in normal lung physiology and pathophysiology (Eaton et al. 2009). ENaC appears to be expressed in both ATI and ATII cells (Guidot et al. 2006). The channel plays a prominent role in sodium uptake from alveolar fluid, and its involvement in alveolar clearance in normal and diseased lungs has been widely demonstrated (Lazrak et al. 2000, Matthay et al. 2002, Sartori and Matthay 2002, Berthiaume and Matthay 2007). K^+ channels are also expressed in ATI and ATII cells (Guidot et al. 2006, Leroy et al. 2004), and they can participate in transepithelial Na^+ and Cl^- exchange (Leroy et al. 2004), as well as alveolar fluid clearance (Sakuma et al. 1998). Apart from ENaC, several other ion channels such as acid-sensing ion channels (ASIC) or ion pumps and transporters like the sodium-calcium exchanger, Na^+/K^+-ATPase or the $Na^+/K^+/Cl^-$ co-transporter contribute to the sodium homeostasis of a cell. Previous work showed an effect of TNF-α on ENaC (Fukuda et al. 2001). ENaC is located at the apical side of the cell, and in addition there is evidence that TIP peptides rather work from the apical than basolateral side (Hamacher et al. 2010). A549 cells express ENaC (Lazrak et al. 2000), potassium channels (Karle et al. 2004) and a cyclic nucleotide-gated ion channel (Xu et al. 1999), but no co-expression of ASIC and ENaC in the A549 cell line has been reported. Therefore, based on these previous findings, A549 cells were chosen for the structure-activity relationship studies on ENaC. However, TIP peptides could affect directly or indirectly also other channels than ENaC and also ion pumps and transporters, which are responsible for sodium homeostasis.

TNF-α has been shown to activate amiloride-sensitive sodium currents in alveolar epithelium (Fukuda et al. 2001). In accordance, several *in situ, ex vivo* and *in vivo* studies have indicated that the lectin-like domain of TNF-α promotes amiloride-sensitive oedema reabsorption and alveolar fluid clearance (Berthiaume 2003, Elia et al. 2003, Braun et al. 2005, Vadasz et al. 2008, Lucas et al. 2009, Hamacher et al. 2010). The seemingly contradictory roles of TNF-α in pulmonary oedema can be explained by the spatial separation of the different functions of TNF-α, with its lectin-like domain which activates, and its receptor-binding sites which inhibit oedema reabsorption (Dagenais et al. 2004, Bao et al. 2007), being located in different domains in the native molecule (Hribar et al. 1999, Braun et al. 2005, Vadasz et al. 2008,

Lucas et al. 2009, Hamacher et al. 2010). Native murine TNF-α (mTNF) has been shown to produce a similar amiloride-sensitive increase in ALC in mice expressing TNF receptors as in mice genetically deficient for the TNF receptors, indicating a TNF receptor-independent mechanism for amiloride sensitive ALC (Elia et al. 2003). A mutant mouse TNF-α with amino acid changes T104A, E106A and E109A in the lectin-like domain, has no effect on Na^+ uptake in flooded rat lungs *in situ*, unlike the wild type mTNF, which increases uptake (Elia et al. 2003). Furthermore, wild-type mTNF, but not mutant, stimulates the amiloride-sensitive Na^+ uptake in A549 cells *in vitro* (Fukuda et al. 2001). The mouse TIP peptide also has been shown to improve alveolar fluid balance in injured isolated rabbit lungs (Vadasz et al. 2008). More recently it has been demonstrated that human TIP peptide improved rat lung function after transplantation, reducing ROS generation and neutrophil infiltration (Hamacher et al. 2010). The latter study also provided evidence for the role of ENaC as the primary site of action of the TIP peptide in monolayers of rat type II alveolar epithelial cells, as the peptide activated transepithelial current only when introduced to the apical side of the cells (Hamacher et al. 2010). Taken together, these observations indicate that the receptor-binding sites of TNF-α inhibit, whereas its lectin-like domain activates oedema reabsorption and support a therapeutic role for TIP peptides in treatment of pulmonary oedema and ALI/ARDS.

4.1. Structure-activity relationship of TIP peptides

Native TNF-α is a homotrimer with the lectin-like domain of each subunit (in human TNF-α the sequence of amino acid residues C101 to E116) located close together at the tip of the structure, whereas the TNF receptor-binding sites are located in the basolateral regions of the molecule. Initially characterised for its trypanolytic effect (Lucas et al. 1994), the lectin-like domain of TNF-α has been shown to activate amiloride-sensitive Na^+ uptake in lung microvascular endothelial cells (Hribar et al. 1999) and in the alveolar epithelial cell line A549 (Fukuda et al. 2001). Therefore, synthetic peptides that mimic the lectin-like domain of TNF-α were synthesized. Replacement of C101 by a glycine residue (G2) and addition of N-terminal (C1) and C-terminal cysteine (C17) residues, linked by a disulphide bridge, resulted in the 17-residue cyclic peptide, AP301. The disulphide bond in analogue AP301 may be susceptible to reduction and scission leading to complications in medical use. Therefore, the focus of the new peptide design described in the thesis was replacement of the disulphide bridge of the original TIP analogue, AP301, with other molecular arrangements. The amino acid residues T105, E107 and E110 of human TNF-α corresponding to T6, E8 and E11 of

AP301, were shown to be essential for the ENaC-activating effect of TNF-α and the analogue AP301 peptide (Lucas et al. 1994, Hribar et al. 1999). From the TIP-domain of TNF-α, a series of synthetic TIP peptides, AP302, AP303, AP309, AP310, AP314, AP317, AP318, AP319, AP321, AP322 as well as cyclic, linear and mutant AP301 was derived.

A comparison of the ENaC-activating effect of all the TIP peptides allows tentative conclusions to be drawn regarding the influence of three main structural features of the TIP-domain and AP301 on ENaC. These features are firstly, the T105, E107, E110 triad of residues at the tip of the TNF-α molecule previously shown to be necessary for the trypanolytic, chitobiose-binding and ENaC-activating effects of TNF-α and AP301 (Lucas et al. 1994, Hribar et al. 1999, Fukuda et al. 2001, Marquart et al. 2007, Hamacher et al. 2010), secondly, a hydrophobic region introduced by P113 and bulky, hydrophobic side chains of adjacent residues W114 and Y115, and thirdly, the presence of either a positively-charged N-terminal amino group, or a negatively-charged C-terminal carboxyl group or both of these. In addition, it has been demonstrated that only the cyclic TIP peptide is active.

The importance of residues T105, E107 and E110 (corresponding to T6, E8 and E11 in AP301) is substantiated in the present study as the mutant TIP peptide, in which these residues are replaced by alanine, has no effect on the sodium current in A549 cells, whereas AP301 does have an effect ($EC_{50} = 54.3 \pm 0.8$ nM). All novel peptides contain T6, E8 and E11, which have been shown to be essential for the ENaC-activating effect of AP301. The inactive TIP peptide AP302 lacks residues equivalent to P113, W114 and Y115 of human TNF-α, and therefore the bulky hydrophobic region of AP301. Furthermore, studying the ENaC-activating effect of these TIP peptides, it became obvious that a free positively-charged N-terminal amino group on residue 1 and/or a free negatively-charged carboxyl group on residue 17 is essential for activity. The most active peptides have either a free positively-charged amino group at the N-terminal in the position of residue 1 – this is the case for AP309 and AP310 – or they have a free negatively-charged carboxyl group at the C-terminal in the position of residue 17, as is the case for AP318 and AP319. TIP peptides which lack a free positively-charged N-terminal amino group on residue 1 as well as a free negatively-charged carboxyl group on residue 17 (AP314, AP317, AP321, AP322), did not affect ENaC. The importance of the charged groups in the linker part of the peptides for activity can be better appreciated by comparison of the activity of pairs of peptides differing only in the presence or absence of a charged group on the linker portion of the molecule. Specifically, peptide AP309 and peptide AP322 differ solely in that AP309 has a charged amino group on residue 1. AP309 has an EC_{50} of 38.3 nM, whereas AP322 is inactive. Peptide AP310 and peptide

AP314 also differ solely in the presence of a charged amino group on residue 1 in AP310 and its absence in AP314. AP310 has an EC_{50} of 45.4 nM, whereas AP314 is inactive. Similar comparison concerning the presence of a free carboxyl group show that peptide AP318, which has a free carboxyl group on residue 17, has an EC_{50} of 24.8 nM, whereas AP317, which lacks a carboxyl group is inactive. TIP peptides AP301 and AP303, which are approximately identical in their ability to activate amiloride-sensitive Na^+ current, (EC_{50} of 54.3 ± 0.8 and 56.0 ± 0.8 nM, respectively), each have both a positively-charged, N-terminal amino group and a negatively-charged, C-terminal carboxyl group. Therefore, it seems that the presence of charge, positive on the N-terminal residue 1 or negative on the C-terminal residue 17 (or 19 in the case of AP303) is essential for the ENaC-activating effect of the TIP peptides. All active TIP peptides were highly selective for ENaC with a tendency towards less selectivity in molecules without a free positively-charged N-terminal amino group.

It is well know that cyclic peptides are more stable than their linear counterparts, and the fact that the linear peptide was inactive seems to indicate that the structural arrangement of the residues is critical for the ENaC-activating effect. Furthermore, we demonstrated that a solution of AP301, which has been nebulized, retains the ENaC activating effect of AP301. Therefore, delivery of AP301 as an aerosol by inhalation to the patient will have no detrimental effect on the pharmacological activity of AP301.

4.2. Mechanism of action on ENaC

Effects on macroscopic Na^+ current were confirmed by single channel current measurements. Besides open probability, mean open times, number of bursts, and duration of bursts were increased by TNF-α as well as AP301 and AP318, resulting in an increased macroscopic current. Single channel conductivity of 9.4 ± 0.1 pS was not changed by the test compounds. TEA-sensitive K^+ current was measured with a conductivity of 261 ± 20 pS (n=6). This estimated conductance is very close to the value of 242 ± 33 pS reported for the TEA-sensitive Ca^{2+}-activated K^+ channel in A549 cells (Ridge et al. 1997). Single K^+ channel parameters were not changed significantly by TNF-α and AP301, which confirms the data obtained with whole-cell recordings.

The binding site for TIP peptides is unidentified, however, patch clamp experiments gave evidence for an extracellularly located site since the TIP peptides acted only when applied to the bathing solution in whole-cell experiments or to the pipette in the inside-out configuration. A cyclic disulfide heptadecapeptide (TIP17ox) derived from the lectin-like 17-amino acid domain of human TNF-α (100–116) was demonstrated to bind specifically to

N,*N*-diacetylchitobiose, a disaccharide present in many glycan structures of glycoproteins (Marquardt et al. 2007). The specific binding of the TNF-TIP domain to chitobiose and other carbohydrate motifs in glycoproteins may explain the high proteolytic stability of these peptides in biological fluids. Although the TIP domain forms a loop structure in the native TNF-α protein, the authors showed by high-resolution ESI-FTICR mass spectrometry that a homologous linear heptadecapeptide (TIP17rd) binds with comparable affinity to chitobiose, suggesting that cyclisation is not essential for carbohydrate binding. This is in contrast to our findings as the linear form of the lead compound AP301 did not show any activating effect on ENaC. To study a theoretical interaction of the TIP peptides with sugar moieties on the cellular membrane, deglycosylation of the A549 cell membrane was performed with PNGase F. Previous studies on deglycosylated channels have been performed on voltage-gated sodium channels of *Electrophorus electricus*, which have approximately 30% carbohydrates. After enzymatic deglycosylation no net change in protein secondary structure from the deglycosylation procedure was observed. Cronin et al. (2005) demonstrated that the sugars of the voltage-gated sodium channels are not essential for functional or structural integrity, but they do appear to have a modulating effect on the conductance properties of these channels. However, in our experiments we could not find any effect on conductivity of epithelial sodium channels after deglycosylation. The ENaC-activating effect, however, got lost in deglycosylated cells as demonstrated with patch clamp experiments in the whole-cell and inside-out configuration. These data imply a role of sugar moieties on the cell surface for the binding of TIP peptides to the cellular membrane.

4.3. *Pore-forming bacterial toxins and pneumonal oedema*

Listeriosis can lead to potentially lethal pulmonary complications in newborns and immune compromised patients, characterized by extensive permeability oedema. The Listeria-toxin LLO induces a dose-dependent hyperpermeability in monolayers of human lung microvascular endothelial cells *in vitro*. Zwaferink et al. (2008b) showed that IFN-β can increase the damage and death caused when macrophages are exposed to LLO. IFN-β is primarily associated with a protective response to viral infection, but its important role in other pathological situations, such as tumor immunity and bacterial infection, is becoming more apparent. Treatment of macrophages with IFN-β increased the ability of sublytic LLO concentrations to cause transient permeability of the plasma membrane. This effect pertains directly to the extent of pore formation at the plasma membrane. We could show that pre-treatment of macrophages with IFN-β critically increased the extent of pore formation by

LLO as well as the rate of cell death. At higher LLO concentrations, IFN-β enhanced the complete breakdown of membrane integrity and cell death. This activity of IFN-β required Stat1. Perturbation of the plasma membrane by LLO resulted in activation of the p38MAPK pathway. IFN-β pretreatment enhanced LLO-mediated signaling through this pathway, consistent with its ability to increase membrane damage. p38MAPK activation in response to LLO was independent of TLR4, a putative LLO receptor, and inhibition of p38MAPK neither enhanced nor prevented LLO-induced death. IFN-β caused cells to express increased amounts of caspase 1 and to produce a detectable caspase 1 cleavage product after LLO treatment. Contrasting previous reports (Nelson et al. 1999, Bantel et al. 2001) with another pore-forming toxin, this pathway did not aid cell survival as caspase1-deficient cells were equally sensitive to lysis by LLO. Key lipogenesis enzymes were suppressed in IFN-β-treated cells, which may exacerbate the membrane damage caused by LLO. More detailed studies of events surrounding pore formation and repair will be needed to delineate how these processes are affected by IFN-β. The inhibitory effect of IFN-β on lipogenesis pathways may prove important. There are two possibilities for the action of IFN-I on LLO. Given that binding and pore formation by LLO is dependent on membrane composition, it is conceivable that IFN-β causes changes in this such that the extent of pore formation is increased. Alternatively, closure of pores and cell survival requires a membrane resealing process (McNeil and Kirchhausen 2005), which may be influenced by lipogenesis pathways. Inhibition of this could extend the damage caused by pore formation, leading to increased death stemming directly or indirectly from the continued ion movement and osmotic stress.

The permeability increasing activity of LLO, which is accompanied by an increased reactive oxygen species generation (ROS), RhoA activation and myosin light chain (MLC) phosphorylation, can be completely inhibited by the protein kinase C α/β inhibitor GÖ6976, indicating a crucial role for PKC in the induction of barrier dysfunction. The TNF-derived human TIP peptide blunts LLO-induced hyperpermeability *in vitro*, upon inhibiting LLO induced protein kinase C-α activation, ROS generation and MLC phosphorylation and upon restoring the RhoA/Rac 1 balance. These results indicate that the lectin-like domain of TNF-α has a potential therapeutic value in protecting from LLO-induced pulmonary endothelial hyperpermeability (Xiong et al. 2010). Amiloride, which inhibits TIP peptide-mediated Na^+ uptake, also inhibits LLO-mediated MLC phosphorylation. Recently, the α-subunit of the epithelial sodium channel, which has been shown to be crucial for the channel's activity, has been shown to be expressed in endothelial cells (Kusche-Vihrog et al. 2008, Wang et al. 2009). These results thus suggest a link between Na^+ uptake and regulation of permeability in

endothelial cells, which requires further investigation. As such, the TIP peptide might represent an interesting candidate for the treatment of infection-associated permeability, since it is able to restore both alveolar liquid clearance as well as endothelial barrier function (Xiong et al. 2010).

Infections with PVL-positive *Staphylococcus aureus* strains were rare, but emerged worldwide within the last years. The β-barrel pore-forming toxin PVL is comprised of two subunits termed LukF-PV and LukS-PV, and it is associated with serious lung infections. Both subunits are secreted separately and are thought to oligomerize on the surface of specific cells to assemble the final pore (Colin et al. 1994, Jayasinghe and Bayley 2005). However, we could demonstrate that the two subunits had to be added to the bathing solution concomitantly and not consecutively in order to allow pore-forming activity of PVL. This effect was observed independent of site of application as Na^+, K^+ and Ca^{2+} conducting PVL pores were induced after extra- as well as intracellular application.

Permeabilsation of the plasma membrane by pore-forming toxins leads to changes in cytoplasmic ion composition, which have been previously shown to modulate inflammatory gene expression (Dragneva et al. 2001, Taneike et al. 2002, Aroian and Van der Goot 2007). For example, treatment of renal epithelial cells with α-haemolysin toxin leads to IL-8 production in a calcium dependent manner (Uhlén et al. 2000). To determine whether pore formation is a pre-requiste for inflammatory cytokine synthesis following rPVL treatment, we treated macrophages with different doses of both single subunits of rPVL (LukS or LukF) or an equimolar combination of both subunits and performed whole cell patch clamp experiments. No pore formation was observed following treatment of cells with single subunits of toxin but multiple ion channels were open following a 1 min treatment with both subunits. These data are in line with previous observations, showing that both subunits of rPVL in an equimolar ratio are required to perform a pore (Colin et al. 1994, Jayasinghe and Bayley 2005). Significantly, although single subunits are incapable of inducing a pore in macrophages, they are capable of inducing TNF-α gene expression, albeit at lower levels than rPVL. These data indicate that although pore formation precedes inflammatory gene expression, inflammatory gene expression is dependent on cellular pathways which are independent of pore formation. A microarray profiling approach to show that PVL induces a highly specific inflammatory transcriptional response in alveolar macrophages was applied. Biochemical and genetic studies indicated that this response is independent from PVLs pore forming ability and is mediated via NF-kB, through a TLR2 dependent mechanism (Zivkovic, paper in print).

4.4. Conclusion

The results of the present thesis show that TIP peptides which have an activating effect on amiloride-sensitive ENaC in A549 cells possess i) the triad of residues equivalent to T105, E107 and E110 of human TNF-α, ii) the group of adjacent hydrophobic residues equivalent to P113, W114 and Y115 of human TNF-α, and iii) either a positively-charged N-terminal amino group or a negatively-charged C-terminal carboxyl group or both of these, whereas peptides which lack one or more of these features do not exert such an effect.

As a link between amiloride-sensitive Na^+ uptake and regulation of permeability in endothelial cells is reported, the TIP peptides might represent an interesting candidate for the treatment of infection-associated permeability oedema. The TNF-derived human TIP peptide is able to blunt LLO-induced hyperpermeability *in vitro*. The presented data show that pre-treatment of macrophages with IFN-β critically increased the extent of pore formation by LLO as well as the rate of cell death. On the other hand, for PVL the data indicate a highly specific inflammatory transcriptional response in alveolar macrophages which is independent of PVL's pore forming ability that was not affected by TIP peptides.

5. LIST OF ABBREVIATIONS

ALC	alveolar liquid clearance
ALI	acute lung injury
ARDS	acute respiratory distress syndrome
ASICs	acid-sensing ion channels
ATI (TI)	alveolar type I cells
ATII (TII)	alveolar type II cells
CFTR Cl$^-$	channel cystic fibrosis transmembrane regulator
CNG channel	pimozide-sensitive cyclic nucleotide-gated cation channel
ENaC	amiloride-sensitive epithelial sodium channel
HSC	highly selective epithelial sodium channel
IFN-I	type I interferon
IFN-β	interferon β
IL-8	interleukin 8
LLO	Listeriolysin O
LukF-PV	Staphylococcal leukocidin, component of PVL
LukS-PV	Staphylococcal leukocidin, component of PVL
MRSA	methicillin resistant *Staphylococcus aureus*
NF-κB	nuclear factor kappa B
NSC	non-selective cation channel
PGNase	N-glycosidase F (Peptide-N4-(acetyl-ß-glucosaminyl)-asparagine amidase)
PMNs	polymorphonuclear cells
PVL	Panton-Valentine Leukocidin
ROS	reactive oxygen species
St. aureus	*Staphylococcus aureus*
TEA	tetraethylammonium chloride
TIP	lectin-like domain of TNF-α
TLR	Toll-like receptors
TNF-α	Tumor necrosis factor α

6. TABLES

Table 1: Cross-linking solutions to replace the disulphide bridge of AP301 in TIP peptide analogues.

Table 2: Potency of ENaC-activating TIP peptides.

Table 3: Selectivity of ENaC-activating TIP peptides.

Table 4: The data of whole cell patch clamping in A549 cells with nebulised and un-nebulized AP301 in different concentrations.

Table 5: Effect of TNF-α, AP301 and AP318 on single channel kinetics at E_h= -60 mV.

Table 6: Effect of TNF-α, AP301 and AP318 on single channel kinetics at E_h= +60 mV.

Table 7: Effect of deglycosylation on TNF-α-, AP301- and AP318-induced ENaC activation.

Table 8: Open probability and single channel conductivity (Conduct.) of ENaC at E_h= -60 mV in untreated and glycosylated A549 cell membranes.

7. FIGURES

Figure 1: The distal airway epithelium contains alveolar type I and type II cells and Clara cells.

Figure 2: Sodium is transported through channels on the apical membrane.

Figure 3: Structure of ENaC.

Figure 4: Block of ENaC by amiloride.

Figure 5: Clinical correlations of ENaC regulation.

Figure 6: Structure and effect of TNF-α on Na^+ current.

Figure 7: Structure of TNF-α.

Figure 8: Analysis of sequence residue in chain A of human TNF-α.

Figure 9: Human TNF-α around TIP or lectin-like domain (C101-E116) according to structure PDB ID:1A8M, and models for the TIP-peptides AP301, AP302, AP303 and mutant peptide based on the 1A8M template.

Figure 10: Model for how PVL might mediate tissue necrosis.

Figure 11: PVL is a β-barrel pore-forming toxin, comprised of two subunits termed LukF-PV and LukS-PV.

Figure 12: Pore formation after exposure to wild-type *Listeria monocytogenes* and LLO.

Figure 13: Patch clamp technique in the cell-attached mode.

Figure 14: All models of patch clamping.

Figure 15: TIP peptide 301, 2D chemical structure.

Figure 16: Effect of AP301 on ENaC.

Figure 17: Effect of AP301 on current-voltage (IV) relationship.

8. REFERENCES

Alberti-Segui C, Goeden KR, Higgins DE (2007) Differential function of Listeria monocytogenes listeriolysin O and phospholipases C in vacuolar dissolution following cell-to-cell spread. *Cell Microbiol* **9**: 179-195

Alvarez de la Rosa D, Canessa CM, Fyfe GK, Zhang P (2000) Structure and regulation of amiloride-sensitive sodium channels. *Annu Rev Physiol* **62**: 573-594

Aroian R, van der Goot FG (2007) Pore-forming toxins and cellular non-immune defenses (CNIDs). *Curr Opin Microbiol* **10**: 57-61

Auerbuch V, Brockstedt DG, Meyer-Morse N, O'Riordan M, Portnoy DA (2004) Mice lacking the type I interferon receptor are resistant to Listeria monocytogenes. *J Exp Med* **200**: 527-533

Baba Moussa L, Werner S, Colin DA, Mourey L, Pedelacq JD, Samama JP, Sanni A, Monteil H, Prevost G (1999) Discoupling the Ca^{2+}-activation from the pore-forming function of the bi-component Panton-Valentine leucocidin in human PMNs. *FEBS Letters* **461**: 280-286.

Babini E, Geisler HS, Siba M, Gründer S (2003) A New Subunit of the Epithelial Na^+ Channel Identifies Regions Involved in Na^+ Self-inhibition. *J Biol Chem* **278**: 28418-28426

Baldwin RL, Mirzabekov T, Kagan BL, Wisnieski BJ (1995) Conformation and ion channel activity of lymphotoxin at neutral and low pH. *J Immunol* **154**: 790-798

Baldwin RL, Stolowitz ML, Hood L, Wisnieski BJ (1996) Structural changes of tumor necrosis factor alpha associated with membrane insertion and channel formation. *Proc Natl Acad Sci USA* **93**: 1021-1026

Bantel H, Sinha B, Domschke W, Peters G, Schulze-Osthoff K, Janicke RU (2001) -Toxin is a mediator of Staphylococcus aureus-induced cell death and activates caspases via the intrinsic death pathway independently of death receptor signaling. *J Cell Biol* **155**: 637-648

Bao HF, Zhang ZR, Liang YY, Ma JJ, Eaton DC, Ma HP (2007) Ceramide mediates inhibition of the renal epithelial sodium channel by tumor necrosis factor-alpha through protein kinase C. *Am J Physiol: Renal Physiol* **293**: F1178-F1186

Barsig J, Kaufmann SH (1997) The mechanism of cell death in Listeria monocytogenes-infected murine macrophages is distinct from apoptosis. *Infect Immun* **65**: 4075-81

Bavdek A, Gekara NO, Priselac D, Gutierrez Aguirre I, Darji A, Chakraborty T, Macek P, Lakey JH, Weiss S, Anderluh G (2007) Sterol and pH interdependence in the binding, oligomerization, and pore formation of Listeriolysin O. *Biochemistry* **46**: 4425-4437

Berthiaume Y (2003) Tumor necrosis factor and lung edema clearance: the tip of the iceberg? *Am J Respir Crit Care Med* **168**: 1022-1023

Berthiaume Y, Folkesson HG, Matthay MA (2002) Lung edema clearance: 20 years of progress: invited review: alveolar edema fluid clearance in the injured lung. *J Appl Physiol* **93**: 2207-2213

Berthiaume Y, Matthay MA (2007) Alveolar edema fluid clearance and acute lung injury. *Respir Physiol Neurobiol* **159**: 350-359

Bhalla V, Hallows K (2008) Mechanisms of ENaC regulation and clinical implications. *J Am Soc Nephrol* **19**: 1845-1854

Borjesson A, Norlin A, Wang X, Andersson R, Folkesson HG (2000) TNF-alpha stimulates alveolar liquid clearance during intestinal ischemia-reperfusion in rats. *Am J Physiol: Lung Cell Mol Physiol* **278**: L3-L12

Boyle-Vavra S, Daum RS (2007) Community-acquired methicillin-resistant Staphylococcus aureus: the role of Panton-Valentine leukocidin. *Lab Invest* **87**: 3-9

Braun C, Hamacher J, R. Morel D, Wendel A, Lucas R (2005) Dichotomal Role of TNF in Experimental Pulmonary Edema Reabsorption. *J Immunol* **175**: 3402-3408

Brochiero E, Dagenais A, Privé A, Berthiaume Y, Grygorczyk R (2004) Evidence of a functional CFTR Cl⁻ channel in adult alveolar epithelial cells. *Am J Physiol Lung Cell Mol Physiol* **287**: L382-L392

Bubeck Wardenburg J, Bae T, Otto M, DeLeo FR, Schneewind O (2007) Poring over pores: alpha-hemolysin and Panton-Valentine leukocidin in Staphylococcus aureus pneumonia. *Nat Med* **13**: 1405-1406

Carrero JA, Calderon B, Unanue ER (2004a) Listeriolysin O from Listeria monocytogenes is a lymphocyte apoptogenic molecule. *J Immunol* **172**: 4866-4874

Carrero JA, Calderon B, Unanue ER (2004b) Type I interferon sensitizes lymphocytes to apoptosis and reduces resistance to Listeria infection. *J Exp Med* **200**: 535-540

Carrero JA, Calderon B, Unanue ER (2006) Lymphocytes are detrimental during the early

innate immune response against Listeria monocytogenes. *J Exp Med* **203**: 933-940

Chraibi A, Horisberger JD (1999) Stimulation of Epithelial Sodium Channel Activity by the Sulfonylurea Glibenclamide. *J Pharmacol* **290**: 341-347

Chu S (2008) Sodium channel ENaC expression in lung epithelia. SciTopics, http://www.scitopics.com/Sodium_channel_ENaC_expression_in_lung_epithelia.html

Colin DA, Monteil H (2003) Control of the Oxidative Burst of Human Neutrophils by Staphylococcal Leukotoxins. *Infect Immun* **71**: 3724-3729

Colin DA, Mazurier I, Sire S, Finck-Barbancon V (1994) Interaction of the two components of leukocidin from Staphylococcus aureus with human polymorphonuclear leukocyte membranes: sequential binding and subsequent activation. *Infect Immun* **62**: 3184-3188

Dagenais A, Frechette R, Yamagata Y, Yamagata T, Carmel JF, Clermont ME, Brochiero E, Masse C, Berthiaume Y (2004) Downregulation of ENaC activity and expression by TNF-alpha in alveolar epithelial cells Am J Physiol: *Lung Cell Mol Physiol* **286**: L301-L311

Davis IC, Matalon S (2007) Epithelial sodium channels in the adult lung - important modulators of pulmonary health and disease. *Adv Exp Med Biol* **618**: 127-140

Decoursey TE, Jacobs ER, Silver MR (1988) Potassium current in Rat Type II Alveolar epithelial cells. *J Physiol* **395**: 487-505

Dragneva Y, Anuradha CD, Valeva A, Hoffmann A, Bhakdi S, Husmann M (2001) Subcytocidal attack by staphylococcal alpha-toxin activates NF-kappaB and induces interleukin-8 production. *Infect Immun* **69**: 2630-2635

Eaton DC, Helms MN, Koval M, Bao HF, Jain L (2009) The contribution of epithelial sodium channels to alveolar function in health and disease. *Annu Rev Physiol* **71**: 403-423

Eck MJ, Sprang SR (1989) The structure of tumor necrosis factor-alpha at 2.6 A resolution. Implications for receptor binding. *J Biol Chem* **264**: 17595-605

Elia N, Tapponnier M, Matthay MA, Hamacher J, Pache JC, Brundler MA, Totsch M, De Baetselier P, Fransen L, Fukuda N, Morel DR, Lucas R (2003) Functional identification of the alveolar edema reabsorption activity of murine tumor necrosis factor-alpha. *Am J Respir Crit Care Med* **168**: 1043-1050

Folkesson HG, Matthay MA (2006) Alveolar epithelial ion and fluid transport: recent progress. *Am J Respir Cell Mol Biol* **35**: 10-19

Fukuda N, Jayr C, Lazrak A, Wang Y, Lucas R, Matalon S, Matthay MA (2001) Mechanisms of TNF alpha stimulation of amiloride-sensitive sodium transport across alveolar epithelium. *Am J Physiol Lung Cell Mol Physiol* **280**: L1258-L1265

Garty H, Palmer L (1997) Epithelial sodium channels: function, structure, and regulation. *Physiol Rev* **77**: 359-96

Gekara NO, Jacobs T, Chakraborty T, Weiss S (2005) The cholesterol-dependent cytolysin listeriolysin O aggregates rafts via oligomerization. *Cell Microbiol* **7**: 1345-1356

Gekara NO, Westphal K, Ma B, Rohde M, Groebe L, Weiss S (2007) The multiple mechanisms of Ca^{2+} signalling by listeriolysin O, the cholesterol-dependent cytolysin of Listeria monocytogenes. *Cell Microbiol* **9**: 2008-2021

Genestier AL, Michallet MC, Prévost G, Bellot G, Chalabreysse L, Peyrol S, Thivolet F, Etienne J, Lina G, Vallette FM, et al (2005) Staphylococcus aureus Panton-Valentine leukocidin directly targets mitochondria and induces Bax-independent apoptosis of human neutrophils. *J Clin Invest* **115**: 3117-3127

Geoffroy C, Gaillard JL, Alouf JE, Berche P (1987) Purification, characterization, and toxicity of the sulfhydryl-activated hemolysin listeriolysin O from Listeria monocytogenes. *Infect Immun* **55**: 1641-1646

Gilbert RJC (2005) Inactivation and activity of cholesterol-dependent cytolysins: what structural studies tell us. *Structure* **13**: 1097-1106

Gilbert RJC, Jimenez JL, Chen S, Tickle IJ, Rossjohn J, Parker M, Andrew PW, Saibil HR (1999) Two structural transitions in membrane pore formation by pneumolysin, the pore-forming toxin of Streptococcus pneumoniae. *Cell* **97**: 647-655

Gillet Y, Issartel B, Vanhems P, Fournet JC, Lina G, Bes M, Vandenesch F, Piemont Y, Brousse N, Floret D, et al (2002) Association between Staphylococcus aureus strains carrying gene for Panton-Valentine leukocidin and highly lethal necrotising pneumonia in young immunocompetent patients. *Lancet* **359**: 753-759

Glomski IJ, Gedde MM, Tsang AW, Swanson JA, Portnoy DA (2002) The Listeria monocytogenes hemolysin has an acidic pH optimum to compartmentalize activity and prevent damage to infected host cells. *J Cell Biol* **156**: 1029-1038

Guidot DM, Folkesson HG, Jain L, Sznajder JI, Pittet JF, Matthay MA (2006) Integrating acute lung injury and regulation of alveolar fluid clearance. *Am J Physiol: Lung Cell Mol Physiol* **291**: L301-L306

Guzman CA, Domann E, Rohde M, Bruder D, Darji A, Weiss S, Wehland J, Chakraborty T, Timmis KN (1996) Apoptosis of mouse dendritic cells is triggered by listeriolysin, the major virulence determinant of Listeria monocytogenes. *Mol Microbiol* **20**: 119-126

Haerteis S, Krueger B, Korbmacher C, Rauh R (2009) The delta-subunit of the epithelial sodium channel (ENaC) enhances channel activity and alters proteolytic ENaC activation. *J Biol Chem* **284**: 29024-29040

Hamacher J, Stammberger U, Roux J, Kumar S, Yang G, Xiong C, Schmid RA, Fakin RM, Chakraborty T, Hossain HM, Pittet JF, Wendel A, Black SM, Lucas R (2010) The lectin-like domain of tumor necrosis factor improves lung function after rat lung transplantation - potential role for a reduction in reactive oxygen species generation. *Crit Care Med* **38**: 871-878

Hamill OP Marty A, Neher E, Sakmann B, Sigworth FJ (1981) Improved patch-clamp techniques for high resolution current recording from cells and cell-free membrane patches. *Pflügers Arch* **391**: 85-100

Hazemi P, Tzotzos SJ, Fischer B, Andavan GS, Fischer H, Pietschmann H, Lucas R, Lemmens-Gruber R. (2010) Essential structural features of TNF-α lectin-like domain derived peptides for activation of amiloride-sensitive sodium current in A549 cells. *J Med Chem* **53**: 8021-8029

Hribar M, Bloc A, van der Goot FG, Fransen L, De Baetselier P, Grau GE, Bluethmann H, Matthay MA, Dunant Y, Pugin J, Lucas R (1999) The lectin-like domain of tumor necrosis factor-alpha increases membrane conductance in microvascular endothelial cells and peritoneal macrophages. *Eur J Immunol* **29**: 3105-3111

Hummler E, Planes C (2010) Importance of ENaC-mediated sodium transport in alveolar fluid clearance using genetically-engineered mice. *Cell Physiol Biochem* **25**: 63-70

Jayasinghe L, Bayley H (2005) The leukocidin pore: Evidence for an octamer with four LukF subunits and four LukS subunits alternating around a central axis. *Protein Sci* **14**: 2550-2561

Ji HL, Bishop LR, Anderson SJ, Fuller CM, Benos DJ (2004) The Role of Pre-H2 Domains of α- and δ-Epithelial Na$^+$ Channels in Ion Permeation, Conductance, and Amiloride Sensitivity. *J Biol Chem* **279**: 8428–8440

Ji HL, Su XF, Kedar S, Li J, Barbry P, Smith PR, Matalon S, Benos DJ *(*2006*)* δ-Subunit Confers Novel Biophysical Features to αβγ-Human Epithelial Sodium Channel (ENaC) via a Physical Interaction. *J Biol Chem* **281**: 8233–8241

Johnson ER, Matthay MA (2010) Acute lung injury: epidemiology, pathogenesis, and treatment. *J Aerosol Med Pulm Drug Delivery* **23**: 243-252

Johnson MD, Bao HF, Helms MN, Chen XJ, Tigue Z, Jain L, Dobbs LG, Eaton DC (2006) Functional ion channels in pulmonary alveolar type I cells support a role for type I cells in lung ion transport. *Proc Natl Acad Sci USA* **13**: 4964-4969

Jonas D, Walev I, Berger T, Liebetrau M, Palmer M, Bhakdi S (1994) Novel path to apoptosis: small transmembrane pores created by staphylococcal-toxin in T lymphocytes evoke internucleosomal DNA degradation. *Infect Immun* **62**: 1304-1312

Kaneko J, Kamio Y (2004) Bacterial Two-component and Hetero-heptameric Pore-forming Cytolytic Toxins: Structures, Pore-forming Mechanism, and Organization of the Genes. *Biosci Biotech Biochem* **68**: 981-1003

Kathariou S, Metz P, Hof H, Goebel W (1987) Tn916-induced mutations in the hemolysin determinant affecting virulence of Listeria monocytogenes. *J Bacteriol* **169**: 1291-1297

Kayal S, Charbit A (2006) Listeriolysin O: a key protein of Listeria monocytogenes with multiple functions. *FEMS Microbiol Rev* **30**: 514-529

Kellenberger S, Schild L (2002) Epithelial sodium channel/degenerin family of ion channels: A variety of functions for a shared structure. *Physiol Rev* **82**: 735-767

Kemp PJ, Kim K-J, Borok Z, Crandall ED (2001) Re-evaluating the Na conductance of adult rat alveolar type II pneumocytes: evidence for the involvement of cGMP activated cation channels. *J Physiol* **536**: 693-701

Knapp S, Florquin S, Golenbock DT, van der Poll T (2006) Pulmonary LPS-binding protein inhibits the LPS-induced lung inflammation in vivo. *J Immunol* **176**: 3189-3195

Kusche-Vihrog K, Sobczak K, Bangel N, Wilhelmi M, Nechyporuk-Zloy V, Schwab A, Schillers H, Oberleithner H (2008) Aldosterone and amiloride alter ENaC abundance in vascular endothelium. *Pflugers Arch* **455**: 849–857

Labandeira-Rey M, Couzon F, Boisset S, Brown EL, Bes M, Benito Y, Barbu EM, Vazquez V, Höök M, Etienne J, Vandenesch F, Bowden MG (2007) Staphylococcus aureus Panton-Valentine Leukocidin Causes Necrotizing Pneumonia. *Science* **315**: 1130-1133

Lazrak A, Samanta A, Matalon S (2000) Biophysical properties and molecular characterization of amiloride-sensitive sodium channels in A549 cells. *Am J Physiol: Lung Cell Mol Physiol* **278**: L848-L857

Lazrak A, Samanta A, Venetsanou K, Barbry P, Matalon S (2000) Modification of biophysical properties of lung epithelial Na(+) channels by dexamethasone. *Am J Physiol: Cell Physiol* **279**: C762-C770

Leroy C, Dagenais A, Berthiaume Y, Brochiero E (2004) Molecular identity and function in transepithelial transport of K(ATP) channels in alveolar epithelial cells. *Am J Physiol: Lung Cell Mol Physiol* **286**: L1027-L1037

Levis RA, Rae JL (1992) Constructing a patch-clamp setup. *In*: Methods in Enzymology, Rudy B, Iverson LE (eds). Academic Press Inc., San Diego, **207**: pp 14-66

Lu M, Echeverri F, Kalabat D, Laita B, Dahan DS, Smith RD, Xu H, Staszewski L, Yamamoto J, Ling J, Hwang N, Kimmich R, Li P, Patron E, Keung W, Patron A, Moyer BD (2008) Small molecule activator of the human epithelial sodium channel. *J Biol Chem* **283**: 11981-11994

Lucas R, Magez S, De Leys R, Fransen L, Scheerlinck JP, Rampelberg M, Sablon E, De Baetselier P (1994) Mapping the lectin-like activity of tumor necrosis factor. *Science* **263**: 814-817

Lucas R, Verin AD, Black SM, Catravas JD (2009) Regulators of endothelial and epithelial barrier integrity and function in acute lung injury. *Biochem Pharmacol* **77**: 1763-1772

Marquardt A, Bernevic B, Przybylski M (2007) Identification, affinity characterisation and biological interactions of lectin-like peptide-carbohydrate complexes derived from human TNF-alpha using high-resolution mass spectrometry. *J Pept Sci* **13**: 803-810

Matthay MA, Folkesson HG, Clerici C (2002) Lung epithelial fluid transport and the resolution of pulmonary edema. *Physiol Rev* **82**: 569-600

McNeil PL, Kirchhausen T (2005) An emergency response team for membrane repair. *Nat Rev Mol Cell Biol* **6**: 499-505

Miles G, Jayasinghe l, Bayley H (2006) Assembly of the Bi-component Leukocidin Pore Examined by Truncation Mutagenesis. *J Biol Chem* **281**: 2205-2214

Morin C, Sirois M, Echave V, Gomes MM, Rousseau E (2007) Functional effects of 20-HETE on human bronchi: hyperpolarization and relaxation due to BKCa channel activation. *Am J Physiol Lung Cell Mol Physiol* **293**: L1037-L1044

Nelson KL, Brodsky RA, Buckley JT (1999) Channels formed by subnanomolar concentrations of the toxin aerolysin trigger apoptosis of T lymphomas. *Cell Microbiol* **1**: 69-74

Nichols D, Chmiel J, Berger M (2008) Chronic inflammation in the cystic fibrosis lung: alterations in inter- and intracellular signalling. *Clin Rev Allergy Immunol* **34**: 146-162

Oiu W, Laheri A, Leung S, Guggino SE (2000) Hormones increase mRNA of cyclic-nucleotide-gated cation channels in airway epithelia. *Pflügers Arch – Eur J Physiol* **441**: 69-77

O'Connell RM, Saha SK, Vaidya SA, Bruhn KW, Miranda GA, Zarnegar B, Perry AK, Nguyen BO, Lane TF, Taniguchi T, et al (2004) Type I interferon production enhances susceptibility to Listeria monocytogenes infection. *J Exp Med* **200**: 437-445

O'Grady SM, Lee SY (2003) Chloride and potassium channel function in alveolar epithelial cells. *Am J Physiol Lung Cell Mol Physiol* **284**: L689-L700

O'Hara FP, Guex N, Word JM, et al (2008) A geographic variant of the Staphylococcus aureus Panton-Valentine leukocidin toxin and the origin of community-associated methicillin resistant S. aureus USA300. *J Infect Dis* **197**:187–192

Park JM, Ng VH, Maeda S, Rest RF, Karin M (2004) Anthrolysin O and other Gram-positive cytolysins are Toll-like receptor 4 agonists. *J Exp Med* **200**: 1647-1655

Ramachandran R, Heuck AP, Tweten RK, Johnson AE (2002) Structural insights into the membrane-anchoring mechanism of a cholesterol-dependent cytolysin. *Nat Struct Mol Biol* **9**: 823-827

Repp H, Pamukci Z, Koschinski A, Domann E, Darji A, Birringer J, Brockmeier D, Chakraborty T, Dreyer F (2002) Listeriolysin of Listeria monocytogenes forms Ca^{2+}-permeable pores leading to intracellular Ca^{2+} oscillations. *Cell Microbiol* **4**: 483-491

Rezaiguia S, Garat C, Delclaux C, Meignan M, Fleury J, Legrand P, Matthay MA, Jayr C (1997) Acute bacterial pneumonia in rats increases alveolar epithelial fluid clearance by a tumor necrosis factor-alpha-dependent mechanism. *J Clin Invest* **99**: 325-335

Ridge FPG, Duszyk M, French AS (1997) A large conductance, Ca-activated K channel in a human lung epithelial cell line (A549). *Biochim Biophys Acta* **1327**: 249-258

Rossier BC, Pradervand S, Schild L, Hummler E (2002) Epithelial sodium channel and the control of sodium balance: Interaction Between Genetic and Environmental Factors. *Annu Rev Physiol* **64**: 877-897

Rossjohn J, Feil SC, McKinstry WJ, Tweten RK, Parker MW (1997) Structure of a cholesterol-binding, thiol-activated cytolysin and a model of its membrane form. *Cell* **89**: 685-692

Sakuma T, Takahashi K, Ohya N, Nakada T, Matthay MA (1998) Effects of ATP-sensitive potassium channel opener on potassium transport and alveolar fluid clearance in the resected human lung. *Pharmacol Toxicol* **83**: 16-22

Sartori C, Matthay MA (2002) Alveolar epithelial fluid transport in acute lung injury: new insights. *Eur Respir J* **20**: 1299-1313

Sayegh R, Auerbach S, Li X, Loftus R, Husted R, Stokes J, Thomas C (1999) Glucocorticoid Induction of Epithelial Sodium Channel Expression in Lung and Renal Epithelia Occurs via trans-Activation of a Hormone Response Element in the 5´-Flanking Region of the Human Epithelial Sodium Channel α Subunit Gene. *J Biol Chem* **274**: 12431-12437

Schnupf P, Portnoy DA, LA (2006) Phosphorylation, ubiquitination and degradation of listeriolysin O in mammalian cells: role of the PEST-like sequence. *Cell Microbiol* **8**: 353-364

Schuerch DW, Wilson-Kubalek EM, Tweten RK (2005) Molecular basis of listeriolysin O pH dependence. *Proc Natl Acad Sci USA* **102**: 12537-12542

Shehata M (2009) Regulation of the epithelial sodium channel [ENaC] in kidneys of salt-sensitive Dahl rats: Insights on alternative splicing. *Int Arch Med* **3**: 14-19

Spöhr F, Busch CJ, Reich C, Motsch J, Gebhard MM, Kuebler WM, Bloch KD, Weimann J (2007) 4-Aminopyridine restores impaired hypoxic pulmonary vasoconstriction in endotoxemic mice. *Anesthesiology* **107**: 597-604

Staali L, Monteil H, Colin DA (1998) The staphylococcal pore-forming leukotoxins open Ca^{2+} channels in the membrane of human polymorphonuclear neutrophils. *J Membr Biol* **162**: 209-216

Staub O, Abriel H, Plant P, Ishikawa T, Kanelis V, Saleki R, Horisberger JD, Schild L, Rotin D (2000) Regulation of the epithelial Na^+ channel by Nedd4 and ubiquitination. *Kidney Int* **57**: 809-815

Stockinger S, Materna T, Stoiber D, Bayr L, Steinborn R, Kolbe T, Unger H, Chakraborty T, Levy DE, Muller M, Decker T (2002) Production of type I IFN sensitizes macrophages to cell death induced by Listeria monocytogenes. *J Immunol* **169**: 6522-6529

Taneike I, Zhang HM, Wakisaka-Saito N, Yamamoto T (2002) Enterohemolysin operon of Shiga toxin-producing Escherichia coli: a virulence function of inflammatory cytokine production from human monocytes. *FEBS Lett* **524**: 219-224

Tilley SJ, Orlova EV, Gilbert RJC, Andrew PW, Saibil HR (2005) Structural basis of pore

formation by the bacterial toxin pneumolysin. *Cell* **121**: 247-256

Tillie-Leblond I, Guery BP, Janin A, Leberre R, Just N, Pittet JF, Tonnel AB, Gosset P (2002) Chronic bronchial allergic inflammation increases alveolar liquid clearance by TNF-alpha-dependent mechanism. *Am J Physiol: Lung Cell Mol Physiol* **283**: L1303-L1309

Trinh NT, Privé A, Kheir L, Bourret JC, Hijazi T, Amraei MG, Noël J, Brochiero E (2007) Involvement of KATP and KvLQT1 K^+ channels in EGF-stimulated alveolar epithelial cell repair processes. *Am J Physiol Lung Cell Mol Physiol* **293**: L870-L882

Tweten RK (2005) Cholesterol-dependent cytolysins, a family of versatile pore-forming toxins. *Infect Immun* **73**: 6199-6209

Uhlén P, Laestadius A, Jahnukainen T, Söderblom T, Bäckhed F, Celsi G, Brismar H, Normark S, Aperia A, Richter-Dahlfors A (2000) Alpha-haemolysin of uropathogenic E. coli induces Ca^{2+} oscillations in renal epithelial cells. *Nature* **405**: 694-697

Vadasz I, Schermuly RT, Ghofrani HA, Rummel S, Wehner S, Muhldorfer I, Schafer KP, Seeger W, Morty RE, Grimminger F, Weissmann N (2008) The lectin-like domain of tumor necrosis factor-alpha improves alveolar fluid balance in injured isolated rabbit lungs. *Crit Care Med* **36**: 1543-1550

Van der Goot, FG, Pugin J, Hribar M, Fransen L, Dunant Y, De Baetselier P, Bloc A, Lucas R (1999) Membrane interaction of TNF is not sufficient to trigger increase in membrane conductance in mammalian cells. *FEBS Lett* **460**: 107-111

Vandenesch F, Naimi T, Enright MC, Lina G, Nimmo GR, Heffernan H, Liassine N, Bes M, Greenland T, Reverdy ME, Etienne J (2003) Community-acquired methicillin-resistant staphylococcus aureus carrying panton-valentine leukocidin genes: worldwide emergence. *Emerg Infect Dis* **9**: 978-984

Verghese GM, Ware LB, Matthay BA, Matthay MA (1999) Alveolar epithelial fluid transport and the resolution of clinically severe hydrostatic pulmonary edema. *J Appl Physiol* **87**: 1301-1312

Waldmann R, Champigny G, Bassilana F, Voilley N, Lazdunski M (1995) Molecular Cloning and Functional Expression of a Novel Amiloride-sensitive Na^+ Channel. *J Biol Chem* **270**: 27411–27414

Wang S, Meng F, Mohan S, Champaneri B, Gu Y (2009) Functional ENaC channels expressed in endothelial cells: a new candidate for mediating shear force. *Microcirculation* **16**: 276–287

Ware LB, Matthay MA (2001) Alveolar fluid clearance is impaired in the majority of patients with acute lung injury and the acute respiratory distress syndrome. *Am J Respir Crit Care Med* **163**: 1376-1383

Xiong C, Yang G, Kumar S, Aggarwal S, Leustik M, Snead C, Hamacher J, Fischer B, Umapathy NS, Hossain H, Wendel A, Catravas JD, Verin AD, Fulton D, Black SM, Chakraborty T, Lucas R (2010) The lectin-like domain of TNF protects from listeriolysin-induced hyperpermeability in human pulmonary microvascular endothelial cells - a crucial role for protein kinase C-alpha inhibition. *Vascul Pharmacol* **52**: 207-213

Yang LM, Rinke R, Korbmacher C (2006) Stimulaion of the epithelial sodium channel (ENaC) by cAMP involves putative ERK phosphorylation sites in the C termini of the channel's β- and γ- subunit. *J Biol Chem* **281**: 9859-9868

Zemans R, Matthay M (2004) Bench-to-beside review: The role of the alveolar epithelium in the resolution of pulmonary edema in acute lung injury. *Crit Care* **8**: 469-477

Zwaferink H, Stockinger S, Reipert S, Decker I (2008a) Stimulation of inducible nitric oxide synthase expression by interferon β increases necrotic death of macrophages upon Listeria monocytogenes infection. *Infect Immun* **76**: 1649-1656

Zwaferink H, Stockinger S, Hazemi P, Lemmens-Gruber R, Decker T (2008b) IFN-beta increases listeriolysin O-induced membrane permeabilization and death of macrophages. *J Immunol* **180**: 4116-4123

9. APPENDIX

9.1. Abstract

Pulmonary oedema is a major complication of acute lung injury, severe pneumonia, and acute respiratory distress syndrome. Ventilation strategies apart, no standard treatment exists for pulmonary permeability oedema. Therefore, novel therapies activating sodium uptake from the alveolar fluid could improve clinical outcome. The involvement of Na^+ transporters in alveolar fluid clearance in the mammalian lung has been well established in recent years. Transport via amiloride-sensitive epithelial sodium channel (ENaC) in particular is one of the major pathways for Na^+ entry across alveolar and distal epithelial cells. ENaC plays a prominent role in sodium uptake from alveolar fluid and is the major component in alveolar fluid clearance in normal and diseased lungs. The lectin-like domain of TNF-α has been shown to activate amiloride-sensitive sodium uptake in type II alveolar epithelial cells. Therefore, several synthetic peptides that mimic the lectin-like domain of TNF-α (TIP) were synthesized and their ability to enhance sodium current through ENaC was studied in A549 cells with the patch clamp technique. Replacement of C101 by a glycine residue (G2) and addition of N-terminal (C1) and C-terminal cysteine (C17) residues, linked by a disulphide bridge, resulted in the 17-residue cyclic peptide, AP301. The disulphide bond in analogue AP301 may be susceptible to reduction and scission leading to complications in medical use. Therefore, the focus of the new peptide design described in the thesis was replacement of the disulphide bridge of the original TIP analogue, AP301, with other molecular arrangements. The data from structure-activity relationship studies suggest that TIP peptides which have an activating effect on amiloride-sensitive ENaC in A549 cells possess the triad of residues equivalent to T105, E107 and E110 of human TNF-α, and the group of adjacent hydrophobic residues equivalent to P113, W114 and Y115 of human TNF-α. Furthermore, a free positively charged N-terminal amino group on residue 1 and/or a free negatively charged carboxyl group on residue 17 of the TIP peptide is essential for the ENaC-activating effect. Peptides which lack one or more of these features do not exert such an effect. All active TIP peptides were highly selective for ENaC with a tendency towards less selectivity in molecules without a free positively-charged N-terminal amino group. A solution of AP301, which has been nebulized, retains the ENaC activating effect of AP301. Therefore, delivery of AP301 as an aerosol by inhalation to the patient will have no detrimental effect on the pharmacological activity of

AP301. Effects on macroscopic Na$^+$ current were confirmed by single channel current measurements. Open probability, mean open times, number of bursts, and duration of bursts were increased by TNF-α as well as AP301 and AP318, whereas single channel conductivity was not changed by the test compounds. Patch clamp experiments gave evidence for an extracellularly located binding site for TIP peptides. The specific binding of the TNF-TIP domain to *N,N*-diacetylchitobiose, a disaccharide present in many glycan structures of glycoproteins, was demonstrated previously. After deglycosylation of the A549 cell membrane with PNGase F, no effect on channel conductivity was found, however, the ENaC-activating effect got lost in deglycosylated cells.

Infections with *Listeria* and *Staphylococcus aureus* can lead to potentially lethal pulmonary complications, characterized by extensive permeability oedema. The bacterial toxin Listeriolysin O (LLO) is a cholesterol-dependent cytotoxin, which induces hyperpermeability in monolayers of human lung microvascular endothelial cells *in vitro*. It is reported that pore-formation and signaling events are linked to cell death induced by LLO and some other pore-forming toxins. When macrophages were pretreated with IFN-β the extent of pore formation by LLO as well as the rate of cell death critically increased. Given that binding and pore formation by LLO is dependent on membrane composition, it is conceivable that IFN-β causes changes in this such that the extent of pore formation is increased. Panton-Valentine Leukocidin (PVL) is a β-barrel pore-forming toxin comprised of two subunits termed LukF-PV and LukS-PV. PVL secreting *Staphylococcus aureus* strains emerged worldwide in the last years and were found associated with serious lung and skin infections in humans, indicating the potential threat of serious infections. Data indicate a highly specific inflammatory transcriptional response in alveolar macrophages which is independent of PVL's pore forming ability. The two components had to be added to the bathing solution concomitantly but not consecutively in order to allow pore-forming activity of PVL. This effect was observed independently of the site of application as Na$^+$, K$^+$ and Ca^{2+} conducting PVL pores were induced after extra- as well as intracellular application. TIP peptides showed no effect on PVL-induced pore formation.

As a link between amiloride-sensitive Na$^+$ uptake and regulation of permeability in endothelial cells is reported, the TIP peptides might represent an interesting candidate for the treatment of infection-associated permeability oedema. Indeed, it could already be demonstrated that the TNF-derived human TIP peptide is able to blunt LLO-induced hyperpermeability *in vitro*.

9.2. Zusammenfassung

Lungenödem ist eine schwerwiegende Komplikation im Rahmen einer Lungenverletzung, schwerer Pneumonie und akutem Lungenversagen. Neue Therapiemöglichkeiten wie Aktivierung des Natriumtransports und dadurch bedingten Wassertransports aus der alveolären Flüssigkeit könnte die Prognose eines Permeabilitätsödems verbessern. Insbesondere der Transport über den Amilorid-sensitiven epithelialen Natriumkanal (ENaC) ist einer der Hauptwege für Na^+ über alveoläre und distale Epithelzellen. ENaC spielt eine wichtige Rolle beim Natriumtransport aus der Alveolarflüssigkeit und ist eine wesentliche Komponente in der alveolären Clearance in gesunden und kranken Lungen. Die Lectin-Domäne von TNF-α kann die Amilorid-sensitive Natriumaufnahme in Typ II alveolären Epithelzellen aktivieren. Ziel war daher die Wirkung von synthetischen Peptiden, die die Lectin-Domäne von TNF-α (TIP) nachbauen, auf ENaC in A549 Zellen mit Hilfe der Patch Clamp Technik zu untersuchen. Austausch von C101 durch Glycin (G2) und Hinzufügen von N-terminalen (C1) und C-terminalen Cystein (C17) Resten, verbunden durch eine Disulfidbrücke, ergab das cyclische Peptid AP301. Die Disulfidbrücke in AP301 kann nachteilig sein und daher sollten neue AP301-Analoge getestet und eine Struktur-Wirkungsbeziehung aufgestellt werden. Die Daten zeigen, dass TIP Peptide, die einen ENaC-aktivierenden Effekt in A549 Zellen haben, einerseits die Triade von Gruppen besitzen, die äquivalent mit T105, E107 und E110 des humanen TNF-α sind, und andererseits auch die angrenzende Gruppe der hydrophoben Reste besitzen, die äquivalent mit P113, W114 und Y115 vom humanen TNF-α sind. Weiters ist eine freie positiv geladene N-terminale Aminogruppe an Rest 1 und/oder eine freie negativ geladene Carboxylgruppe an Rest 17 der TIP Peptide essentiell für die ENaC-aktivierende Wirkung. Peptide ohne eine oder mehrere dieser Eigenschaften hatten keine Wirkung. Alle aktiven TIP Peptide waren hoch selektiv für ENaC mit einer Tendenz zu geringerer Selektivität in Molekülen ohne eine freie positiv geladene N-terminale Aminogruppe. Eine AP301-Lösung, die vernebelt und kondensiert wurde, behielt ihre ENaC-aktivierende Wirkung. Deshalb ist die Anwendung in Ärosol-Form zur Inhalation für Patienten geeignet, ohne Verlust der pharmakologischen Wirksamkeit. Die Wirkungen auf den makroskopischen Na^+ Strom wurden durch die Einzelkanalstrom-messungen bestätigt. Die Öffnungswahrscheinlichkeit, mittlere Öffnungszeit sowie Anzahl und Dauer der Bursts wurden durch TNF-α und auch AP301 und AP318 signifikant erhöht, wohingegen die Einzelkanalleitfähigkeit durch die Testsubstanzen nicht verändert wurde.

Patch Clamp Experimente weisen auf eine extrazelluläre Bindungsstelle für TIP Peptide hin. Eine spezifische Bindung der TNF-TIP Domäne an *N,N*-Diacetylchitobiose, ein in vielen Glykanstrukturen von Glykoproteinen vorkommendes Dissaccharid, ist bekannt. Deglycosylierung der A549 Zellmembran mit PNGase F bewirkte keine Veränderung der Kanalleitfähigkeit, jedoch ging die ENaC-aktivierende Wirkung in deglykosylierten Zellen verloren.

Infektionen mit *Listeria* und *Staphylococcus aureus* können zu möglichen letalen pulmonalen Komplikationen mit ausgeprägtem Permeabilitätsödem führen. Das bakterielle Toxin Listeriolysin O (LLO) gehört zur Gruppe der Cholesterol-abhängigen Cytotoxine, das Hyperpermeabilität in Einzelschichten humaner pulmonaler mikrovaskulärer Endothelial-zellen *in vitro* induzieren kann. Es wird angenommen, dass über Porenbildung und Signalwege der von LLO und anderen porenbildenden Toxinen induzierte Zelltod erfolgt. Vorbehandlung von Makrophagen mit IFN-β verstärkte die LLO-induzierte Porenbildung und den Zelltod drastisch. Da die Bindung und Porenbildung durch LLO vom Membranaufbau abhängig ist, wäre eine IFN-β bedingte erhöhte Porenbildung denkbar. Panton-Valentine Leukocidin (PVL) ist ein β-barrel porenbildendes Toxin, das aus zwei Komponenten besteht, LukF-PV und LukS-PV. PVL sezernierende *Staphylococcus aureus* Stämme traten in den letzten Jahren vermehrt auf und wurden mit schweren Lungen- und Hautinfektionen in Zusammenhang gebracht. Die Ergebnisse deuten auf eine hoch spezifische inflammatorische transkriptionale Reaktion in alveolären Makrophagen hin, die unabhängig von der porenbildenden Eigenschaft von PVL ist. Die zwei Toxin-Komponenten müssen gemeinsam der Badlösung zugesetzt warden. Eine sukzessive Applikation führt nicht zur Porenbildung. Die Bildung von Na^+, K^+ und Ca^{2+} leitenden Poren wurde sowohl nach extra- als auch intrazellulärer Applikation festgestellt.

Da ein Zusammenhang zwischen Amilorid-sensitivem Na^+ Transport und Regulation der Permeabilität in Endothelzellen besteht, könnten die TIP Peptide ein interessanter Ansatzpunkt in der Therapie von infektionsassoziierten Permeabilitätsödemen sein. Es konnte bereits gezeigt werden, dass ein humanes TNF-TIP Peptid eine LLO-induzierte Hyperpermeabilität *in vitro* abschwächen kann.

9.3. Curriculum vitae

First name:	Parastoo
Surname:	Hazemi
Date and place of birth:	03.04.1981 in Tehran, Iran
Nationality:	Iranian
Email:	parastoo_hazemi@yahoo.com

Education:	1987 – 1991	Primary school, Tehran
	1991 – 1999	Secondary school, Tehran
	1999	Higher school certificate
	1999 – 2005	Study of Pharmacy at the Azad University, Tehran
	13.09.2005	Academic degree "Doctor of Pharmacy"
	2007 – 2011	PhD study at the Department of Pharmacology and Toxicology at the University of Vienna, Austria

Internships:	07/2000 – 10/2000	Azad-Pharmacy, Tehran
	07/2001 – 10/2001	Hasti-Pharmacy, Tehran
	07/2002 – 12/2002	Hasti-Pharmacy, Tehran

Professional career:	03/2002 – 03/2004	Pharmaceutical representative for Shafayab Pharmacy Co., Tehran
	09/2003 – 07/2005	Pharmacist, Sima-Pharmacy, Tehran
	06/2008 – 09/2010	Research assistant, Apeptico Forschung und Entwicklung GmbH, Vienna

Language skills:	Farsi (Persian):	Mother tongue
	German:	Very good knowledge, written and spoken
	Englisch:	Good knowledge, written and spoken

Publications:

Zwaferink H, Stockinger S, Hazemi P, Lemmens-Gruber R, Decker T (2008) IFN-β increases Listeriolysin O-induced membrane permeabilisation and lytic death of macrophages. *Journal of Immunology* **180**: 4116-4123.

Hazemi P, Tzotzos SJ, Fischer B, Andavan GS, Fischer H, Pietschmann H, Lucas R, Lemmens-Gruber R (2010) Essential structural features of TNF-α lectin-like domain derived peptides for activation of amiloride-sensitive sodium current in A549 cells. *Journal of Medicinal Chemistry* **53**: 8021-8029.

Zivkovic A, Sharif O, Stich K, Doninger B, Colinge J, Bilban M, Mesteri I, Hazemi P, Lemmens-Gruber R, Knapp S (2010) Toll-like receptor 2 mediates innate immunity and lung inflammation to Staphylococcal Panton Valentine Leukocidin in vivo. *Journal of Immunology* [Epub ahead of print].

Poster presentation:

Fischer B, Tzotzos SJ, Pietschmann H, Fischer H, Lucas R, Hazemi P, Lemmens-Gruber R, Hartmann E, Markstaller K, Mascher H (2010) Development of inhalation therapy for prevention and treatment of acute lung injury. Annual Congress of the European Respiratory Society, Barcelona, Spain, September 18-22.